Assessment and Real Time Implementation of Wireless Communications Systems and Applications in Transportation Systems

Ángel Carro Lagoa

Doctoral Thesis UDC / 2021

Advisors: Miguel González López
José Antonio García Naya

PhD Program in Information Technology and Mobile Network Communication

UNIVERSIDADE DA CORUÑA

Avaliación e Implementación en Tempo Real de Sistemas de Comunicacións sen Fíos e Aplicacións en Sistemas de Transporte

Ángel Carro Lagoa

Tese de Doutoramento UDC / 2021

Directores: Miguel González López
José Antonio García Naya

Programa de Doutoramento en Tecnoloxías da Información e das Comunicacións en Redes Móbiles

UNIVERSIDADE DA CORUÑA

Evaluación e Implementación en Tiempo Real de Sistemas de Comunicaciones Inalámbricos y Aplicaciones en Sistemas de Transporte

Ángel Carro Lagoa

Tesis Doctoral UDC / 2021

Directores: Miguel González López
José Antonio García Naya

Programa de Doctorado en Tecnologías de la Información y de las Comunicaciones en Redes Móviles

UNIVERSIDADE DA CORUÑA

Ángel Carro Lagoa

CERTIFICA / *CERTIFICA* / *CERTIFIES*

Que a presente memoria é o resultado do meu propio traballo de investigación e que o traballo doutros autores está citado axeitadamente.

Que la presente memoria es el resultado de mi propio trabajo de investigación y que el trabajo de otros autores está citado apropiadamente.

That the present report is the result of my own research work and that the work done by other authors is appropriately cited.

A Coruña, *19 de abril de 2021 / 19 de abril de 2021 / April 19, 2021*

Ángel Carro Lagoa

Miguel González López
José Antonio García Naya

CERTIFICAN / *CERTIFICAN* / *CERTIFY*

Que a presente tese titulada "Avaliación e implementación en tempo real de sistemas de comunicacións sen fíos e aplicacións en sistemas de transporte" foi realizada por Ángel Carro Lagoa baixo a nosa dirección no Departamento de Enxeñaría de Computadores da Universidade da Coruña e preséntase para obter o grao de Doutor.

Que la presente tesis titulada "Evaluación e implementación en tiempo real de sistemas de comunicaciones inalámbricos y aplicaciones en sistemas de transporte" fue realizada por Ángel Carro Lagoa bajo nuestra dirección en el Departamento de Ingeniería de Computadores de la Universidade da Coruña y se presenta para obtener el grado de Doctor.

That the present thesis titled "Assessment and real time implementation of wireless communications systems and applications in transportation systems" was done by Ángel Carro Lagoa under our supervision in the Department of Computer Engineering at the University of A Coruña and it is submitted to obtain the Ph.D. degree.

Os directores da tese / *Los directores de la tesis* / *The Ph.D. supervisors*.
A Coruña, 19 de abril de 2021 / *19 de abril de 2021* / *April 19, 2021*.

Dr. Miguel González López
Profesor Titular de Universidade
Dpto. de Enxeñaría de Computadores
Universidade da Coruña

Associate Professor
Dept. of Computer Engineering
University of A Coruña

Dr. José Antonio García Naya
Profesor Contratado Doutor
Dpto. de Enxeñaría de Computadores
Universidade da Coruña

Associate Professor
Dept. of Computer Engineering
University of A Coruña

Tese de Doutoramento / *Tesis Doctoral* / *Doctoral Thesis*

Título:	Avaliación e implementación en tempo real de sistemas de comunicacións sen fíos e aplicacións en sistemas de transporte
***Título*:**	*Evaluación e implementación en tiempo real de sistemas de comunicaciones inalámbricos y aplicaciones en sistemas de transporte*
***Title*:**	*Assessment and real time implementation of wireless communications systems and applications in transportation systems*
Autor / *Autor* / *Author*:	Ángel Carro Lagoa
Directores / *Directores* / *Supervisors*:	Miguel González López José Antonio García Naya
Data / *Fecha* / *Date*:	19 de abril de 2021 / *19 de abril de 2021* / *April 19, 2021*

Tribunal / *Tribunal* / *Evaluation Committee*

Presidente / *Presidente* / *President*:	Raquel Barco Moreno
Vogal / *Vocal* / *Member*:	José Rodríguez Piñeiro
Secretaria / *Secretaria* / *Secretary*:	Luis Castedo Ribas

Agradecimientos

Son muchas las personas a las que me gustaría agradecer su ayuda a lo largo de estos años. En primer lugar, quiero agradecer a mis directores de tesis, José Antonio y Miguel, su esfuerzo, dedicación y paciencia. Sus ideas y consejos han hecho posible este trabajo.

También quiero agradecer a Luis Castedo el haberme brindado la oportunidad de pertenecer a este grupo de investigación y su apoyo durante tantos años.

Esta tesis tampoco sería posible sin la ayuda y talento de Pedro, con quien tuve la suerte de compartir muchos años de trabajo. Gracias a él, todas las horas dedicadas a pelearnos con las FPGAs y a desentrañar las misteriosas causas de los problemas que nos íbamos encontrando, fueron mucho más llevaderas y entretenidas.

Igualmente, debo agradecer a Xosé, entre otras cosas, el haber obtenido las medidas de propagación en el metro junto a José Antonio. Quiero agradecer también a Tomás su ayuda en la interpretación y adaptación de estas medidas a las necesidades del simulador.

La paciencia de Tiago con mis constantes consultas e interrupciones ha sido de gran ayuda, sobre todo en mis inicios en el grupo. No me puedo olvidar del apoyo recibido y de los buenos momentos durante las comidas en el campus con José, Néstor, Tiago y Pedro. También quiero darle las gracias a Paula, que siempre ha estado ahí para echarme una mano cuando lo necesitaba.

Tampoco me puedo olvidar de los buenos ratos pasados en los descansos (y otros eventos sociales) junto a todos los compañeros del GTEC que he ido conociendo durante estos años: Adriano, Aida, Belén, Darian, Diego, Fran Laport, Héctor, Ismael, Iván, Javi, José Francisco, Josmary, Manuel, Marc, Óscar Blanco, Óscar Fresnedo, Santi, Sonia y Valentín. Asimismo, quiero mencionar al resto de profesores del GTEC que he tenido el placer de conocer: Adriana, Carlos, Dani, Fran, José Juan Lamas, Julio, Paula Castro y Roberto. También quiero agradecer a Cris toda la ayuda prestada con el papeleo de la Universidad.

Además, me gustaría agradecer a Antonio J. Rodríguez que me permitiera participar en su investigación sobre la aceleración con FPGAs de las simulaciones de modelos multicuerpo.

Por último, dedico esta tesis a mi familia y amigos, especialmente a mis padres y hermano, que siempre me han dado ánimos para terminarla, y a Maryem, que ha estado a mi lado ayudándome durante todo este tiempo.

Resumo

Os sistemas de comunicación sen fíos de cuarta e quinta xeración (4G e 5G) utilizan unha capa física (PHY) baseada en modulacións multiportadora para a transmisión de datos cun gran ancho de banda. Este tipo de modulacións proporcionan unha alta eficiencia espectral á vez que permiten corrixir de forma sinxela os efectos da canle radio.

Estes sistemas utilizan OFDMA como mecanismo para a repartición dos recursos radio dispoñibles entre os diferentes usuarios. Este repartimento realízase asignando un subconxunto de subportadoras a cada usuario nun instante de tempo determinado. Isto aporta unha gran flexibilidade ó sistema que lle permite adaptarse tanto ós requisitos de calidade de servizo dos usuarios como ó estado da canle radio.

A capa de acceso ó medio (MAC) destes sistemas encárgase de configurar os diversos parámetros proporcionados pola capa física OFDMA, ademais de xestionar os diversos fluxos de información de cada usuario, transformando os paquetes de capas superiores en paquetes da capa física.

Neste traballo estúdase o deseño e implementación das capas MAC e PHY de sistemas de comunicación 4G ademais da súa aplicabilidade en sistemas de transporte ferroviarios.

Por unha parte, abórdase o deseño e implementación en tempo real do estándar WiMAX. Estúdanse os mecanismos necesarios para establecer comunicacións bidireccionais entre unha estación base e múltiples dispositivos móbiles. Ademais, estúdase como realizar esta implementación nunha arquitectura hardware baseada en DSPs e FPGAs, na que se implementan as capas MAC e PHY. Dado que esta arquitectura ten uns recursos computacionais limitados, tamén se estudan as necesidades de cada módulo do sistema para poder garantir o funcionamento en tempo real do sistema completo.

Por outra parte, tamén se estuda a aplicabilidade dos sistemas 4G a sistemas de transporte públicos. Os sistemas de comunicacións e sinalización son unha parte vital para os sistemas de transporte ferroviario e metro. As comunicacións sen fíos utilizadas por estes sistemas deben ser robustas e proporcionar unha alta fiabilidade para permitir a supervisión, control e seguridade do tráfico ferroviario.

Para levar a cabo esta avaliación de viabilidade realízanse simulacións de redes de comunicacións LTE en contornos de transporte ferroviarios, comprobando o cumprimento dos requisitos de fiabilidade e seguridade. Realízanse diferentes simulacións do sistema de comunicacións para poder ser avaliadas e seleccionar a configuración e arquitectura do sistema máis axeitada en función do escenario considerado. Tamén se efectúan simulacións de redes baseadas en Wi-Fi, dado que é a solución máis utilizada nos metros, para confrontar os resultados cos obtidos para LTE.

Para que os resultados das simulacións sexan realistas débense empregar modelos de propagación radio axeitados. Nas simulacións utilízanse tanto modelos deterministas como modelos baseados nos resultados de campañas de medida realizadas nestes escenarios.

Nas simulacións empréganse os diferentes fluxos de información destes escenarios para comprobar que se cumpren os requisitos de calidade de servicio (QoS). Por exemplo, os fluxos críticos para o control ferroviario, como European Train Control System (ETCS) ou Communication-Based Train Control

(CBTC), necesitan unha alta fiabilidade e un retardo mínimo nas comunicacións para garantir o correcto funcionamento do sistema.

Resumen

Los sistemas de comunicación inalámbricos de cuarta y quinta generación (4G y 5G) utilizan una capa física (PHY) basada en modulaciones multiportadora para la transmisión de datos con un gran ancho de banda. Este tipo de modulaciones han demostrado tener una alta eficiencia espectral a la vez que permiten corregir de forma sencilla los efectos del canal radio.

Estos sistemas utilizan OFDMA como mecanismo para el reparto de los recursos radio disponibles entre los diferentes usuarios. Este reparto se realiza asignando un subconjunto de subportadoras a cada usuario en un instante de tiempo determinado. Esto aporta una gran flexibilidad al sistema que le permite adaptarse tanto a los requisitos de calidad de servicio de los usuarios como al estado del canal radio.

La capa de acceso al medio (MAC) de estos sistemas se encarga de configurar los diversos parámetros proporcionados por la capa física OFDMA, además de gestionar los diversos flujos de información de cada usuario, transformando los paquetes de capas superiores en paquetes de la capa física.

En este trabajo se estudia el diseño e implementación de las capas MAC y PHY de sistemas de comunicación 4G además de su aplicabilidad en sistemas de transporte ferroviarios.

Por una parte, se aborda el diseño e implementación en tiempo real del estándar WiMAX. Se estudian los mecanismos necesarios para establecer comunicaciones bidireccionales entre una estación base y múltiples dispositivos móviles. Además, se estudia cómo realizar esta implementación en una arquitectura hardware basada en DSPs y FPGAs, en la que se implementan las capas MAC y PHY. Dado que esta arquitectura tiene unos recursos computacionales limitados, también se estudian las necesidades de cada módulo del sistema para poder garantizar el funcionamiento en tiempo real del sistema completo.

Por otra parte, también se estudia la aplicabilidad de los sistemas 4G a sistemas de transporte públicos. Los sistemas de comunicaciones y señalización son una parte vital para los sistemas de transporte ferroviario y metro. Las comunicaciones inalámbricas utilizadas por estos sistemas deben ser robustas y proporcionar una alta fiabilidad para permitir la supervisión, control y seguridad del tráfico ferroviario.

Para llevar a cabo esta evaluación de viabilidad se realizan simulaciones de redes de comunicaciones LTE en entornos de transporte ferroviarios, comprobando si se cumplen los requisitos de fiabilidad y seguridad. Se realizan diferentes simulaciones del sistema de comunicaciones para poder ser evaluados y seleccionar la configuración y arquitectura del sistema más adecuada en función del escenario planteado. También se efectúan simulaciones de redes basadas en Wi-Fi, dado que es la solución más utilizada en los metros, para comparar los resultados con los obtenidos para LTE.

Para que los resultados de las simulaciones sean realistas se deben utilizar modelos de propagación radio apropiados. En las simulaciones se utilizan tanto modelos deterministas como modelos basados en los resultados de campañas de medida realizadas en estos escenarios.

En las simulaciones se utilizan los diferentes flujos de información de estos escenarios para comprobar que se cumplen sus requisitos de calidad de servicio. Por ejemplo, los flujos críticos para

el control ferroviario, como European Train Control System (ETCS) o Communication-Based Train Control (CBTC), necesitan una alta fiabilidad y un retardo bajo en las comunicaciones para garantizar el correcto funcionamiento del sistema.

Abstract

The fourth and fifth generation wireless communication systems (4G and 5G) use a physical layer (PHY) based on multicarrier modulations for data transmission using high bandwidth. This type of modulations has shown to provide high spectral efficiency while allowing low complexity radio channel equalization.

These systems use OFDMA as a mechanism for distributing the available radio resources among different users. This allocation is done by assigning a subset of subcarriers to each user in a given instant of time. This provides great flexibility to the system that allows it to adapt to both the quality of service requirements of users and the radio channel state.

The media access layer (MAC) of these systems is in charge of configuring the multiple OFDMA PHY layer parameters, in addition to managing the data flows of each user, transforming the higher layer packets into PHY layer packets.

This work studies the design and implementation of MAC and PHY layers of 4G communication systems as well as their applicability in rail transport systems.

On the one hand, the design and implementation in real time of the WiMAX standard is addressed. The required mechanisms to establish bidirectional communications between a base station and several mobile devices are also evaluated. Moreover, a MAC layer and PHY layer implementation is presented, using a hardware architecture based in DSPs and FPGAs. Since this architecture has limited computational resources, the requirements of each processing block of the system are also studied in order to guarantee the real time operation of the complete system.

On the other hand, the applicability of 4G systems to public transportation systems is also studied. Communications and signaling systems are a vital part of rail and metro transport systems. The wireless communications used by these systems must be robust and provide high reliability to enable the supervision, control and safety of rail traffic.

To carry out this feasibility assessment, LTE communications network simulations are performed in rail transport environments to verify that reliability and safety requirements are met. Several simulations are carried out in order to evaluate the system performance and select the most appropriate system configuration in each case. Simulations of Wi-Fi based networks are also carried out, since it is the most used solution in subways, to compare the results with those obtained for LTE.

To perform the simulations correctly, appropriate radio propagation models must be used. Both deterministic models and models based on the results of measurement campaigns in these scenarios are used in the simulations.

The simulations use the different information flows present in the railway transportation systems to verify that its quality of service requirements are met. For example, critical flows for railway control, such as the European Train Control System (ETCS) or Communication-Based Train Control (CBTC), require high reliability and low delay communications to ensure the proper functioning of the system.

Table of Contents

List of Figures

List of Tables

Chapter I

Introduction

Wireless communications systems have greatly evolved since the emergence of the first generation of wireless cellular technology in the 80s. The following generations provided a huge increase in data rates, spectral efficiency, security, and coverage. The last 4G and 5G generations use multicarrier modulations given their high spectral efficiency, simple channel equalization and flexible multiple access schemes. The well-known and widely adopted orthogonal frequency-division multiplexing (OFDM) modulation with cyclic prefix (CP) has been selected because of its multiple advantages such as low implementation complexity thanks to the fast Fourier transform (FFT) algorithm [ZAI+16]. The orthogonal frequency-division multiple access (OFDMA) scheme is also used in these wireless communication standards to provide flexibility in the radio resource sharing between users with high spectral efficiency.

Worldwide Interoperability for Microwave Access (WiMAX) is the commercial name adopted for the IEEE 802.16 wireless communication standards. This was one of the competing technologies to be selected as the 4G mobile communication standard. Although Long Term Evolution (LTE) finally became the world's 4G standard, Mobile WiMAX is a similar technology based on an OFDMA physical layer (PHY) and a connection-oriented medium access control layer (MAC) with good quality of service (QoS) support. WiMAX is still being used for broadband wireless access (BWA) and in some specific environments such as airport surface communications (known as AeroMACS).

Real-time transceiver prototyping is an important tool for testing and verifying system performance under real-world conditions. The use of testbeds is a less expensive alternative than developing a prototype, but the hardware restrictions to achieve real-time operation are not considered in the implementation and algorithm selection. Prototype development requires to consider the usage of alternative low-complexity algorithms to avoid processing bottlenecks and obtain an efficient and realistic implementation. The obtained prototype allows for evaluating the total performance loss of the combined low-complexity algorithms in realistic environments.

The implementation of digital radio communication systems is usually carried out in dedicated chips or application-specific integrated circuits (ASICs) to minimize the power requirements of the device. These implementations are very efficient, but lack the flexibility

needed to support new waveforms or protocols. Software-defined radio (SDR) systems try to minimize the dedicated hardware components in transceivers and substitute them by software modules running in more general processors such as digital signal processors (DSPs). This idea was popularized by Joseph Mitola III [MIT92; MIT95; MIT99] in the 90s and has gained interest in military and research environments as well as in commercial deployments, thanks to the great increase in computing power of microprocessors and the advances in heterogeneous computing.

Over the last decades, the railway industry has been evolving their conventional signaling systems to communication-based systems demanding reliable and fault-tolerant infrastructures. The European Rail Traffic Management System (ERTMS) was adopted in all European countries for mainline railway operations using GSM for Railways (GSM-R) as the radio transmission technology. Other example of these modern communication-based signaling systems is the communications-based train control (CBTC) standard, which is usually used in subway and urban rail transport to provide high-resolution train location determination and continuous train-to-wayside data communications. CBTC allows for reducing the distance between trains, increasing the line capacity. CBTC systems are usually deployed using proprietary solutions based on IEEE 802.11 (Wi-Fi) technology for radio communications.

In this thesis we focus on subway environments where there are many other services that demand wireless connectivity such as video surveillance or passenger information. Separate radio technologies are usually considered to provide these additional services (e.g., Terrestrial Trunked Radio (TETRA) for public safety) which results in increased costs due to the deployment and maintenance of several network infrastructures. Using only one modern wireless technology for all the services would reduce operational costs and would simplify the installation of new applications. This common wireless communication system should support all the different QoS requirements of these applications, specially the mission critical ones. The Wi-Fi networks used for CBTC include several proprietary modifications to adapt the 802.11 standard to the railway environment needs. These enhancements usually focus on using a fast handover method to support the high mobility of the trains, providing better QoS mechanisms and security. However, Wi-Fi still has problems with the limited transmission range and with potential interference as it uses unlicensed frequency bands. In fact, after some incidents with interference in the 2.4 GHz band in Chinese subways, China authorities forced the use of LTE instead of Wi-Fi for new deployments of CBTC in 2014, assigning the 1.8 GHz band to subway operators.

LTE and its 5G evolution has gained several interest for railway applications. GSM-R will be replaced by the International Union of Railways (UIC) Future Railway Mobile Communication System (FRMCS) which is included in the latest 5G standards (3GPP releases 15 and 16). The 3rd Generation Partnership Project (3GPP) has also included public safety features into LTE to replace TETRA. CBTC is also being deployed using LTE in countries which provide a licensed band for subway operators such as China and Australia. LTE is better

suited for subway environments than Wi-Fi as it provides better mobility support and QoS mechanisms with higher spectral efficiency and range. The major problem for LTE adoption in subways is the need to use licensed bands, requiring an agreement between subway operator and the owner of the licensed band rights.

Radio communication deployments in subways require a great effort in planning and conducting measurement campaigns to ensure the coverage along the entire line. Radiating cable ("leaky feeder") or distributed antennas can be used to provide radio coverage in tunnels. Although radiating cable solutions provide more stable coverage, distributed antennas solutions are preferred because of their lower cost. However, radio planning is more complex with antennas. Several factors affect radio propagation inside tunnels such as its dimensions and shape, position of antennas, operating frequency, size of the trains, etc. Measurement campaigns should be performed before a deployment [TOL15] to correctly adjust the used channel model and predict the coverage in the tunnel with accuracy. It is also important to perform network simulations in order to evaluate the performance and prevent possible problems.

Network simulators are very useful to validate, optimize and test the efficiency and performance of networks under different scenarios and configurations. They allow for studying the expected network behavior in complex environments where it is very difficult to conduct real tests. For this reason, modeling and simulating subway network deployments is very useful as it helps in the network planning and the parameter configuration. However, there are some common pitfalls that should be avoided such as using unrealistic or unverified models with excessive simplifications [SUÁ+15a]. The subway simulations should use verified communication models with adapted and accurate mobility and channel models. In this way, the simulation results will allow for assessing the feasibility of the network planning with the selected technology.

1.1 Thesis Overview

This work studies the design and implementation of MAC and PHY layers of a 4G communication system (Mobile WiMAX) using an SDR architecture made up of DSPs and field programmable gate arrays (FPGAs). The applicability of 4G (LTE) in rail transport systems is also evaluated by using a system-level network simulator customized for subway environments.

Chapter 2 describes the most relevant characteristics of Mobile WiMAX MAC and PHY layers. The chapter focus on the mandatory features of the IEEE 802.16e standard that need to be implemented in a Mobile WiMAX transceiver.

Chapter 3 presents the design and real-time implementation of Mobile WiMAX transceivers. The MAC and PHY layers of the mobile and the base stations are implemented allowing real-time bidirectional communications using time-division duplexing (TDD). A performance evaluation of the transceivers is also carried out using a channel emulator and the scenarios recommended by the WiMAX Forum.

Chapter 4 evaluates the suitability of different communication technologies for subway environments. LTE and Wi-Fi deployments are simulated using tunnel propagation channels based on deterministic models and real channel measurements. The ns-3 network simulator is enhanced to match the subway scenario conditions. The results of a measurement campaign are used to perform realistic simulations in that scenario. The developed deterministic channel model combines several works found in the literature allowing the definition of complex scenarios. This channel model is used to perform simulations on the same subway line with different technologies and deployments.

1.2 Contributions

The work presented in this thesis led to the co-authored publications listed in Sections 1.2.1 and 1.2.2. During the research of this thesis, the author also collaborated in the research projects described in Section 1.2.3.

1.2.1 Journal Papers

1. Ángel Carro-Lagoa, Pedro Suárez-Casal, José A. García-Naya, Paula Fraga-Lamas, Luis Castedo, and Antonio Morales-Méndez. "**Design and implementation of an OFDMA-TDD physical layer for WiMAX applications**". *EURASIP Journal on Wireless Communications and Networking*, vol. 2013, no. 1, 2013, p. 243. ISSN: 1687-1499. DOI: 10.1186/1687-1499-2013-243
2. Pedro Suárez-Casal, Ángel Carro-Lagoa, José A. García-Naya, Paula Fraga-Lamas, Luis Castedo, and Antonio Morales-Méndez. "**A real-time implementation of the Mobile WiMAX ARQ and physical layer**". *Journal of Signal Processing Systems*, vol. 78, no. 3, 2015, pp. 283–297. ISSN: 1939-8115. DOI: 10.1007/s11265-014-0890-3
3. Antonio J. Rodríguez, Roland Pastorino, Ángel Carro-Lagoa, Karl Janssens, and Miguel Á. Naya. "**Hardware acceleration of multibody simulations for real-time embedded applications**". *Multibody System Dynamics*, 2020, pp. 1–19. DOI: 10.1007/s11044-020-09738-w

1.2.2 International Conference Papers

1. Pedro Suárez-Casal, Ángel Carro-Lagoa, José A. García-Naya, and Luis Castedo. "**A Multicore SDR Architecture for Reconfigurable WiMAX Downlink**". *Proc. of 13th Euromicro Conference on Digital System Design: Architectures, Methods and Tools (DSD), 2010.* 2010, pp. 801–804. DOI: 10.1109/DSD.2010.108

2. Ángel Carro-Lagoa, Pedro Suárez-Casal, P. Fraga-Lamas, J. A. García-Naya, L. Castedo, and A. Morales-Méndez. "**Real-Time Validation of a SDR Implementation of TDD WiMAX Standard**". *Proc. of 2013 Wireless Innovation Forum European Conference on Communications Technologies and Software Defined Radio (SDR-WInnComm-Europe 2013)*. 2013
3. José Rodríguez-Piñeiro, José A. García-Naya, Ángel Carro-Lagoa, and Luis Castedo. "**A testbed for evaluating LTE in high-speed trains**". *Proc. of 16th Euromicro Conference on Digital System Design (DSD 2013)*. 2013, pp. 175–182.
DOI: 10.1109/DSD.2013.27
4. Ángel Carro-Lagoa, Tomás Domínguez-Bolaño, José Rodríguez-Piñeiro, Miguel González-López, and José A. García-Naya. "**Feasibility of LTE for train control in subway environments based on experimental data**". *Proc. of 2019 27th European Signal Processing Conference (EUSIPCO)*. 2019, pp. 1–5.
DOI: 10.23919/EUSIPCO.2019.8903070

1.2.3 Research Projects

The work performed in this thesis contributed to the following projects:

- SeaMAX (2007-2009): The aim of this project was to study of the feasibility of WiMAX technology in coastal maritime environments. A real-time channel emulator was developed on an FPGA-based development kit. This channel emulator was configured to test Fixed WiMAX equipment in coastal maritime environments.
  - Funding entity: Wireless Galicia.
  - Funding: €31 625.
  - Duration: 1 year and 11 months.
- MoWi (2008-2011): This project was funded by Indra Sistemas S.A. to design and implement a Mobile WiMAX prototype. The project was performed in three phases. First, the PHY layer was implemented in FPGAs and DSPs. Then, the prototype was modified with tactical countermeasures to support military scenarios. Finally, the MAC layer was partially implemented.
- GNUTEST (2010-2013): In this project, the GNU Radio toolkit and the Ettus USRP hardware were tested for several applications. One of the applications was the transmission and reception of Mobile WiMAX signals.
  - Reference: 10TIC003CT.
  - Funding entity: Galician Economy and Industry Department, Xunta de Galicia.
  - Funding: €123 343.25.
  - Duration: 3 years.
- TECRAIL (2011-2014): This project was aimed at adapting IP-based 4G technologies for railway environments, centering on railway signaling, automated driving, on-board

communications, and train-to-ground communications. Several simulations with Mobile WiMAX signals were performed to test the effects of high-speed environments in the decoding of OFDM signals. Also, a testbed based on Ettus USRP devices was developed for performing measurement campaigns on railway environments, focusing on the generation and processing of LTE signals.
  - Reference: IPT-2011-1034-370000.
  - Funding entity: Ministry of Science and Innovation, Government of Spain.
  - Funding: €245 791.
  - Duration: 3 years and 3 months.
- INRA-CBTC (2018-2021): The project is intended to develop a set of tools for the validation of an LTE network specifically adapted to the railway environment. These tools evaluate the fulfillment of the CBTC requirements by measuring the performance of the deployed network in terms of PER, delay, and jitter.
  - Funding entity: CAF Signalling S.L. and the CDTI entity of the Spanish Ministry of Science and Innovation.
  - Funding: €262 487.86.
  - Duration: 2 years and 7 months.

The author also participated in the following projects related with other topics:

- CIUDAD2020 (2011-2014): The objective of this project was to develop new citizen-oriented services in areas such as energy, transportation, and environmental control. We focused on the information and communications architecture that should integrate the different services. This architecture was based on an Enterprise Service Bus (ESB).
  - Reference: IPT-20111006.
  - Funding entity: ATOS Origin and the CDTI entity of the Spanish Ministry of Science and Innovation.
  - Funding: €120 000.
  - Duration: 3 years and 3 months.
- SmartMonitor (2013-2014): This project was focused on developing a monitoring data collection system for enterprise infrastructure management and monitoring. A distributed system was developed in two phases to provide fault-tolerant, reliable and scalable data collection. The system supports several communication protocols to monitor and perform actions on the enterprise infrastructure.
- SmartPort Coruña and Smart VIPort (2015-2016): The aim of these projects was to adapt and evolve the monitoring system to the ports of A Coruña and Vigo, Spain. Furthermore, the integration of several systems involved in port operations was addressed.
- PortsPlatform (2018-2019): This project was focused on the improvement and customization of the monitoring system to the environment of several ports of Spain.
- Navantia-UDC "The Shipyard of the Future" (2015-2021): This project is carried out by the mixed research unit Navantia-UDC in two phases. One research line is the integrated

services system, which aims to integrate several communications and services inside the vessel with a common infrastructure. We are focused on providing location services for the crew members using computer vision and deep learning techniques.

- References: IN853A 2015/01 and IN853B 2018/02.
- Funding entity: Galician Innovation Agency (GAIN), Xunta de Galicia.
- Funding: €387 435.31 and €99 707.45.
- Duration: 7 years.

Chapter II

OFDMA based PHY and MAC Layers – Mobile WiMAX

Wireless communications systems have to cope with various physical phenomena that the electromagnetic signal experiences as it propagates. Typical effects of wireless channels are propagation losses, multipath, fading, doppler, and interference.

Multi-carrier systems make it possible to combat these effects efficiently. Specifically, orthogonal frequency-division multiplexing (OFDM) is the basis for various communication standards focused on cellular mobile communications or wireless local area networks. Orthogonal frequency division multiple access (OFDMA) is a very flexible scheme based on OFDM that modern communication systems use to share the radio spectrum between multiple users.

This chapter shows the mechanisms that need to be implemented in physical and medium access layers (PHY and MAC) of OFDMA based systems. Mobile WiMAX standard is used as reference.

This chapter is based on the following co-authored publications:

- Ángel Carro-Lagoa, Pedro Suárez-Casal, José A. García-Naya, Paula Fraga-Lamas, Luis Castedo, and Antonio Morales-Méndez. "**Design and implementation of an OFDMA-TDD physical layer for WiMAX applications**". *EURASIP Journal on Wireless Communications and Networking*, vol. 2013, no. 1, 2013, p. 243. ISSN: 1687-1499. DOI: 10.1186/1687-1499-2013-243
- Pedro Suárez-Casal, Ángel Carro-Lagoa, José A. García-Naya, Paula Fraga-Lamas, Luis Castedo, and Antonio Morales-Méndez. "**A real-time implementation of the Mobile WiMAX ARQ and physical layer**". *Journal of Signal Processing Systems*, vol. 78, no. 3, 2015, pp. 283–297. ISSN: 1939-8115. DOI: 10.1007/s11265-014-0890-3

This chapter is structured as follows. Section 2.1 introduces WiMAX and 802.16 standards. Sections 2.2 and 2.3 describe the OFDMA-TDD Mobile WiMAX PHY and MAC layers. Section 2.4 shows the changes and enhancements introduced by the WiMAX Advanced Air

Interface. Finally, Section 2.5 presents the concluding remarks.

2.1 Mobile WiMAX

Worldwide Interoperability for Microwave Access (WiMAX) is a wireless communication standard developed to provide broadband wireless access (BWA) over large distances. The term WiMAX was adopted by the WiMAX Forum, an organization created to promote the interoperability between the IEEE 802.16 family of wireless communication standards.

In late 90s, IEEE started the working group IEEE 802.16 to create a point-to-multipoint (PMP) air interface alternative to cable and digital subscriber lines. The original standard was modified to produce the IEEE 802.16d standard for fixed applications [IEE04b]. IEEE 802.16d uses OFDM with time division multiple access (TDMA) as the transmission scheme. In 2005, mobility support was incorporated based on scalable OFDMA (SOFDMA), resulting in the amendment 802.16e [IEE06], also known as Mobile WiMAX. Four years later, the standard IEEE 802.16-2009 [IEE09] was released to support both fixed and mobile wireless communications. A complete survey of the historical evolution of the standard up to 2010 can be found in [PAR+12].

In 2011, WiMAX evolved to 802.16m [IEE11], which focuses on providing an advanced air interface to fulfill the requirements of IMT-Advanced while maintaining backward compatibility with existing specifications. In 2012, the standard was split in two versions:

Air Interface for BWA Standard 802.16-2012 [IEE12a] consolidates material from 802.16j-2009 for relay-based networks and the amendment 802.16h-2010, which implements coexistence enhancement for license-exempt operation. Finally, 802.16-2017 [IEE18] was released including several enhancements: support for machine-to-machine (M2M) applications, higher reliability networks, multi-tier networks and operation with channel bandwidth from 100 kHz up to 1.25 MHz.

WirelessMAN-Advanced Air Interface for BWA
Standard 802.16.1-2012 [IEE12b] specifies the enhanced air interface designated as "IMT-Advanced" by the ITU-R consolidating the 802.16m amendment. The 802.16.1b-2012 [IEE12c] and 802.16.1a-2013 [IEE13] ammendments were published to add support for M2M applications and higher reliability networks, respectively.

Together with Long Term Evolution (LTE), WiMAX was one of the competing radio access technologies to be used by the fourth generation (4G) of mobile communication systems. Although LTE finally became the world's 4G standard, WiMAX is an interesting modern wireless communication system to be studied. This chapter will focus on IEEE 802.16e (Mobile WiMAX) from now on. The most salient technical features of Mobile WiMAX are:

Scalable OFDMA PHY Mobile WiMAX PHY layer architecture allows for easily scaling bandwidth and throughput. The OFDMA PHY chooses the fast Fourier transform (FFT) size based on the available bandwidth so subcarrier spacing is constant. Also, the use of

OFDM modulation provides resiliency to multipath propagation and allows for operating in non-line-of-sight (NLoS) conditions.

TDD and FDD support The IEEE standards support both time-division duplexing (TDD) and frequency-division duplexing (FDD) modes. The initial release of Mobile WiMAX only included TDD profiles. FDD profiles were added by the WiMAX Forum in release 1.5. However, all existing WiMAX deployments only use TDD.

High throughput As an example, the OFDMA-PHY in SISO TDD mode using 10 MHz bandwidth and 64-QAM 3/4 can provide up to 14.9 Mbit/s in DL and 11.6 Mbit/s in UL with a 26:21 downlink-to-uplink rate. Better results can be obtained using the FDD mode, higher bandwidth and multiple-antenna techniques.

AMC and dynamic resource allocation WiMAX supports several modulations and coding schemes which can be selected for each user in each frame, based on channel conditions. Resource assignment in uplink (UL) and downlink (DL) is controlled by a scheduler at the base station. The standard allows for the allocation of available resources in time and frequency, and has flexible mechanisms for transmitting resource allocation information frame by frame. In addition, resources can be allocated in the space domain when optional adaptive antenna systems (AASs) are used.

Mobility Mobile WiMAX supports hard and soft handover so applications such as VoIP can work seamlessly. The system also integrates energy-saving mechanisms to extend the battery life of mobile station (MS) devices.

Reliability Automatic repeat request (ARQ) is supported in MAC layer to increase connection reliability. WiMAX also supports hybrid automatic repeat request (HARQ), which is an effective combination of forward error correction (FEC) and ARQ.

QoS WiMAX defines five quality of service (QoS) classes to support several application types.

Security WiMAX MAC layer contains a security sublayer that supports robust security algorithms such as EAP-based authentication, AES-CCM encryption, and CMAC and HMAC message authentication.

WiMAX PHY is in charge of multiplexing user and system data together with control signaling in order to ensure a proper utilization of the radio resources. The WiMAX physical layer specifies how to map and how to allocate those resources as either reference signals or to form various physical channels. IEEE 802.16 specifications define three different PHY layers: single-carrier (SC) transmission, OFDM, and OFDMA. Among them OFDMA is the most attractive given its flexibility and ability to support multiple users at the same time. OFDMA is based on OFDM modulation and allows a WiMAX base stations (BSs) to divide the available subcarriers into subchannels that can be assigned to different users. OFDMA enables a large flexibility in the radio interface since users can be assigned different bandwidths, time durations and modulation orders according to their demanded QoS and the available bandwidth.

There exist two basic methods to achieve two-way communication in a wireless communication system: FDD and TDD. The FDD technique has been preferred by the first

Table 2.1: Mobile WiMAX profiles.

WiMAX Profile	Channel Bandwidth	Sampling Frequency	FFT Size	Subcarrier Spacing
# 1	3.5 MHz	4 MHz	512	7.81 kHz
# 2	5 MHz	5.6 MHz	512	10.94 kHz
# 3	7 MHz	8 MHz	1024	7.81 kHz
# 4	8.75 MHz	10 MHz	1024	9.77 kHz
# 5	10 MHz	11.2 MHz	1024	10.94 kHz

generation of wireless systems mainly optimized for symmetric voice traffic. However, with the advent of high-speed data services, TDD is more flexible supporting variable and asymmetric data traffic. WiMAX specifies both FDD as well as TDD operating modes. In addition, only TDD offers an efficient and flexible support for the ad-hoc and multihop communication scenarios considered in 802.16-2012.

2.2 802.16e OFDMA PHY Layer

This section describes the primary features of the Mobile WiMAX PHY. For a more detailed description see [NUA07], [YAN10] or [IEE09, Chapter 8.4].

Mobile WiMAX is based on the OFDMA physical layer defined in the IEEE 802.16e standard. It supports both TDD and FDD operation modes while allowing for variable bandwidth and a scalable number of subcarriers ranging from 128 to 2048. Furthermore, the WiMAX Forum specifies five mandatory profiles for interoperability as shown in Table 2.1. Such profiles combine different FFT sizes, bandwidths, and sampling frequencies. Note that profiles #3 and #5 are scaled versions of #1 and #2, respectively, as they maintain the same subcarrier frequency spacing but use more bandwidth. Also, the difference between channel bandwidth and sampling frequency is because the edge subcarriers are not used (guard tones) to allow for adequate RF filtering and to avoid interfering contiguous channels.

Fig. 2.1 shows the basic building blocks of an IEEE 802.16e transmitter. The main blocks are channel coding, subchannelization and the final OFDM modulator with the inverse fast Fourier transform (IFFT) and the cyclic prefix addition. Channel coding transforms data bits into constellation symbols (e.g., QPSK) with the required redundancy. The subchannelization block generates the frames in frequency domain by placing the data, pilot and preamble symbols in their assigned places following the frame structure. Data and pilot subcarriers transmitted in either the uplink or the downlink go through a process of scrambling (*subcarrier randomization*) just before the IFFT operation, and then a cyclic prefix (CP) is appended at its output. The size

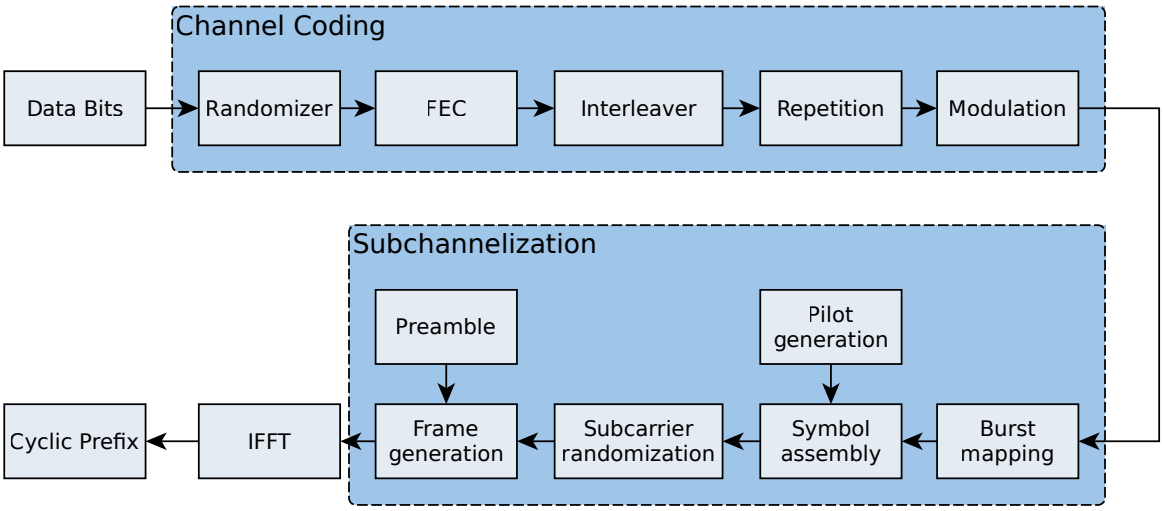

Figure 2.1: Block diagram of an IEEE Std 802.16e transmitter.

of this CP is defined as a ratio of the FFT size and can be variable, being valid values 1/4, 1/8, 1/16, and 1/32, although the WiMAX Forum only requires the support of the 1/8 value.

2.2.1 TDD Frame Structure

OFDMA is a multi-user version of OFDM to allow users to transmit and receive data simultaneously. This is done by distributing groups of subcarriers at different times among users. These subsets of subcarriers are called subchannels and are dynamically assigned to users (or groups of users) according to their needs. Other basic terms are defined in the standard to specify the frame structure:

Frame The largest structure at the PHY with a fixed duration. The TDD frames contain both an UL subframe and a DL subframe.

Permutation zone A set of adjacent OFDM symbols in which a particular method of subcarrier assignment and structuring is used. The DL or UL subframes can contain more than one permutation zone.

Slot The slot unit is the minimum possible data allocation unit and it is used to specify the data time-frequency regions of the bursts. Depending on the permutation scheme used, a slot is defined in a different way although it always encompasses 48 data subcarriers.

Data region A set of slots defined by a two-dimensional allocation of several adjacent subchannels in a group of contiguous OFDMA symbols.

Burst The data assigned to one or more users mapped into one data region. The allocated slots use the same modulation and coding configuration.

Segment A subdivision of the available OFDMA subchannels (that may include all available subchannels). The segments can be assigned to sectors, facilitating the use of frequency reuse techniques.

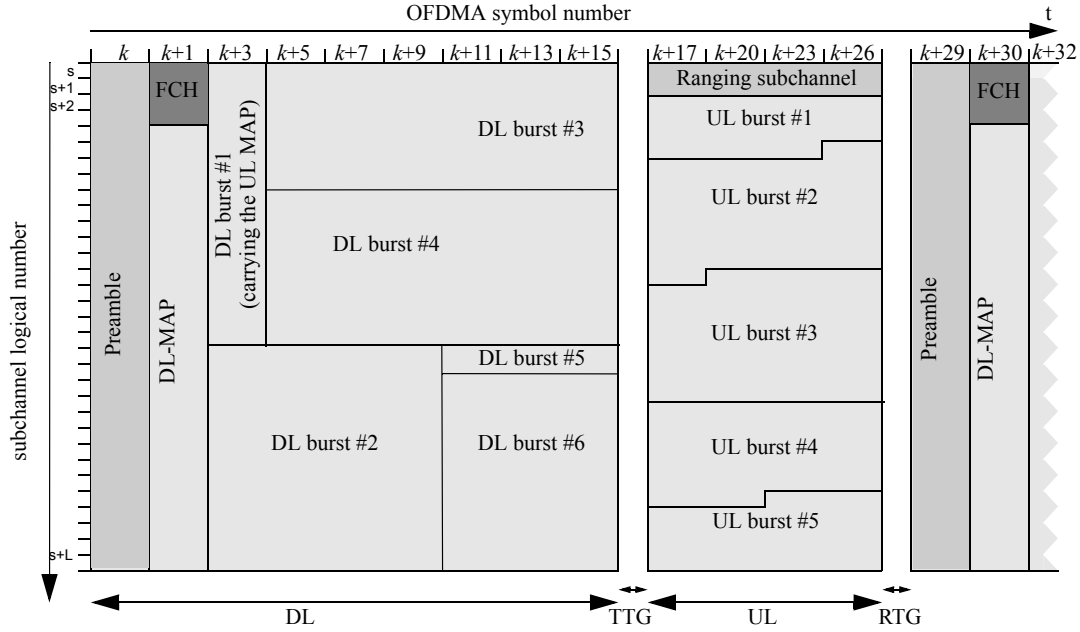

Figure 2.2: TDD frame structure example ©2009 IEEE [IEE09].

Fig. 2.2 shows an example of a Mobile WiMAX TDD frame. Each frame contains one DL subframe and one UL subframe. The first symbol in the DL subframe is a preamble symbol whose subcarriers are chosen from a predefined set. The first two symbols after the preamble are reserved to send the frame control header (FCH) and downlink map (DL-MAP) messages, which describe the mapping of the bursts inside the downlink subframe. If an uplink map (UL-MAP) message is sent to set the uplink configuration, it should be transmitted on the first burst defined in the DL-MAP.

The 802.16e standard allows to use several frame sizes, but the WiMAX Forum only specifies the 5 ms frame size as mandatory. The transmit/receive transition gap (TTG) and receive/transmit transition gap (RTG) values are set according to the 5 ms frame duration and depend on the used WiMAX profile. Also note that the total number of OFDM symbols (DL and UL) in a frame also depends on each profile: 47 symbols for 10 and 5 MHz profiles, 42 for 8.75 MHz, and 33 for 7 and 3.5 MHz. The downlink-to-uplink ratio can vary from 3:1 to almost 1:1.

Uplink resources are shared among MSs, and their allocation and scheduling is centralized on the BS. The latter decides how many slots are assigned to each MS depending on their QoS parameters and bandwidth requirements. Additionally, ranging regions can be defined in the uplink to allow MSs to perform network entry, improve uplink synchronization parameters, or send special feedback messages, among other tasks.

As shown in Fig. 2.2, the time-frequency shape of data regions is different in DL and UL. In DL, the data regions are rectangular, being defined by the number of subchannels and OFDMA symbols they occupy. In UL, only the number of slots is needed to define each data region. They are reserved first in the time axis, using all the available OFDMA symbols of a subchannel

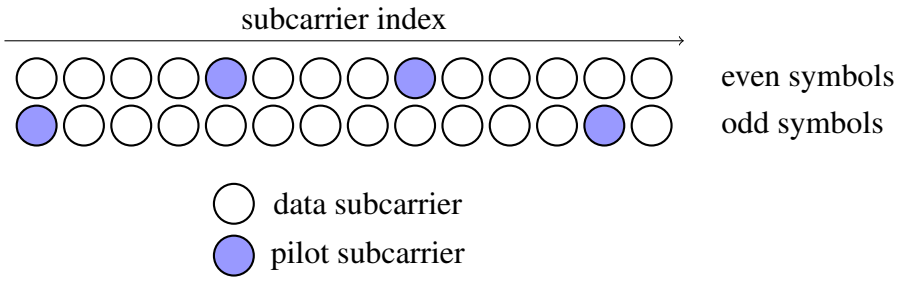

Figure 2.3: DL PUSC cluster structure.

before using the next subchannel. However, the UL ranging regions are rectangular. Finally, the data mapping on data regions is performed in the frequency axis, first filling all the subchannels of one OFDMA symbol before using the next symbol.

The standard defines different OFDMA symbol structures that can be used in the permutation zones: partial usage of subchannels (PUSC), full usage of subchannels (FUSC), optional PUSC, optional FUSC, tile usage of subchannels (TUSC), and adaptive modulation and coding (AMC). With the exception of AMC, all symbol structures are distributed subcarrier permutations where the subcarriers of each subchannel are distributed over all available bandwidth. The main advantage of these permutations is the frequency diversity and the interference averaging between adjacent sectors or cells. The AMC mode uses a contiguous subcarrier permutation that allows for the choice of the best frequencies for each user.

According to the WiMAX Forum, only the PUSC symbol structure is mandatory as the DL shall contain one PUSC permutation zone at the beginning of the frame.

2.2.1.1 Downlink PUSC

The downlink PUSC symbol structure uses pilot, data and guard subcarriers. Each OFDMA symbol is divided into clusters, which are sets of pilot and data carriers. A different cluster structure is defined depending on whether the symbol is odd or even as shown in Fig. 2.3. The pilot subcarriers are transmitted with a $\pm 4/3$ value so they are boosted by 2.5 dB compared to normal data subcarriers.

For every FFT size (N_{FFT}), the standard specifies the number of guard subcarriers (left and right guards), the number of used subcarriers including pilots and DC (N_{used}), and the number of clusters and subchannels as shown in Table 2.2. One subchannel is made up of two clusters, having a total of 24 data subcarriers (and 4 pilots) in one OFDMA symbol. This way, a slot in a DL PUSC zone is defined as one subchannel over two OFDMA symbols so the slots contains 48 data subcarriers.

Every OFDMA symbol is divided into guards, DC subcarrier and physical clusters. The physical clusters are mapped to logical clusters using a renumbering sequence that distributes them among all the available spectrum. The logical clusters are divided into 6 *major groups*, each of them having a number of subchannels assigned as shown in Table 2.3. The data

Table 2.2: DL and UL PUSC parameters for 512 and 1024 FFT size.

	DL PUSC		UL PUSC	
N_{FFT}	512	1024	512	1024
Left guards	46	92	52	92
Right guards	45	91	51	91
N_{used}	421	841	409	841
Clusters/Tiles	30	60	102	210
Subchannels	15	30	17	35

Table 2.3: Subchannels and logical clusters mapping into major groups for 512 and 1024 FFT size.

	$N_{FFT} = 512$		$N_{FFT} = 1024$	
Major group	Clusters	Subchannels	Clusters	Subchannels
0	0-9	0-4	0-11	0-5
1	-	-	12-19	6-9
2	10-19	5-9	20-31	10-15
3	-	-	32-39	16-19
4	20-29	10-14	40-51	20-25
5	-	-	52-59	26-29

subcarriers of a subchannel are distributed among all the assigned *major group* subcarriers using a permutation formula defined in the standard.

Each of the *major groups* is assigned to one of the three segments that can be used. Each segment should have at least one *major group* assigned. This way it is possible to use all or part of the available spectrum in a segment, adding more flexibility to the sectorization and frequency reuse configuration [YAN10, Chapter 5.9.2].

2.2.1.2 Uplink PUSC

The uplink PUSC symbol structure differs from the downlink to suit the requirements of uplink transmissions. Each symbol is divided into a set of tiles, whose structure can be seen in Fig. 2.4. Because contiguous tiles may be transmitted by different users (or there may be no transmission at all), information from adjacent tiles cannot be used to make channel estimates. Therefore, the pilots are placed in the corner positions of the tiles so that the channel inside the tile can be estimated from these pilots only. Moreover, one out of every three symbols is transmitted without pilots, so it is necessary to perform a two-dimensional channel estimation.

The subchannels are made up of six tiles. This way, a slot is defined as one subchannel

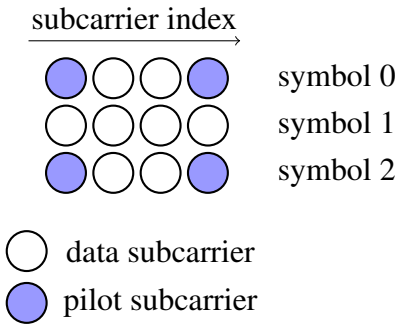

Figure 2.4: UL PUSC tile structure.

in three OFDMA symbols, with a total 48 data subcarriers and 24 pilots. The high number of pilot subcarriers allows for a better channel estimation than in DL PUSC clusters. The OFDMA symbol structure parameters are summarized in Table 2.2.

The procedure to map the slots data into the data subcarriers is analog to the DL PUSC method and also supports the use of up to three segments. The subcarriers are distributed in several steps so the tiles of a subchannel are not physically adjacent. Also, a subchannel rotation scheme is also defined so the assigned subchannels for a data burst changes every three OFDMA symbols, behaving like a frequency hopping technique. The ranging subchannels are not affected by these subcarrier permutation mechanisms.

2.2.2 OFDMA Ranging

In multiuser mobile environments, time and frequency estimations obtained at MSs cannot be directly used to construct the uplink signal because the relative distance and speed with respect to the BS is not known [MKP07]. In the IEEE 802.16e standard, this problem is solved with the so-called ranging process. In such a process, MSs transmit CDMA code sequences generated from a shift register in specific regions of the uplink, reserved for this purpose by the BS in a contention-based policy. At the receiver side, the BS must detect the arrival of ranging codes and estimate the synchronization parameters from them. Finally, these parameters are sent back to the MSs in a MAC management message and used to construct the synchronized uplink frames to be transmitted by the MSs.

Two types of ranging regions are defined: initial ranging, used during network entry; and periodic ranging, used when the MSs are already connected. In the case of initial ranging, OFDM symbols containing ranging codes must be transmitted by MSs in pairs as shown in Fig. 2.5: the first symbol with a CP and the second one with a cyclic postfix, hence allowing a wider time synchronization window.

Ranging codes are sequences of 144 BPSK symbols generated from the output of a pseudorandom binary sequence (PRBS). Different sets of codes are used depending on the purpose of the MS: initial ranging, periodic ranging, bandwidth requests, or handover. When

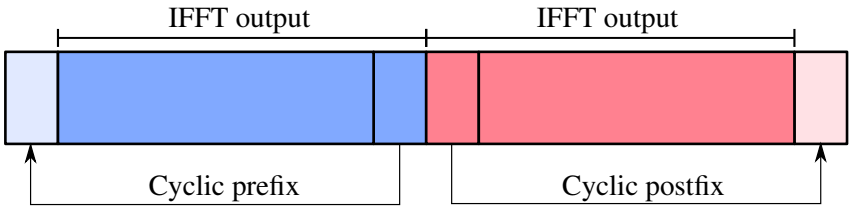

Figure 2.5: OFDM symbol structure for initial ranging with two symbols.

a MS decides to start a ranging process, it selects a code randomly from the corresponding set and then maps it to a ranging region. This mapping in a PUSC zone is done in a distributed fashion and only groups of four BPSK symbols are guaranteed to be transmitted in contiguous subcarriers. The BS must identify the ranging code sent by the MS in order to estimate the uplink synchronization errors.

2.2.3 Channel Coding

As shown in Fig. 2.1, the channel coding stage consists of the following steps: data randomization, channel coding, bit-interleaving, repetition coding, and symbol mapping.

Data randomization is performed in both the uplink and the downlink employing the output of a maximum-length shift-register sequence initialized at the beginning of every FEC block. Such a FEC block consists of an integer number of slots.

Channel coding is performed on a per-FEC-block basis employing one of the schemes defined in the standard, namely, tail-biting convolutional code (TBCC), block turbo code (BTC), convolutional turbo code (CTC), or low-density parity check (LDPC). Additionally, variable coding rate and modulation are supported, thus enabling for AMC capabilities.

In the bit-interleaving phase, each FEC block is processed by a two-step permutation. In the first step, the adjacent coded bits are mapped onto nonadjacent subcarriers, which provides frequency diversity and improves decoder performance. The second permutation distributes the positions of the bits inside the constellation to avoid long runs of lowly reliable bits.

The FEC blocks can be further processed by repetition coding with factors of 2, 4, or 6, to increase the resilience of important control data. Finally, the coded bits are mapped into Gray-mapped QPSK, 16-QAM, or 64-QAM constellations at the modulation stage.

The TBCC is specified as mandatory in the standard, supporting the following modulation and coding rate configurations: QPSK 1/2, QPSK 3/4, 16-QAM 1/2, 16-QAM 3/4, 64-QAM 1/2, 64-QAM 2/3, and 64-QAM 3/4.

2.3 802.16e MAC Layer

The MAC layer provides an interface between the higher-level network and transport layers and the physical layer. The packets received from the higher-level layers, called MAC service data

units (MSDUs), are reorganized into MAC protocol data units (MPDUs) and sent to the PHY layer. The reverse operation is done at the receiver side.

The MAC layer is divided into three sublayers: the convergence sublayer (CS), the common part sublayer (CPS), and the security sublayer. The CS maps the external network data into MSDUs allowing the MAC layer to be used with several protocols, such as Internet Protocol (IP) or Ethernet. Therefore, the CS has a set of classification rules which are used to assign the appropriate service flow to the higher-level layer packets. The CS can perform other tasks to reduce the overheads of the higher-level layers like payload header suppression (PHS) or RObust Header Compression (ROHC). The CPS is the core subsystem of the WiMAX MAC, providing all the needed mechanisms for connection establishment and maintenance, bandwidth allocation, QoS provisioning, etc. The security sublayer is embedded inside the CPS to provide authentication, secure key exchange and encryption functionalities.

The standard provides an example of MAC service access point (SAP), although it is implementation specific. The purpose of the example is to illustrate the information that should be exchanged between the CS and the CPS.

WiMAX MAC layer is connection-oriented. When a subscriber station (SS) accomplishes the network entry process, a set of connections is provided to the new node in order to communicate with the BS. All the connections have a unique 16-bit connection identifier (CID). There are two kinds of connections, management connections and transport connections. The management connections can be bidirectional and they are used for sending the different MAC management messages. The management connections are:

Broadcast Used by the BS to send messages to all the SSs.

Ranging Used during the ranging process.

Basic Unique for each SS. Used to send time-urgent messages.

Primary Used to send delay tolerant messages.

Secondary Optional connection that can transport standard-based messages.

Although basic, primary and secondary management connections are unique for each SS, the basic connection is used to identify the SS in the management messages.

The transport connections are unidirectional and they are used for sending the user data. They are always associated with a service flow which defines the QoS parameters and the classification rules.

2.3.1 MPDU Generation

MSDUs arriving from higher-level layers must be classified on MAC connections before transmission. These connections have associated the relevant parameters to packet transmission, such as the QoS requirements and the encryption keys. All information carried into MPDUs is always linked to a unique connection, but a wide range of possibilities regarding its generation is supported. Fragments of different MSDUs can be packed into a MPDU, and a MSDU can be

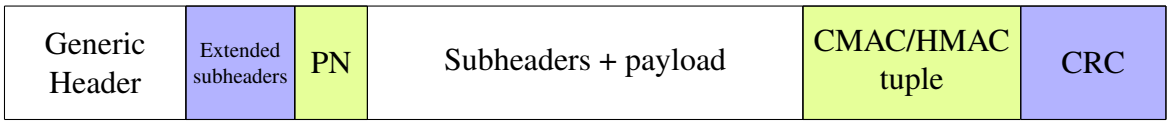

Figure 2.6: MPDU packet format.

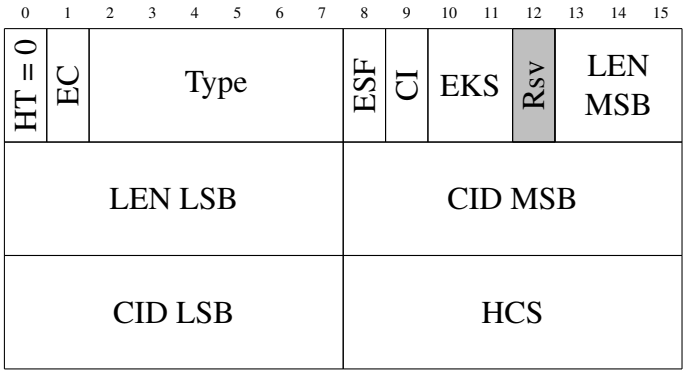

Figure 2.7: Generic MAC header format.

split into several MPDUs. Also, if a group of MPDUs is going to be transmitted under the same physical modulation and coding, they can be concatenated into the same physical burst, even if they come from different MAC connections.

Besides routing traffic from higher-level layers, MPDUs can also carry management messages of the MAC layer. These messages are meant to control processes which are exclusive of this layer, such as conveying information about the structure of the downlink and uplink subframes, managing network entry and initialization of new MSs, or completing secure authentication and key exchanges. In this case dedicated MAC connections are used, while packing and fragmentation of messages is not allowed.

The MPDU packet structure is illustrated in Fig. 2.6. All the MPDUs begin with a fixed-length MAC header which can be followed by a set of optional fields and the the payload with the information to be transmitted. If the connection associated with the MPDU has an associated security association (SA), the MPDU should be encrypted and two new fields should be added: packet number (PN) and HMAC/CMAC tuple. This tuple is also used in authenticated management messages.

In Fig. 2.7, the fields of the fixed-size (6 bytes) generic MAC header are shown. The CID and the length fields indicate the destination connection of the data and the length of the complete MPDU, respectively. The header check sequence (HCS) field is used to verify the header data fidelity. The remaining fields are mainly used to specify the presence of optional fields or subheaders, including the cyclic redundancy check (CRC) field, or the use of encryption.

There are other type of MPDUs with only a header and no payload, such as the bandwidth request (BR) header. They are used exclusively in the uplink and their purpose is to signal control information to the BS in a very compact form. These headers have the HT field set to

one to differentiate them from the generic MAC header.

WiMAX MAC layer provides three mechanisms to process the MSDUs, generate the MPDUs, and map them into bursts:

Concatenation Several MPDUs can be concatenated in the same burst.

Fragmentation One MSDU can be fragmented in several MPDUs.

Packing Several MSDUs with the same CID can be packed in one MPDU.

These three mechanisms can be combined in different ways to efficiently share the radio resources between the users. The behavior of these mechanisms is different depending on the connection configuration, e.g., fixed-length MSDUs can be packed in an more efficient way than variable-length MSDUs because there is no need to include packing subheaders in the MPDUs.

The concatenation mechanism allows to send data to different users or connections in the same burst. To identify when there are no more MPDUs in a burst, the unused bytes can be padded with stuff bytes (0xFF) or can be formatted with a special MPDU.

2.3.2 ARQ Mechanism

The ARQ mechanism allows for the retransmission of erroneous decoded MPDUs and works at MAC connection level. To provide this functionality, the MSDUs are divided in fixed-length blocks and numbered by assigning a block sequence number (BSN) to each block. The transmitter and receiver sides use a fixed-size window to manage the block states. The receiver side sends ARQ feedback messages to inform the state of its window, so the transmitter knows which blocks need to be retransmitted. The ARQ mechanism is managed by the transmitter and receiver state machines using timers to control the state changes of each block.

The ARQ performance is influenced by several parameters such as block size, window size and maximum waiting interval of the timers. These parameters are established on connection creation, and they are stored in the service flow associated to the connection. The ARQ feedback intensity is not specified in the standard and it is left to the designer's choice.

2.3.3 Scheduling and QoS

Scheduling in 802.16e is centralized in the BS. The BS determines how many slots are assigned to each SS or connection in the DL and in the UL. The SS is limited by the total burst size assigned in each UL subframe, but it decides which connections can send data in that space. These mechanisms are implemented by two different schedulers: outbound transmission scheduling and UL request/grant scheduling. The former selects the data to be sent in each bandwidth allocation and is performed by the BS in the DL, and the SS in the UL. The latter determines the bandwidth assigned to each SS so they can transmit data or request more bandwidth. These schedulers base their decisions on the QoS information and the scheduling service of each connection. This information is stored in the service flows associated with each connection.

Table 2.4: QoS parameters defined for each service class. Parameters marked as (✔) are optional.

QoS Parameters	UGS	rtPS	ertPS	nrtPS	BE
Traffic priority	✖	(✔)	(✔)	(✔)	(✔)
Max. sustained traffic rate	✔	(✔)	(✔)	(✔)	(✔)
Min. reserved traffic rate	(✔)	✔	✔	✔	✖
Minimum traffic burst	✖	(✔)	(✔)	(✔)	✖
Tolerated jitter	✔	✖	(✔)	✖	✖
Maximum latency	✔	✔	✔	✖	✖
Unsolicited Grant Interval	✔	✖	✔	✖	✖
SDU size	(✔)	✖	✖	✖	✖
Unsolicited Polling Interval	✖	✔	✖	✖	✖

The service flows plays a fundamental role in the 802.16e QoS. A service flow is defined as a MAC transport service that allows for unidirectional transport of packets either in DL or UL directions. They are created on the network entry procedure and are characterized by a set of QoS parameters such as latency, jitter and throughput assurances. They also indicate the service class that modifies the UL request/grant scheduling algorithm behavior or their corresponding DL data delivery service. The service classes are:

UGS The unsolicited grant service provides fixed-size grants on a real-time periodic basis. This avoids the need of SS requests reducing the overhead and latency. This class is useful for voice over Internet Protocol (VoIP) applications.

rtPS The real-time polling service supports real-time service flows with variable-size packets by providing periodic opportunities to specify the size of the needed grants. This class is appropriate for audio and video streaming.

ertPS The extended rtPS combines the advantages of unsolicited grant service (UGS) and real-time polling service (rtPS) by providing periodic grants of dynamically configurable size. This class is useful for VoIP applications with activity detection.

nrtPS The non-real-time polling service is used for non-real-time services with variable-size packets. The BS provides periodic BR opportunities but does not guarantee maximum latency. This class can be used for delay tolerant applications such as FTP.

BE The best effort service does not have minimum throughput or delay requirement. No BR opportunities are provided, so only contention request opportunities are used to notify the need of bandwidth assignment. This class should be used for low priority applications like data transfer or web browsing.

The QoS parameters defined for each service class are specified in Table 2.4, including the optional values.

Finally, a SS can use three different mechanisms to request more bandwidth:

Piggyback request Specify the requested increase in bandwidth or the need to be polled in a grant management subheader included in a MPDU of the connection.

Bandwidth stealing Insert a BR header in space assigned to send data.

Contention-based Use a ranging slot to send a CDMA code to inform the BS the need to send a BR. The BS would assign UL space to the SS so it can send its BR.

2.3.4 Convergence Sublayer

The CS maps the different higher layer packets to MSDUs, isolating the MAC CPS from higher layers. The CS carries out the next tasks:

- Accept packets from higher layer protocols.
- Classify the higher layer packets determining the connection to be used to transmit them.
- Process the packets if required depending on the classification (e.g. apply PHS).
- Deliver and receive the CS protocol data units (PDUs) to/from the MAC CPS.

Depending on the higher layer, these tasks are performed in different ways. Three different CS specifications are defined in the standard: ATM CS, packet CS, and the Generic Packet CS. Only the packet CS is described as mandatory by the WiMAX Forum.

2.3.4.1 Packet CS

The packet CS provides a interface between the MAC CPS and packet based protocols, such as IP or Ethernet. The input service data units (SDUs) are processed if PHS or ROHC are activated, in other case, the generated PDUs are equal to the SDUs.

The most important function of the CS is the classification of the higher layer packets. This task is carried out by applying the classification rules defined in the service flows. These classification rules define the criteria by which a SDU should be accepted by a connection. The used criteria can be the source or destination IP addresses, as well as the port number, or any other IP header fields. If several connections accept a SDU, it will be assigned to the higher priority connection, while if the packet does not match any classification rule, it should be discarded. The result of the classification process is the CS PDU and the corresponding CID.

When a classification rule is selected, PHS or ROHC can be enabled for that rule. In this case, the SDU will be processed using the associated mechanism to generate the resulting PDU.

2.3.5 Security Sublayer

The security sublayer provides authentication and privacy to the SS in the network. To fulfill the security needs, two protocols are defined: a key management protocol and an encapsulation protocol.

2.3.5.1 PKM Protocol

The key management protocol used in the standard is privacy key management (PKM) version 2. The PKM protocol carries out the secure distribution of the keying data to the SS and authentication tasks. The standard allows for using the Extensible Authentication Protocol (EAP) authentication protocol, defining messages to carry EAP payloads, but without specifying a particular variant of EAP and letting higher layer processes to define the requirements of this implementation. Once the authentication process is finished, the MAC layer receives as a result an authentication key shared between base station and the subscriber station, which is used to generate keying material. The PKM protocol also specifies management messages to define security associations and to distribute traffic keys.

2.3.5.2 Encapsulation Protocol

The encapsulation protocol specifies the rules to encrypt and authenticate the MPDUs using a set of cryptographic suites. WiMAX Forum selects advanced encryption standard (AES) in CCM mode and cipher-based message authentication code (CMAC) as the required algorithms.

In order to authenticate management messages, CMAC tuples generated with the AES algorithm can be appended to them, although payloads are always transmitted as clear text. In the case of MPDUs transmitted over traffic connections with a security association enabled, their payloads are ciphered with AES in CCM mode. In this mode two fields are appended to the encrypted payload: a PN value which is unique for each packet to avoid replay attacks, and an authentication code.

This encapsulation protocol does not cipher headers of MPDUs in any case.

2.3.6 Network Entry

A network entry protocol is defined to allow MSs to attach to the base station. This protocol starts when a MS sends a ranging code in a region specified for this purpose by the base station in the uplink (see Section 2.2.2). Once the arrival of a sequence of this type is detected, the base station can estimate synchronization parameters such as time, frequency or power offset, and send them back to the transmitting MS to improve synchronization. This process can be repeated until the base station considers the synchronization parameters are within acceptable thresholds, and finally a pair of CIDs for the basic and primary management connections are assigned. From this point, both stations can exchange management messages using these CIDs, and to check if some message is lost in this stage, a set of timers is defined.

These timers define a maximum waiting time and a number of retries to restart the network entry protocol if necessary, until a successful connection is established. This stage performs the exchange of capabilities of both stations, as well as the authentication and registration steps. Optionally, provisioned service flows can be defined at the end of this protocol.

2.4 WirelessMAN-Advanced Air Interface

The IEEE 802.16m standard introduces a completely new definition of MAC and PHY known as Advanced Air Interface (AAI). The configurability of the parameters is reduced to a large extent, but additional features such as multiple-input-multiple-output (MIMO) and HARQ are now mandatory to accomplish the minimum requirements of the standard, and also backward compatibility is mandatory. For a more detailed description see [AHM10].

A new profile with a channel bandwidth of 20 MHz and 2048 subcarriers is added while the 3.5 MHz profile is discarded. The new frame structure is divided into superframes of 20 ms. Each superframe is made up of four 5 ms frames. The main difference with the old frame structure is the way the frames are subdivided into subframes to increase the flexibility of the allocation of downlink and uplink zones. Each subframe can be dynamically configured for downlink or uplink transmission.

The synchronization mechanisms have been improved by defining two new preambles: the PA-preamble, with a fixed number of pilot subcarriers regardless the FFT size to be used by the advanced base station (ABS), and the SA-preamble, with a structure and purpose similar to the preamble of the previous release. Also, new ranging preambles are added with extended length and reduced subcarrier spacing for the initial ranging and handover mechanisms.

The new subchannelization scheme is designed to simplify the channel estimation and to reduce the signaling overhead required for the burst placement, and it only depends on the MIMO scheme at use. The AAI defines new MIMO configurations to support Single User MIMO (SU-MIMO) and Multiple User MIMO (MU-MIMO) schemes, both with adaptive and non-adaptive precoding. The WiMAX Forum defines the minimum number of ABS antennas as two, while the advanced mobile station (AMS) can operate with only one antenna.

Channel coding in 802.16m only uses two FEC schemes. On the one hand, CTC is the encoder defined to transmit the data bursts. On the other hand, a TBCC encoder with rate 1/5 is used to encode the control information.

2.5 Conclusions

This chapter describes how OFDMA-based communications systems work. The Mobile WiMAX standard is considered as an example to describe the mechanisms used in the PHY and MAC layers to share radio resources efficiently among different users. The evolution of the different ammendments of the standard is shown as well as a detailed description of the mandatory features of the PHY and MAC layers, which are specified by the WiMAX Forum. Finally, the changes and enhancements introduced in 802.16m AAI are summarized.

The PHY layer has a flexible OFDMA TDD frame structure where only the preamble and the FCH and DL-MAP bursts have fixed positions in it. Different OFDMA symbol structures can be configured in the frame, assigning a contiguous or distributed set of subcarriers for each

user. However, only the DL and UL PUSC symbol structures are mandatory. The DL-MAP and UL-MAP management messages specify the symbol structures used in the DL and UL subframes as well as the configuration of each burst: position, size, modulation and coding, the destination connections, etc.

Rectangular regions in the UL subframes can be reserved for the contention-based transmission of ranging codes from the MSs. These codes are sent by the MSs to synchronize in time and frequency with the BS during initial, periodic or handover ranging. This contention mechanism can also be used by the MSs to send bandwidth request ranging codes to obtain transmission opportunities.

The MAC layer is connection-oriented and made up of three sublayers: the CS, the CPS and the security sublayer. The CS processes and maps upper layer packets (such as IP or Ethernet) into MSDUs. These MSDUs are processed by the CPS to generate MPDUs using the fragmentation and packing mechanisms. The PHY layer bursts are filled with these MPDUs. An ARQ protocol is also defined in the MAC layer and can be enabled for each transport connection.

Regarding QoS, the MAC defines several parameters for each service class that are used by the scheduler to assign resources to the SSs and to prioritize the packets of each connection. The scheduling is centralized in the BS, as it determines the resources granted to each SS. However, the SS scheduler still selects what connections are served in each transmission opportunity.

Chapter III

Real-Time Implementation of TDD Mobile WiMAX

This chapter shows the design and real-time implementation of base station (BS) and mobile station (MS) transceivers compliant with the Mobile WiMAX standard. Both mobile and base stations include transmission and reception chains to enable real-time concurrent downlink (DL) and uplink (UL) communications. This chapter also addresses the verification and validation of the proposed implementation based on the reference scenarios defined by the WiMAX Forum, i.e., the ITU Radiocommunication Sector (ITU-R) M.1225 channel models [ITU97; WIM05].

The time-division duplexing (TDD) version of the orthogonal frequency-division multiple access (OFDMA) physical (PHY) and medium access control (MAC) layers are implemented using an software-defined radio (SDR) architecture. The implementation is limited to the mandatory elements of the standard, supporting the following features:

- PHY layer:
  - Five profiles defined by the WiMAX Forum: 3.5 MHz, 5 MHz, 7.5 MHz, 8.75 MHz, or 10 MHz.
  - TDD frame structure with fixed number of OFDMA symbols in DL and UL.
  - PUSC permutation zone in DL and UL.
  - Modulation and coding using tail-biting convolutional code (TBCC): QPSK 1/2, QPSK 3/4, 16-QAM 1/2, 16-QAM 3/4, 64-QAM 1/2, 64-QAM 2/3, and 64-QAM 3/4.
- MAC layer:
  - Convergence sublayer (CS): Packet classification and payload header suppression (PHS).
  - Common part sublayer (CPS):
    * Management and transport connections.
    * Support for automatic repeat request (ARQ).
    * QoS scheduler and burst mapper.
  - Security sublayer: Key management, authentication and encryption algorithms.

This chapter is mainly based on the following co-authored publications:

- Pedro Suárez-Casal, Ángel Carro-Lagoa, José A. García-Naya, and Luis Castedo. "**A Multicore SDR Architecture for Reconfigurable WiMAX Downlink**". *Proc. of 13th Euromicro Conference on Digital System Design: Architectures, Methods and Tools (DSD), 2010*. 2010, pp. 801–804.
  DOI: 10.1109/DSD.2010.108
- Ángel Carro-Lagoa, Pedro Suárez-Casal, José A. García-Naya, Paula Fraga-Lamas, Luis Castedo, and Antonio Morales-Méndez. "**Design and implementation of an OFDMA-TDD physical layer for WiMAX applications**". *EURASIP Journal on Wireless Communications and Networking*, vol. 2013, no. 1, 2013, p. 243. ISSN: 1687-1499.
  DOI: 10.1186/1687-1499-2013-243
- Pedro Suárez-Casal, Ángel Carro-Lagoa, José A. García-Naya, Paula Fraga-Lamas, Luis Castedo, and Antonio Morales-Méndez. "**A real-time implementation of the Mobile WiMAX ARQ and physical layer**". *Journal of Signal Processing Systems*, vol. 78, no. 3, 2015, pp. 283–297. ISSN: 1939-8115.
  DOI: 10.1007/s11265-014-0890-3
- Antonio J. Rodríguez, Roland Pastorino, Ángel Carro-Lagoa, Karl Janssens, and Miguel Á. Naya. "**Hardware acceleration of multibody simulations for real-time embedded applications**". *Multibody System Dynamics*, 2020, pp. 1–19.
  DOI: 10.1007/s11044-020-09738-w

The structure of the chapter is as follows. Section 3.1 reviews other 802.16 published implementations. Section 3.2 describes the proposed SDR architecture and the used development methodology. The PHY and MAC implementations are described in Section 3.3 and Section 3.4, respectively. Section 3.5 presents the amount of field programmable gate array (FPGA) and digital signal processor (DSP) resources consumed by the implementation while Section 3.6 is devoted to its experimental evaluation over ITU-R wireless channel models. Section 3.7 explains how the proposed hardware architecture can be extended to implement the PHY and MAC of the WirelessMAN-Advanced Air Interface. Finally, Section 3.8 presents the concluding remarks.

3.1 State of the Art

The experimental validation of prototype baseband systems employing real-time hardware demonstrators confronts several challenges such as enormous design complexity, long development time, high costs and manpower, or dealing with insuperable hardware issues.

Few works exist in the literature that address the complete and real-time implementation of OFDMA-TDD mobile communication PHY and MAC. Existing works focus on performance analysis such as path-loss measurements using Fixed WiMAX commercial equipment in rural environments [ISC07], tests in outdoor scenarios employing commercial Mobile WiMAX

equipment [ZTN08], or evaluations of the IEEE 802.16e OFDMA downlink in vehicular environments (ITU-R M.1225) [COL+10]. In this context, references considering simulations [MR10], non-real-time deployments [HU+07; MCR08], and Fixed WiMAX implementations [LB08] were found. However, none of the aforementioned approaches accounts for software constraints or hardware limitations.

Some works consider the real-time implementation of the OFDMA-TDD PHY used in Mobile WiMAX but most of them only consider simplex communications, either downlink [FON+11; CLC07] or uplink [WU+09]. Only two papers were found which consider a bidirectional OFDMA-TDD PHY: an implementation of 802.16e-2005 carried out in a System-on-Chip (SoC) platform [WU+10], and a SoC baseband implementation integrated in a USB device for high mobility scenarios [CHU+11].

Studies that incorporate MAC layer functionalities provide a more realistic evaluation of the actual performance of a wireless communication system, especially when measuring meaningful metrics such as throughput. A detailed description of the WiMAX ARQ mechanism and a performance analysis using a simulated environment can be found in [SAY+07]. Theoretical analysis of the throughput achievable at MAC level taking into account some features of the WiMAX physical layer can be found in [PAR+10]. Some works devoted to study the effect of particular parameters of the WiMAX ARQ or hybrid automatic repeat request (HARQ) mechanisms in order to improve specific metrics are [ARH09; LP09; HEM+08]. These references usually rely on simulations of the physical layer using simplified channel models, thus the behavior of the systems cannot be reliably outlined under more realistic conditions. Implementations of full-featured MAC layers using network processors with a detailed design description and resource utilization can also be found [WWX08].

It is possible to find implementations of individual processing blocks of the standard but not integrated in a complete system. As an example, the design of a channel encoder prototyped in a reconfigurable hardware architecture is presented in [CKH11]. Another example is an FPGA architecture of a fixed sphere decoder for a WiMAX system presented in [KAH09]. There are some implementations that aim to support two standards by extracting common signal processing between them and sharing hardware resources, such as the study of a dual-mode baseband receiver for 802.11n and 802.16e [HCC09], and a 802.16m and LTE downlink implementation [HSU+11].

The work presented in this chapter differs from existing ones in the literature because it presents a hardware architecture for the implementation of both the downlink and the uplink of OFDMA-TDD PHY and MAC for WiMAX applications. We discuss a large number of practical issues and show how they can be solved to fit into the proposed hardware architecture. Although most of the work focuses on Mobile WiMAX, we also explain how the proposed architecture can be used to implement the WirelessMAN-Advanced Air Interface.

3.2 System Architecture Design

The complexity and different functionalities present in a WiMAX transceiver pose several technical design challenges. Thus, it is more appropriate to implement the transceiver on a multicore SDR hardware architecture where each core is adapted to a specific functionality. This approach is much more energy efficient than attempting to implement the whole system on a single very flexible core [PAL+10], although there are several SDR implementations that rely only on a general purpose processor (GPP) such as the OpenLTE implementation based on an Intel Core i7 processor. The PHY layer implementation requires high computing power for the signal processing tasks which is provided by the FPGAs present in the architecture. The WiMAX standard also requires the implementation of other management tasks that are not so compute intensive but they need to be highly reconfigurable or flexible. In these cases, a software implementation in a GPP or DSP is more appropriate and will ease the development process.

The architecture where the transceivers are implemented follows the SDR principles [MIT92] and it is based on the "task" concept. In this case, a task is a set of operations that corresponds to a logical block of the system (e.g. I/Q modulation, synchronization, fast Fourier transform (FFT), etc.) which can be executed in different type of processors. The system is built connecting different tasks in a proper way. The key concept here is the reconfigurability of the tasks constituting the system and how to achieve the required flexibility without losing performance. Reconfigurability denotes the capability of a system to modify its behavior according to configuration parameters.

The architecture has to be flexible in order to support both processing operations and high-level control logic required by the distinct elements of the software design. The kernel of the architecture is constituted by the DSP. It is responsible of executing the higher-level tasks, which requires the highest degree of freedom and the most complex operations, as well as controlling the executions of the remaining elements of the system (mainly the tasks running at different FPGAs). Note that if the architecture does not have a DSP, it is possible to replace it by embedding a processor in the FPGA logic. In fact, there are several FPGAs available in the market that embed a physical processor core in the FPGA chip.

The FPGAs provide much higher processing power than the DSPs. The main drawback, among the disadvantages of FPGAs, is the implementation difficulty of the dynamic tasks that require real-time reconfigurability capabilities. Due to the above reason, it is more recommendable to view the FPGAs as coprocessors of the DSPs. Therefore, those tasks demanding high processing power (i.e. FFT, pulse-shape filtering, synchronization, etc.) are placed on different FPGAs, while the control logic is carried out by the DSP tasks. Unfortunately, these time-consuming tasks also have to be reconfigurable, making impossible to delegate all reconfigurability logic to the DSP.

The remaining of this section explains the development methodology used in the design and

implementation of the system (Sections 3.2.1 and 3.2.2), and the final SDR architecture of the system (Sections 3.2.3 and 3.2.4).

3.2.1 Development Methodology

The use of an appropriate development methodology is essential for a successful system implementation. A good methodology should be able to anticipate possible problems at an early stage. However, this system is composed of two layers with significant differences in its processing requirements and flexibility. On the one hand, the implementation of the MAC layer is purely a software development. On the other hand, the PHY layer is mostly constituted as signal processing tasks requiring specialized hardware. These differences force the use of different methodologies for each layer. For the MAC layer traditional software development methodologies can be used while for the PHY layer it is necessary to define a methodology adapted to its needs.

The MAC layer cannot be implemented independently of the rest of the system since it is strongly coupled to it, as it must communicate with the tasks of the PHY layer and control its operation. For this reason it is necessary to have a software development environment where it is possible to simulate the operation of the MAC layer in conjunction with the rest of the system, so that it is as similar as possible to the final execution environment. For this reason, a development environment has been implemented for the MAC layer that simulates the functionalities of the hardware environment libraries and allows the simulation and debugging of the system in a simpler way in a conventional PC. This simulation environment allows us to perform tests in a simpler and faster way than performing tests on the real hardware, which require a long setup process.

The general methodology followed for the development of the physical layer is divided into the following phases:

1. Theoretical model: division of the system into blocks/tasks specifying its inputs and outputs.
2. Implementation of reference software.
    - Testing of blocks in simulation.
    - Fixed point analysis.
    - Foreseeing implementation problems.
3. Design of real-time system architecture.
4. Implementation of real-time tasks.
5. Integration and testing.

The purpose of this methodology is to anticipate the problems of the advanced phases of system implementation that could force the repetition of previous phases. For this reason, a reference implementation is created in which the algorithms to be implemented in the final phases are studied. This methodology is appropriate for physical layer signal processing tasks.

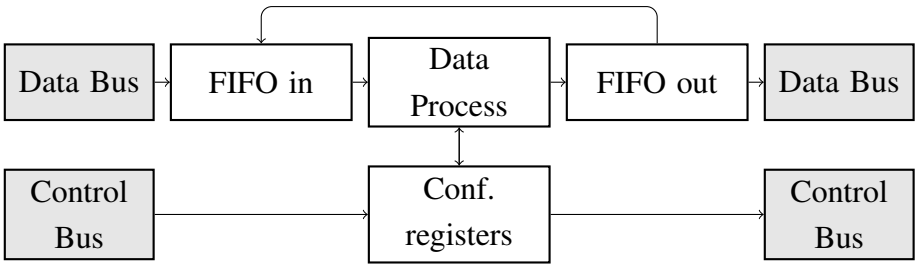

Figure 3.1: Task template for FPGA.

However, the implementation of the MAC layer is strictly a software development process and this methodology is not appropriate.

Special care must be taken in the system architecture definition phase (step 3). In this phase, the SDR hardware structure of the system is decided, as well as the flexibility of each task and how they are mapped to the different modules. In general, the following guidelines should be followed:

- Identify the time-consuming tasks that will be placed on FPGAs. A good design should minimize the number of these tasks.
- Identify the higher level tasks with complex control logic that should be placed on DSPs.
- Decouple the tasks and define the communication protocols between them. An appropriate definition of the tasks yields to the minimization of the dependencies among them.
- Minimize the degree of reconfigurability present on the FPGA tasks.

The obtained task structure is used for the definition of the hardware architecture. The architecture must be adapted to the processing and communications needs of each task. Thanks to the flexible SDR architecture, each task can be placed on a DSP or on an FPGA according to its performance requirements.

In the implementation phase it is very useful to use a template for FPGA tasks. This template defines the task structure and simplifies the implementation and communication protocols. The following subsection explains this task template.

3.2.2 Development of FPGA Tasks

To simplify the implementation of the tasks in the FPGA, the task template shown in Fig. 3.1 is used. This template defines the structure of a task, which is constituted by two different paths: one for the data —including the processing steps— and another for the configuration.

The data path has an input first-in-first-out (FIFO) queue followed by the processing block and, finally, an output FIFO queue. The input queue interacts with the data bus, signaling when it can receive more data from the bus. The output queue checks whether the data bus is ready before sending the data. If the output data bus is blocked for a long time, the output queue will fill up quickly. For this reason, the output queue will notify the input queue to stop sending

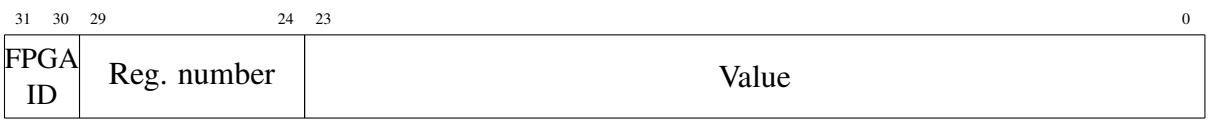

Figure 3.2: Register configuration message format.

data. Thanks to this scheme, several tasks can be chained even when they have different data processing rates.

The configuration path stores the configuration data in several registers. Consequently, the processing block can read this configuration information in order to appropriately configure itself. The processing block can also write output data or status in the registers, so they can be retrieved by the DSP. The messages read from the control bus have the format shown in Fig. 3.2 with the following fields:

FPGA ID Identifies de destination FPGA of the message. The register number space is shared between the tasks of each FPGA.

Reg. number Identifies the target register to configure. The registers 0 to 62 can be written. When the value 63 is used, the message purpose is to read the register indicated by the value field and send it to the output control bus.

Value The new value of the register or the register number to read.

In general, the separation between configuration and data simplifies the task development as no communication packet format needs to be defined for each task: the data path only contains data to be processed and the configuration path is used to specify the task settings. A DSP task that uses this FPGA task only has to configure the registers before sending the data to be processed.

However, this template has a performance penalty when using the FPGA task as a coprocessor. In this case the data is usually processed in blocks, the configuration changes frequently, and the DSP task is interested in the reception of the processed data. The following steps have to be performed for each data block to process:

- Send several registers to the control bus to configure the task.
- Prepare the reception of the data.
- Send the data to be processed to the data bus.
- Wait until all the processed data is received.
- Read the output registers if needed.

The DSP task has to wait until all the data is received before changing the configuration and sending other data block to be processed with the new configuration. This is because the data and configuration buses are independent and the configuration changes cannot be synchronized properly. The FPGA pipelined processing capabilities are underused in these cases.

There are different development tools for the implementation of algorithms in FPGAs. These design tools simplify the development process by reducing the usage of hardware description languages (HDLs). The used tool for the implementation of these tasks is Xilinx

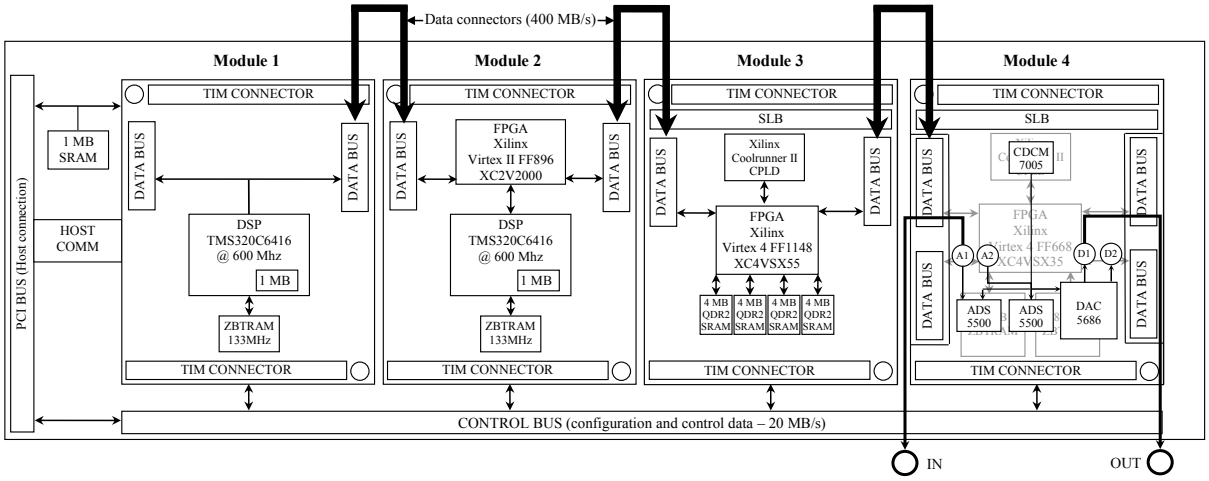

Figure 3.3: Hardware configuration of a station.

System Generator for DSP [XILd]. This tool is specialized in the implementation of signal processing algorithms. It is integrated in the Mathworks Simulink [MAT] software with special blocks that are directly mapped in the FPGA hardware. This integration simplifies the simulation and testing of the designs.

There are other higher level development tools for FPGA design known as high-level synthesis (HLS) tools. These tools allow for implementing the algorithms using high-level programming languages such as C/C++ or SystemC. They are able to convert the source code to a low-level hardware design (register transfer level) based on finite-state machines that control the execution of the data path operations. The hardware design is optimized using directives that customize the resources used for each operation, e.g., a loop can be pipelined so it outputs one value for each clock cycle or it can be unrolled, devoting more hardware to execute all the loop operations at the same time. These HLS tools accelerate the development process, especially of algorithms with complex control code such as a linear equation solver [ROD+20]. However, these tools do not allow for easy configuration of low-level implementation details, leading to increased resource usage. We decided to use System Generator because it is well suited for the implementation of signal processing algorithms and also allows for a detailed control over the final design.

3.2.3 Hardware Platform

In the proposed design for the bidirectional TDD WiMAX transceivers, MS and BS were implemented making use of the same type of hardware elements based on commercial off-the-shelf (COTS) components. As shown in Fig. 3.3, each station makes use of several interconnected FPGAs and DSPs. These components are provided by four different modules placed on a PCI carrier board and communicated by high-speed and low-latency buses.

The first module contains a Texas Instruments TMS320C6416 DSP. The second module

contains another identical DSP together with a Xilinx Virtex-II XC2V2000 FPGA. The third module has a Xilinx Virtex-4 XC4VSX55 FPGA, while the fourth one is equipped with a Virtex-4 XC4VSX35 FPGA together with an analog add-on module containing a dual digital-to-analog converter (DAC) and a pair of analog-to-digital converters (ADCs). The DACs are Texas Instruments DAC5686 [TEXb], with 16 bits of precision and a maximum sampling rate of 160 Msample/s. The ADCs are Texas Instruments ADS5500 [TEXa], with 14 bits of precision and maximum sampling rate of 125 Msample/s. Note that both Virtex-4 FPGAs are equipped with a large number of embedded multipliers, hence enabling intensive signal processing operations.

Two kind of buses were used for communications between modules: data buses, which can achieve up to 400 MB/s; and control buses with a throughput of 20 MB/s used exclusively for configuration messages. Also, the communications between the host PCs and the carrier boards are done through the PCI bus.

3.2.4 SDR Architecture

The architecture was designed following the guidelines shown in Section 3.2.1. The block diagram of the hardware architecture of each station is shown in Fig. 3.4 with the location of each system task and the connections between them. The arrow numbers indicate the number of bits of the communications between tasks, e.g. 16×2 represents complex numbers with 16 bits precision for each component.

The first DSP is devoted to the implementation of the MAC layer. The MAC CS and CPS are implemented in two different tasks. The security sublayer is included in the CPS. Communications between CS and CPS are performed using a custom MAC service access point (SAP) protocol. The CS also interacts with the Host PC to allow for sending and receiving IP packets.

The PHY layer uses the remaining modules of the system. The *PHY Control* task is placed in the second DSP and is the central component of the PHY layer. The remaining PHY tasks are configured and controlled by this central block, which uses the Virtex II FPGA as a coprocessor to perform the forward error correction (FEC) processing. Also, the communications with the MAC CPS are performed using a PHY SAP protocol.

All the FPGA tasks of the system are used in the PHY layer to perform the low-level and compute-intensive processing. The subchannelization tasks (*DL/UL PUSC*) are placed in the DSP because the flexibility needed for them and they do not require too much processing power. However, the other tasks implemented in the DSP (*equalization* and *ranging*) require higher processing resources and are hard to implement on an FPGA because they need to support the different frame structures and configurations. In this case, the decision was to develop an optimized implementation of these tasks on the DSP.

The two FPGA-only modules contain the orthogonal frequency-division multiplexing

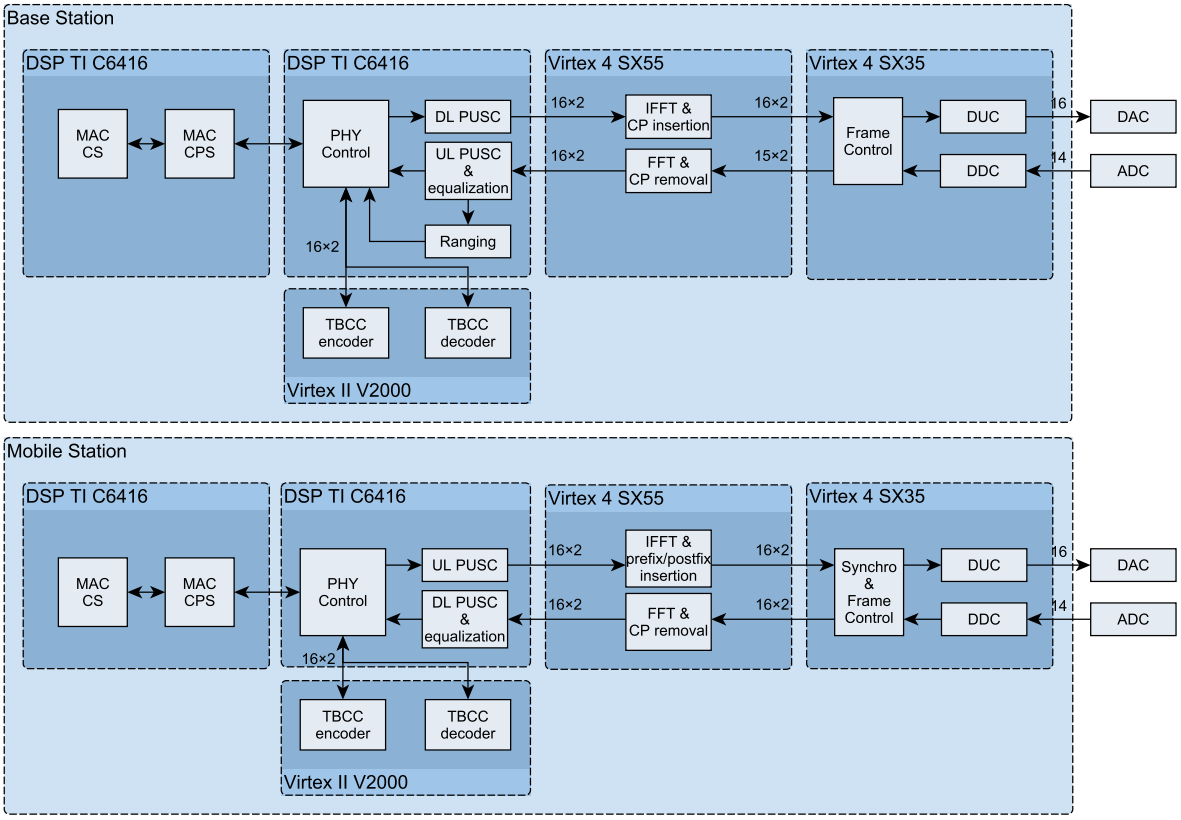

Figure 3.4: Global architecture of the base (top) and mobile (bottom) stations including both the uplink and the downlink building blocks.

(OFDM) signal processing tasks for the downlink and uplink. They communicate with the PUSC tasks and perform the remaining processing of the physical layer, first performing the frequency processing tasks (FFT/IFFT), and then performing the signal processing in time.

3.3 Mobile WiMAX Physical Layer Implementation

This section describes the design and implementation of an OFDMA-TDD PHY compliant with the Mobile WiMAX standard. This implementation is focused on the mandatory parts of the standard for both the BS and the MS, i.e. OFDMA frame structure, partial usage of subchannels (PUSC) permutation scheme in downlink and uplink subframes, ranging, and channel coding with TBCC.

In the block division of the physical layer shown in Fig. 3.4, the central node of all processing is the DSP that uses the blocks located in the FPGAs as coprocessors to perform the most computationally intensive tasks. This allows for high-level logic to be located in the DSP favoring system versatility and reconfigurability.

Most of the signal processing calculations performed in the DSP tasks are done in fixed-point with 16 bits of precision. This is because the architecture of the DSPs is optimized for

this precision. However, more bits are used in some intermediate calculations which require more precision. In the FPGA tasks, the used bit width can be configured as needed in each calculation but it is also common to use 16 bits of precision in these tasks.

3.3.1 Digital Up/Down Conversion

The digital up-converter (DUC) and digital down-converter (DDC) blocks are responsible for adapting the signal to the ADCs and DACs sampling rate and I/Q modulation/demodulation. During upconversion the following tasks are done: upsampling, filtering, and I/Q modulation to a configurable intermediate frequency. The downconverter performs the complementary operations in inverse order, i.e. I/Q demodulation, filtering, and downsampling.

The chosen profiles selected by the WiMAX Forum are supported by means of five different bit streams to the FPGAs, each one with a different up/downsampling factor. Since the converters sampling frequency is fixed at 80 MHz, the up/downsampling factors for each profile are 20, $100/7$, 10, 8, and $50/7$ for profiles #1 to #5, respectively (see Table 2.1 in Section 2.2). In order to efficiently implement these sample-rate conversions, each FPGA bit stream has a different optimized combination of interpolation/decimation filters.

The different filter banks explained in [SUÁ+10] could be used for these task so the used profile could be changed in real-time without the need to update the FPGA bitstream. However, that implementation uses more FPGA resources and provides lower signal quality than using an optimized filter for a given bandwidth. In the MS transceiver this task has to share the FPGA resources with the synchronization task, forcing the use of the optimized non-reconfigurable design.

The add-on module containing the digital converters has a 80 MHz clock used for setting the sample rate of the converters. This clock is used in the DUC and DDC tasks to correctly communicate with the converters. Thanks to the used task template described in Section 3.2.2, the last FIFO queue of the DUC regulates the processing speed of the transmission chain to ensure the required data output rate.

Also, the add-on module can be configured to use an external clock source. This allows for performing tests sharing the same clock source for both stations, increasing the obtained signal quality. Also, an alternative up/downsampling factors could be used by changing the clock frequency. As an example, with a 89.6 MHz clock, the profiles #1 and #4 can be obtained using 16 and 8 up/downsampling factors, respectively.

Only one configuration register is used by these blocks when using one bitstream for each profile:

fc (UFix_24_19) Intermediate transmission frequency in MHz.

3.3.2 Frame Control and Downlink Synchronization

The frame control tasks coordinate the transmission and reception of downlink and uplink signals following the standard TDD frame structure. In the BS, this task is in charge of sending the downlink subframe every 5 ms and starting the reception of the uplink subframe after the transmit/receive transition gap (TTG). In the MS this task is integrated with the downlink synchronization, which notifies when downlink subframes are detected, so that uplink subframe can be sent at the correct time.

The downlink synchronization task performs frame detection and frequency offset estimation at the MS. This task takes advantage of the correlation properties exhibited by the preamble defined in the standard as well as those found in OFDM symbols when the cyclic prefix is included. These properties enable the calculation of the subframe start time and the received signal carrier frequency offset (CFO). Also, a cross-correlation with a quantized portion of the preamble is used to enhance the subframe detection. A more detailed description can be found in [CAR+13b].

The general structure of the frame control and downlink synchronization task is shown in Fig. 3.5. Since ADCs are not equipped with a programmable gain amplifier (PGA), normalization of the received signal is performed after the DDC stage. This is done by first obtaining the average power of the received signal and then calculating a constant *scaling factor* that is applied during the whole downlink subframe. This normalization strategy has been selected because it provides a good compromise between clipping and quantization errors. The *subframe start* time is also notified to the UL transmission control block. This block schedules the emission of the uplink subframe taking into account the subframe size, the TTG and receive/transmit transition gap (RTG) guard intervals, and the offset set by the BS in the ranging process.

These blocks use several configuration registers:

CP_size (UFix_2_0) Selects the cyclic prefix used.
Nfft (UFix_1_0) Selects the FFT size used.
OFDM_symbols_DL (UFix_16_0) The number of OFDM symbols in the downlink subframe.
OFDM_symbols_UL (UFix_16_0) The number of OFDM symbols in the uplink subframe.
TTG (UFix_16_0) The length of the TTG.
RTG (UFix_16_0) The length of the RTG.
synch_threshold (UFix_16_16) The synchronization threshold to detect the subframe start.

Finally, two output registers are also provided by the synchronization task with the energy estimations during the downlink and the RTG guard interval. These registers are read by *PHY Control* task to estimate the signal-to-noise ratio (SNR).

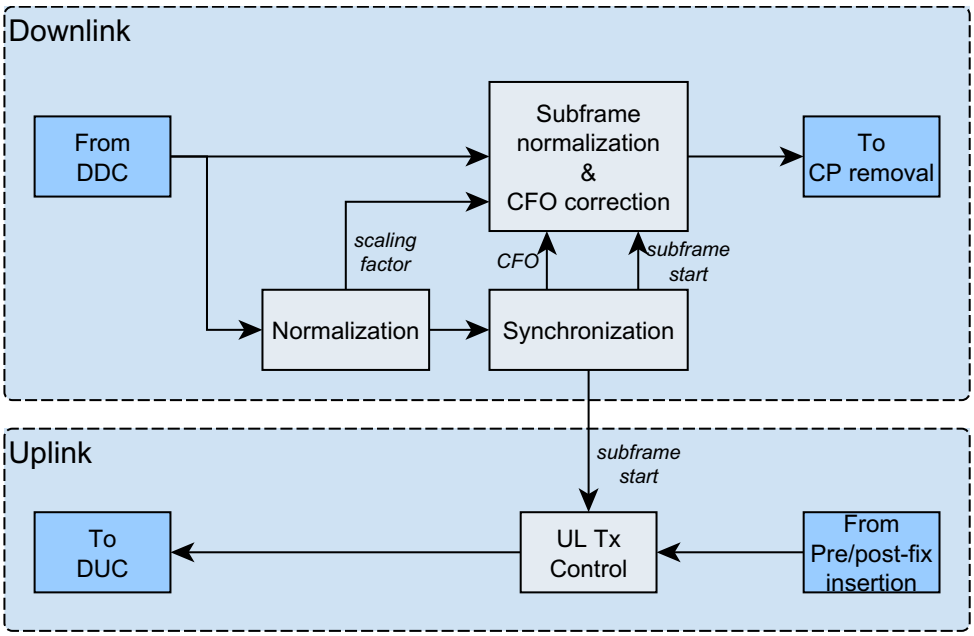

Figure 3.5: Frame detection and synchronization subsystem implemented in the MS.

3.3.3 Ranging and Uplink Synchronization

Physical layers based on OFDMA require that uplink frames arrive at the BS at the same time and with a significant accuracy. This can only be achieved if all users are synchronized with the BS before the communication takes place. WiMAX standard states that the round-trip delay between the MS and the BS must be known beforehand by the MS. This is possible thanks to the so-called ranging step.

As already explained in Section 2.2.2, MSs generate pseudo-noise sequences from a shift register that are transmitted in specific regions of the uplink subframe. Such regions have to be reserved by the BS in a contention-based policy. At the receiver side (in the uplink), the BS detects the arrival of a ranging code and then it estimates the synchronization parameters. Finally, the MS adjusts its synchronization parameters from the base-station estimates sent back to the MS in a MAC management message.

During the initial ranging, OFDM symbols containing ranging codes are transmitted by the MS in pairs, the first one with a cyclic prefix, while the second one also adds a cyclic postfix, hence allowing for a wider time-synchronization margin. In this implementation, the mobile station has a special *cyclic prefix and postfix insertion* block to accomplish this requirement. This block receives the pattern of the prefixes and postfixes for the uplink subframe in a configuration register.

Code detection and time-offset estimation at the BS takes place at the frequency domain over each received OFDM symbol. Let $X(k)$ represent the 144 BPSK received symbols in a ranging subchannel of a single OFDM symbol. An energy threshold is first applied to them to avoid further processing [MAO06]. When the energy threshold is reached, a cross-correlation

of the received symbols, $X(k)$, with all possible ranging codes, $p_c(k)$, is used to determine the ranging code index c. If we denote $t_c(k) = X(k)p_c(k)$ the product of the received symbols times the c-th ranging code, we can write the lag-one autocorrelation of $t_c(k)$ for groups of four consecutive subcarriers as follows [ALT06]

$$R(c) = \sum_{n=0}^{T-1} \sum_{m=0}^{2} t_c(l) t_c^*(l+1), \quad l = 4n + m,$$

where * denotes the complex conjugate and T is the number of tiles of a ranging code[1] . If we assume that the channel coefficients are similar in adjacent subcarriers, the effect of the channel is cancelled in $R(c)$ and only the residual time offset remains. This way, we can define estimators for the ranging code and the time-offset of the uplink signal as follows

$$\hat{c} = \arg\max_{c} \{R(c)\},$$
$$\hat{\phi}_{\mathrm{RNG}} = \mathrm{angle}(R(\hat{c})).$$

Several uplink frequency-offset estimation algorithms can be found in the literature. These algorithms can be divided in three groups, from lower to higher computational complexity: subband, interleaved, and generalized allocation of subcarriers. Ranging in Mobile WiMAX is an example of generalized allocation where the subcarriers reserved to the ranging process can take up any position in the available spectrum. The algorithms defined for this kind of structures are based on a Joint Maximum Likelihood (JML) estimation of the channel response and the frequency offset, but with a very high complexity [MKP07].

The uplink synchronization algorithms selected for this design avoid the complexity of JML algorithms by exploiting the redundancy present in the ranging codes. Once the ranging code is known, frequency-offset can be extracted through reconstruction of the transmitted signal sent by the mobile station. To do so, the received pseudo-noise sequence is mapped back to the OFDM symbol. Since the initial ranging forces mobile stations to transmit the same ranging code twice in two consecutive symbols, this property can be used to extract the frequency offset through a correlation computation.

All these operations involve a considerable computational load. However, the processing requirements are reduced considering that the base station has a reasonable time to respond to initial ranging requests, and will not receive such requests in all frames. Furthermore, this task needs to be flexible enough to adapt to the different frame configurations it can receive. For this reason, it has been decided to perform an optimized implementation of this task in the DSP.

3.3.4 Subchannelization and Channel Equalization

Tasks related with the OFDM modulation are placed in the Virtex-4 SX55 FPGA module. The most important operations are the FFT and IFFT, which have been implemented using the

[1] Set to 36 in the IEEE Std. 802.16e.

Xilinx LogiCORE IP Fast Fourier Transform [XILc], allowing for run-time configuration of the transform point size. The IFFT blocks receive a concatenated sequence of all the OFDM symbol subcarriers (including data, pilots and guards) of each subframe to output the baseband complex signal in time. As this OFDM signal has a high peak-to-average power ratio (PAPR), special care must be taken with the signal peaks which should be clipped to avoid overflows in the fixed point representation. No other PAPR reduction techniques are used in the current implementation.

The FFT and IFFT blocks use these configuration registers:

CP_size (UFix_2_0) Selects the cyclic prefix used.

Nfft (UFix_1_0) Selects the FFT size used.

OFDM_symbols_UL (UFix_16_0) The number of OFDM symbols in the uplink subframe. Only needed in the MS IFFT block.

postfix_mask (UFix_24_0) Defines the OFDM symbols that should be transmitted with cyclic postfix. Used when sending ranging requests in the MS IFFT block.

Subchannelization is implemented in the DL/UL PUSC tasks in the DSP to provide the maximum flexibility with respect to the different FFT sizes, burst mapping, and eventual support of other permutation schemes (see Fig. 3.4). Also, an optimized low-complexity equalization is performed inside the reception tasks in the DSPs.

The subchannelization process involves three steps: interleaving, pilot insertion, and randomization of subcarriers according to some permutation scheme. The BS specifies this structure for each frame using the dedicated downlink map (DL-MAP) and uplink map (UL-MAP) messages. As shown in Section 2.2.1, these messages are always placed in a predefined position in the downlink subframe. Correct decoding of these messages is necessary so the MS can obtain the different bursts from the downlink and transmit its assigned bursts in the uplink.

3.3.4.1 Channel Equalization

Channel estimation and equalization is performed by inverting the pilot subcarriers and linearly interpolating the computed values for the remainder subcarriers. This zero-forcing method has been selected because it offers an acceptable performance with a low-complexity implementation as shown in the literature [YUC+07; PW10; HK09; SHE+10]. The low-complexity of the algorithms is required as the tasks are implemented in the DSPs.

The downlink symbols are equalized independently in the frequency domain. However, the uplink tiles are equalized with a bilinear interpolation algorithm. The UL PUSC tile structure is shown in Fig. 3.6 with the pilots (P_i) and the needed channel estimations in data subcarriers (H_i). The bilinear interpolation is performed by first interpolating in the frequency domain the

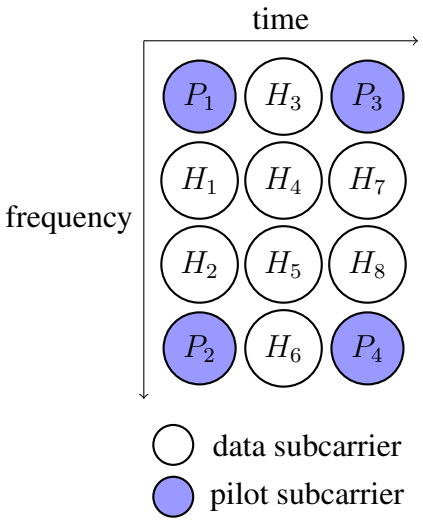

Figure 3.6: UL PUSC tile structure.

first and third symbols,

$$H_1 = \frac{2}{3}P_1 + \frac{1}{3}P_2 \qquad H_2 = \frac{1}{3}P_1 + \frac{2}{3}P_2$$
$$H_7 = \frac{2}{3}P_3 + \frac{1}{3}P_4 \qquad H_8 = \frac{1}{3}P_3 + \frac{2}{3}P_4$$

and then averaging the obtained values to obtain the estimation of the second symbol:

$$H_3 = \frac{P_1 + P_3}{2} \qquad H_4 = \frac{H_1 + H_7}{2} \qquad H_5 = \frac{H_2 + H_8}{2} \qquad H_6 = \frac{P_2 + P_4}{2}$$

The final step involves correcting the data subcarriers multiplying them by the inverse of the channel estimation in each position. To reduce the expensive division operations in the DSP, the P_i values are first inverted so there is no need to perform an inversion of each H_i value. This simplification slightly deteriorates the equalization precision.

3.3.5 Channel Coding

As shown in Fig. 2.1, the channel coding blocks in transmission are: randomizer, FEC encoder, interleaver, repetition coder (optional) and modulation (symbol mapper). The decoding steps are: repetition decoder (averages the received symbols), soft-decisor (symbols to soft-bits), deinterleaver, FEC decoder and randomizer.

These operations are mainly implemented in a Virtex II FPGA (see Fig. 3.4), although the optional repetition coding step performed over the constellation-mapped data and the processing control are both carried out in the DSP, using the FPGA as a coprocessor.

The proposed design supports a variable-rate TBCC coding scheme with constellation sizes varying from QPSK to 64-QAM, both in the downlink and the uplink. The implementation is based on the convolutional encoder [XILa] and Viterbi decoder [XILb] Xilinx IP cores.

There are several techniques to design TBCC using standard convolutional encoders and Viterbi decoders [CS94]. The chosen technique offers a good trade-off between computational complexity and performance. The encoder is implemented adding a cyclic prefix to each FEC block with a size equal to the constraint length (in the case of WiMAX, such a value is set to 7). On the other hand, the decoder concatenates the first bits of the block at the end, and vice versa, hence removing the additional bits from the decoder output.

The size of the chunks added at the beginning and at the end of the blocks is equal to the traceback length of the Viterbi decoder. If a block is shorter than the traceback length, it is just sent three times to the decoder and only the output corresponding to the second repetition is considered.

The soft-decisor obtains the soft-bits from the constellation symbols. These soft-bits together with the puncture pattern are the input to the Viterbi decoder. The soft-decisor uses the simplified demapper described in [TB02] allowing us to implement the operation with low FPGA resources. The obtained soft-bits have a width of 3 bits which are enough to obtain good results. Increasing the soft-bits width has minimal impact on bit error ratio (BER) performance but results in a significant increase in resource usage [XILb].

These tasks use the following configuration registers:

modulation (UFix_2_0) Selects the modulation: 4-QAM, 16-QAM or 64-QAM.

rate (UFix_2_0) Selects the coding rate: 1/2, 2/3 or 3/4.

burst_slots (UFix_16_0) The number of slots in the burst.

seed (UFix_15_0) The seed to initialize the pseudorandom binary sequence (PRBS) generator used in the data randomization block.

Additionally, the decoder computes the error vector magnitude (EVM) of the received symbols and sends this value to the *PHY Control* task. The EVM is obtained employing the soft-decisor to estimate the transmitted symbols:

$$\text{EVM [dB]} = 10\log_{10}\left(\frac{\sum_{i=1}^{M}|R(i)-I(i)|^2}{\sum_{i=1}^{M}|I(i)|^2}\right)$$

where $R(i)$ are the received IQ symbols and $I(i)$ are the constellations points closest to the received symbols, i.e., the decisor output. This metric is used to provide an estimation of the carrier-to-interference-and-noise ratio (CINR), and it is verified that the algorithm provides accurate values of the CINR as long as decision errors are low. Otherwise, the CINR is overestimated.

3.3.6 Physical Layer Control

This task is the central component of the PHY layer. It controls all the operations performed by the remaining PHY tasks, either by setting the configuration registers of each FPGA task

or by interacting with the other DSP tasks. The channel coding and decoding is carried out using the Virtex II as a coprocessor since it includes the FEC and constellation mapping tasks. Only the repetition coding is performed in the DSP as it does not require too much processing power. The subchannelization is controlled by direct communication with the PUSC tasks with a custom protocol.

The communications with the MAC CPS task are performed using the so-called OFDMA PHY SAP specification defined by Intel for its BSs [COR07]. Such a SAP defines the way the MAC and PHY layers exchange the information regarding subframe structure, burst data, ranging codes, etc. This SAP was also extended to support the features of the MSs.

In the SS, the frame control header (FCH) and DL-MAP bursts are decoded in this task so the DL subframe can be equalized and decoded as soon as possible. First the four repetitions of the FCH burst are averaged so it can be decoded and the configuration of the DL-MAP burst can be obtained. Then the DL-MAP burst is retrieved and decoded so the remaining bursts in the DL can be correctly decoded. This way we avoid the delay of forwarding these critical bursts to the MAC tasks to decode them.

3.4 Mobile WiMAX MAC Layer Implementation

As shown in Fig. 3.4 , the MAC layer is implemented in two different tasks: MAC CS and MAC CPS. The security sublayer implementation is included in the CPS. Communications between CS and CPS are performed using a custom MAC SAP protocol.

The MAC CPS task is the main responsible of the operations done inside the MAC Layer: managing the state of the connections, determining or decoding the frame structure, scheduling data delivery for different service classes, adding headers, etc.

Fig. 3.7 shows the operations performed to generate and decode protocol data units (PDUs) in this sublayer. In transmission, SDUs arriving from the CS are queued according to their connection to wait for transmission. When the scheduler decides to send a data SDU, it is first fragmented according to its size. The obtained fragments are packed into PDUs. The data is also encrypted and/or authenticated depending on the service flow configuration. Finally, the PDUs are built following the format explained in Section 2.3.1, including the calculated header check sequence (HCS) and cyclic redundancy check (CRC) codes. These PDUs will be concatenated inside their corresponding burst before the bursts are sent to the PHY.

At reception, the integrity of the received PDUs is first checked by calculating the HCS and CRC codes. The header length field must also be verified in case the HCS fails to detect the errors in the header. The optional decryption and authentication steps also check the data integrity of the PDU. If all the verifications are correct, the fragments of each PDU are unpacked. To reconstruct the original SDU, it is necessary to save the received fragments while the SDU is not complete. If ARQ is not enabled and a fragment is missing, all fragments associated with that SDU are discarded. Finally, the SDUs are stored in a queue to be sent to

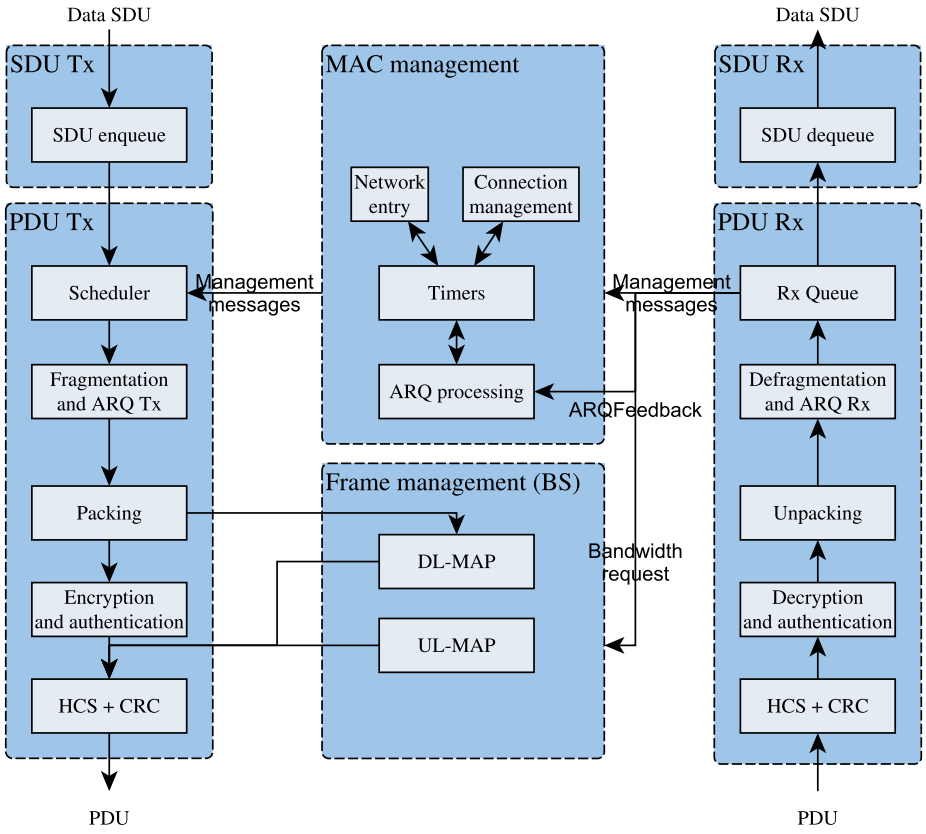

Figure 3.7: Diagram of the packet processing in MAC layer.

the CS when possible.

When ARQ is enabled for the connection, the fragmentation process in Fig. 3.7 is done following the rules of the ARQ process: fragmentation is done according to the ARQ block size and the transmission window is updated. Besides, the received ARQ Feedback messages are used to know whether new or old fragments must be sent, avoiding the retransmission of blocks already received in the other station.

The frame management module is only present on the base station. It manages the resources available on the DL and UL and controls the burst layout. It is therefore also responsible for generating the DL-MAP and UL-MAP messages. To manage the DL subframe, the PDU Tx module informs this module of each new PDU to be transmitted along with its burst profile. In the case of the UL, the received bandwidth requests are used to distribute the resources among the different SS taking into account their quality of service (QoS) requirements.

Since it is the base station that determines the frame structure, the subscriber station uses the information received on the maps to extract the DL bursts and fill its assigned UL burst.

The MAC management module is the central module of the stations that is responsible for following the management protocols specified in the standard. Management messages are generated by this module and are sent like conventional SDUs, although ARQ is never used and

messages are not encrypted, only authenticated. Received management messages are processed in an analogous way and sent to the MAC management module.

3.4.1 Frame Management (BS)

The frame management module is responsible for the accounting of the radio resources available given the current profile configuration. During PDU generation, the available space inside the downlink subframe is checked iteratively, and while it is possible, new fragments are taken from the SDU queues and added to the PDUs. As a result of this process, a DL-MAP management message is also generated with the description of the bursts. This message is also inserted into a PDU, mapped to a burst, and sent to the PHY layer like a regular burst.

Multiple burst-mapping proposals for Mobile WiMAX are presented in [SJT09]. Our implementation uses the so-called Ohseki algorithm [OMI07], a reference algorithm considering complexity, requested bandwidth, and the shape of the downlink burst. The frame management module implements this algorithm and uses information about the burst profile used by the target MS to decide the burst to be used to map its PDUs. Potentially, all users sharing the same burst profile (i.e. modulation and channel coding) would receive all their PDUs inside the same burst.

Resource management in the uplink is more flexible since it is only necessary to indicate the number of slots allocated to each station. The size of such allocations should be decided by the MAC layer considering the QoS constraints and the bandwidth requests received from each user. The current implementation equally distributes all the available bandwidth between the users. The MS manages the available space using a similar scheme in the downlink, but using only one burst with the size assigned in the UL-MAP management message by the BS, hence simplifying the allocation process.

3.4.2 QoS Scheduler

The main function of the scheduler is to select the data to be sent from the connections considering the QoS requirements of each service flow and the space available in each subframe. Additionally, in the BS, it is necessary to implement an UL resource scheduler so the different stations can transmit according to their needs and QoS requirements.

The QoS schedulers in BS and SS try to ensure the QoS requirements by processing the service classes in priority order, in a similar way to the method shown in [SAY+06; BN09]. The deficit round robin (DRR) algorithm [SV96] is also used to process the active connections of each service class in a fair and efficient way.

Fig. 3.8 shows the mechanism used by the scheduler to ensure QoS requirements. The connections are processed in priority order assigning them at least the minimum required bandwidth. If starvation is detected in low priority classes, a small amount of resources are

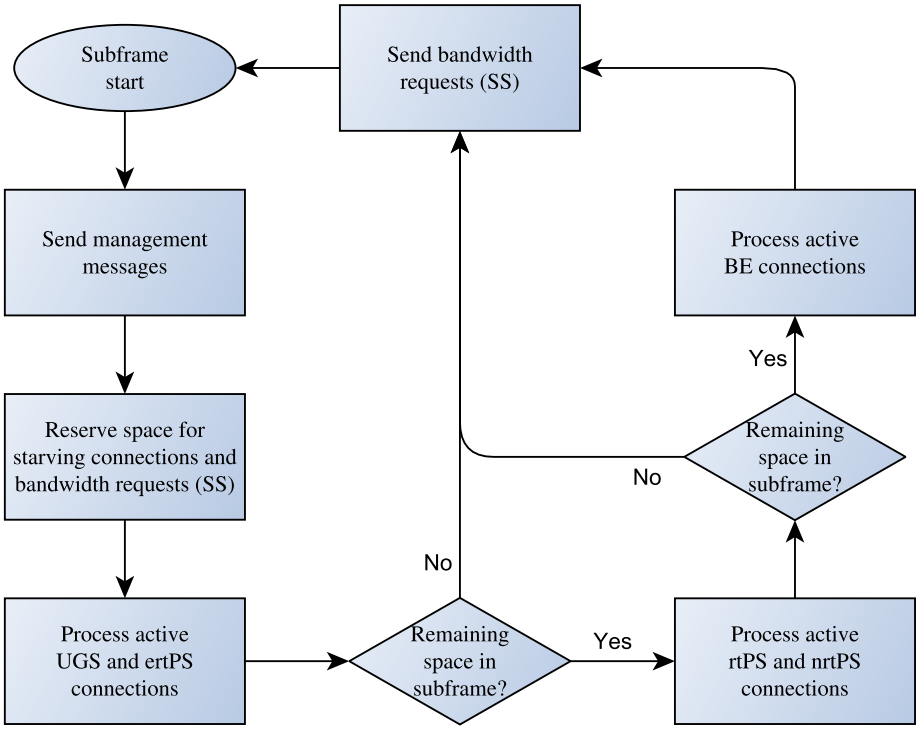

Figure 3.8: Flowchart of the scheduler operations to satisfy the QoS requirements.

reserved for them. The space needed for sending bandwidth requests is also reserved in the subscriber station (SS).

As shown in previous chapter (Table 2.4), the standard defines various QoS parameters depending on the service class. The following parameters are considered in this implementation:

- Minimum Reserved Traffic Rate (MRTR): It defines the minimum average rate to be guaranteed to the service flow.
- Maximum Sustained Traffic Rate (MSTR): It defines the maximum rate that the service flow can reach.
- Traffic Priority: Specifies the priority assigned to a service flow.

Latency and jitter parameters are only defined in the highest priority service classes (UGS and ertPS). The QoS scheduler is designed to minimize the latency in these service classes and therefore it is not necessary to take these parameters into account.

As shown in Fig. 3.8, the connections are grouped in this way:

- Group 0: Management connections.
- Group 1: unsolicited grant service (UGS) and extended rtPS (ertPS).
- Group 2: real-time polling service (rtPS) and non-real-time polling service (nrtPS).
- Group 3: best effort (BE).

Therefore, there is a list of active connections for each group, where connections are added each time data is queued. These lists are then processed using the DRR algorithm, except for Group 0, where management messages have top priority and are all sent.

Table 3.1: DRR parameters for each service class.

Service class	*Quantum*	*MaxBytes*
UGS	MRTR	*Quantum*
ertPS	Between MRTR and MSTR	*Quantum*
rtPS	MRTR	MSTR
nrtPS	MRTR	MSTR
BE	Depends on Traffic Priority	MSTR if defined, ∞ otherwise

The DRR algorithm defines two parameters:

- *DeficitCounter*: It is an integer that accumulates the amount of data that can be extracted from a connection.
- *Quantum*: It is the increment that is made on the *DeficitCounter* each time a connection is accessed.

The original DRR algorithm is only allowed to extract complete packets from the queues, i.e., when the *DeficitCounter* is smaller than the next packet size, the packet cannot be sent. However, 802.16 MAC layer allows fragmenting packets to make a better use of the available space in the bursts. We could fragment the SDUs when the *DeficitCounter* is smaller than the size of the SDU but this would increase the overhead unnecessarily. In our implementation we only fragment an SDU when the remaining space in a burst requires it or to avoid exceeding the MSTR.

In order to implement a scheduler that satisfies the QoS requirements using the DRR algorithm, a data limit for each subframe is defined per connection, depending on its service class. This way the *Quantum* and *MaxBytes* parameters are defined differently for each service class, as shown in Table 3.1.

On the one hand, this configuration ensures a fair resource distribution between connections based on their minimum rate. On the other hand, the data rate never exceeds the maximum allowed rate for each connection. The UGS and ertPS classes are special cases in which a fixed amount of data to be transmitted is assigned for each subframe and therefore the quantum and the limit take the same value. In the case of BE, there is no defined minimum rate and only the Traffic Priority parameter is used to prioritize between connections.

Finally, the UL resource scheduler is implemented by taking bandwidth requests into account, so for each SS a number of slots are allocated according to the needs of its connections. This amount of slots is calculated taking into account the MRTR and MSTR parameters of the connections of each station that have requested bandwidth. A few slots are also periodically assigned to allow stations to send bandwidth requests.

Table 3.2: FPGA resource utilization.

	Virtex-II V2000	Virtex-4 SX55	Virtex-4 SX35
Base Station			
Slices	10131/10752 (94%)	13785/24576 (56%)	6580/15360 (41%)
LUTs	13509/21504 (62%)	18356/49152 (37%)	8261/30720 (26%)
RAMB16s	52/56 (92%)	113/320 (35%)	45/192 (23%)
Multipliers	2/56 (3%)	116/512 (22%)	24/192 (12%)
Power	2.07 W	3.93 W	2.21 W
Mobile Station			
Slices	10131/10752 (94%)	14692/24576 (59%)	15358/15360 (99%)
LUTs	13509/21504 (62%)	19951/49152 (40%)	22625/30720 (73%)
RAMB16s	52/56 (92%)	114/320 (35%)	52/192 (27%)
Multipliers	2/56 (3%)	117/512 (22%)	70/192 (36%)
Power	2.07 W	3.99 W	2.79 W

3.5 Resource Utilization

The hardware architecture described in Section 3.2.3 contains three FPGAs and two DSPs per station. FPGAs are the most critical parts and their size should be large enough to enable the implementation of the tasks assigned to them. Table 3.2 shows the FPGA resource utilization in terms of slices, LUTs, RAMB16s and multipliers after the implementation of the previously described OFDMA-TDD Mobile WiMAX PHY. FPGA designs were implemented using Xilinx System Generator and built with Xilinx ISE. Power consumption estimations of each module were obtained using the Xilinx XPower Analyzer tool and they are also included in Table 3.2. Thanks to the design decisions adopted in the previous section, we were able to successfully implement the whole OFDMA-TDD PHY at both the BS and the MS.

The FPGAs resource allocation shown in Table 3.2 considers separately the cases of the BS and the MS. The main difference between both designs lies in the synchronization block in the MS, which requires 58% of the slices of the Virtex-4 SX35. The quantized cross-correlation algorithm is the most demanding block inside this synchronization module. Another difference is caused by the ability of the MS to add cyclic postfixes to the output of the IFFT. This requirement is necessary for sending the initial ranging codes.

Table 3.3 shows an estimation of the individual FPGA resource utilization of each block obtained when compiling them separately. Notice that this results were obtained before the compiler applied its global optimizations to the design. Additionally, the operation frequency of each block is also shown as well as the critical path delay of each module. The internal FIFO blocks shown in Table 3.3 are used to support the communications between the different modules. Also, the TBCC encoder is subdivided into the Symbol Mapper and the FEC TX

blocks, while the TBCC decoder is made up of the Soft-Decisor and the FEC RX blocks.

The Virtex-4 SX55 is a high-resource FPGA that allowed for the implementation of the FFT blocks without a resource-optimized design, hence a pipelined architecture was used allowing for continuous data processing. However, the Virtex-II V2000 is resource limited, which forced us to optimize the FEC design.

Regarding DSP resources, Table 3.4 shows the memory usage of each PHY task and an estimation of the DSP cycles required for the processing performed inside each task. The MAC tasks are not shown as they do not perform symbol-level or bit-level operations, which are the most demanding. The DSP cycles estimation is obtained from a static analysis of the assembly code generated by the compiler. We also present an estimation of the time required to execute each task in the last column of the table. These time estimations were obtained making the following assumptions:

- The 8.75 MHz profile is used with 1024 subcarriers and a cyclic prefix length of 1/8.
- The frame duration is 5 ms, with 25 symbols in the downlink and 18 symbols in the uplink.
- The subframes are used entirely for data transmission.
- Data subcarriers are modulated in 64-QAM and convolutional coding with rate 3/4.
- Every 16 frames, there is a ranging burst of 30 subchannels and 3 symbols.
- The tasks which use the internal DSP memory are executed at 600 MHz, while the tasks that only use ZBTRAM memory are executed at 100 MHz.
- The data copy between the DSP tasks is performed at 800 MB/s. The communication with the FPGAs does not consume DSP time.

The estimation of the total DSP time used is 958.56 µs and 927.89 µs for the BS and MS, respectively. This is an optimistic estimation since we are not taking into account the time consumed by the kernel as well as context switches and interrupt handling. Furthermore, the delay of the communication with the FPGA and the interdependence between the processing tasks can lead up to long waiting times for FPGA data. This means that a good concurrent processing planning is also needed to fulfill the 5 ms frame duration. In fact, to ensure that no timing problems arise during system evaluation, the experimental results were performed with a 15 ms frame duration. The main bottleneck is in the communications with the channel coding tasks, which are used as coprocessors, and the inefficient use of the FPGA pipelined processing, as explained in Section 3.2.2.

3.6 Experimental Results

In this section we present the results of several tests that were conducted to check the performance of the proposed OFDMA-TDD WiMAX PHY implementation. First, in Section 3.6.1, the results of a unit test of the channel coding tasks are shown to validate the processing performed in these tasks. To check the performance of the complete implementation,

Table 3.3: FPGA resource utilization of each processing block.

Block	Slices	LUTs	RAMB16s	Multipliers	Clock Frequency (critical path)
Virtex-II V2000	10752	21504	56	56	
TX FIFO	64	93	2	0	80 MHz
RX FIFO	88	119	4	0	80 MHz
FEC TX	511	827	4	0	80 MHz (12.47 ns)
Symbol Mapper	72	41	0	0	80 MHz
Soft-Decisor	1500	2597	1	2	80 MHz
FEC RX	2260	3591	6	0	80 MHz
Virtex-4 SX35	15360	30720	192	192	
Synchronization (MS)	9110	16806	39	42	80 MHz
Frame Control (BS)	496	1002	25	0	80 MHz
DUC 10 MHz	2455	3447	16	26	
DUC 8.75 MHz	1305	1784	10	13	160 MHz
DUC 3.5 MHz	1266	1769	10	11	
DDC 10 MHz	4567	6901	12	44	
DDC 8.75 MHz	2466	3904	10	15	160 MHz (12.10 ns)
DDC 3.5 MHz	2947	4918	11	13	
Virtex-4 SX55	24576	49152	320	512	
TX FIFO	182	305	15	0	100 MHz
RX FIFO	182	305	15	0	100 MHz
FFT	7184	9129	19	57	100 MHz (9.47 ns)
IFFT (BS)	7551	9799	66	59	100 MHz
IFFT (MS)	8381	11436	67	60	100 MHz (9.79 ns)

Table 3.4: Static analysis of DSP resource utilization.

Task	DSP Cycles per Frame	ZBTRAM Memory	DSP Memory	Estimated Time (μs)
BS+MS: PHY Control (FEC)		3000K BS 5500K MS	0K BS 0K MS	77.11
Repetition coding	Rep. 2: $56 \cdot n_{slots}$ Rep. 4: $83 \cdot n_{slots}$ Rep. 6: $134 \cdot n_{slots}$			3.32
FEC TX preprocessing	$7 + n_{Bunc}/2$			BS 48.67 MS 28.42
FEC RX postprocessing	$9 + n_{Bunc}/2$			BS 28.44 MS 48.69
BS: TX PUSC DL		2000K	618K	168.00
Frame initialization	$6 + N_{fft} + (3 + N_{fft}/4) \cdot n_{symb}$			12.08
Add burst to frame	$147 \cdot n_{subc} \cdot n_{symb}/2$			88.20
Subcarrier randomization	$(11 + N_{used} \cdot 2) \cdot n_{symb}$			67.72
BS: RX PUSC UL		2000K	327K	463.97
Subcarrier randomization	$8501 + (11 + N_{used} \cdot 2) \cdot n_{symb}$			64.96
Extract burst from frame (equalization included)	$6 + n_{slots} \cdot 1140$			399.01
BS: RX Ranging	$36059 \cdot n_{subc}/6 \cdot n_{srang}/3$	500K	0K	112.68
Energy threshold	$82 \cdot n_{subc}/6 \cdot n_{srang}/3$			0.26
Extract ranging code	$21504 \cdot n_{subc}/6 \cdot n_{srang}/3$			67.20
Extract pilots	$144 \cdot n_{subc}/6 \cdot n_{srang}/3$			0.45
Frequency offset	$14329 \cdot n_{subc}/6 \cdot n_{srang}/3$			44.78
MS: RX PUSC DL		1000K	564K	582.84
Subcarrier randomization	$(11 + N_{used} \cdot 2) \cdot n_{symb}$			67.72
Equalization	$425 \cdot n_{subc} \cdot n_{symb}$			510
Extract burst from frame	$(16 + n_{subc} \cdot 8) \cdot n_{symb}/2$			5.12
MS: TX PUSC UL		1000K	196K	131.14
Frame initialization	$14 + n_{slots} \cdot 7$			2.47
Add burst to frame	$6 + n_{slots} \cdot 182$			63.71
Subcarrier randomization	$8501 + (11 + N_{used} \cdot 2) \cdot n_{symb}$			64.96

we set up an evaluation system that uses a channel emulator that implements different time-varying channel models. This way, the evaluation can be carried out in a repeatable as well as in a reproducible way. This channel emulator is described in Section 3.6.2, and the results of the different tests are shown in the remaining subsections.

3.6.1 Validation of the Channel Coding Blocks

The TBCC encoder and decoder tasks have been tested by using a new AWGN task placed in the Virtex II FPGA. This task works as a coprocessor to emulate an additive white Gaussian noise (AWGN) channel. A test program is used in the DSP to measure the error rate with the different modulation and code rate configurations. This test program performs the following operations:

- Data bursts are generated with random bytes.
- This data is sent to the TBCC encoder task to obtain the constellation mapped symbols.
- Noise is added to the symbols using the AWGN task.
- The symbols are decoded with the TBCC decoder to obtain the received bytes.
- The sent and received bytes are compared to count the number of bit errors.

These steps are repeated until a good measurement of the BER is obtained by processing up to $500 \cdot 10^6$ uncoded bits. This process is performed for each noise level and modulation and coding rate. Fig. 3.9 shows the obtained coded BER results with respect to the E_b/N_0. As expected, curves move to the right as the spectral efficiency increases. Also, the 4-QAM results match the BER performance curves in [XILb] for a convolutional code with constraint length 7, showing the correct implementation of the blocks. The 16-QAM and 64-QAM curves achieve the expected performance for a Viterbi decoder with 3 soft-bits, which is about 2 dB better than hard decision decoding.

3.6.2 ITU-R Channel Emulator

In order to validate the real-time implementation as well as to assess the performance of the system, a channel emulator was implemented on a Xilinx Xtreme DSP Development Kit consisting of a Virtex-4 FPGA plus a couple of DACs and ADCs (see Fig. 3.10).

The channel emulator is made up of a channel coefficient generator, an interpolator, a channel filtering stage, and an AWGN generator. It accepts parameters such as the average power and delay of each tap, the noise power, and the intermediate frequency of the input signal. The coefficient interpolation factor as well as the Doppler power spectrum are defined at compilation time and they are fixed during the emulation.

The WiMAX Forum [WIM05] recommends the usage of the ITU-R M.1225 [ITU97] channel models for the evaluation of WiMAX solutions. Three channel models are selected by the WiMAX Forum: Pedestrian A, Pedestrian B, and Vehicular A. The pedestrian channels assume a speed of 3 km/h, while the Vehicular A channel model can be configured with a speed

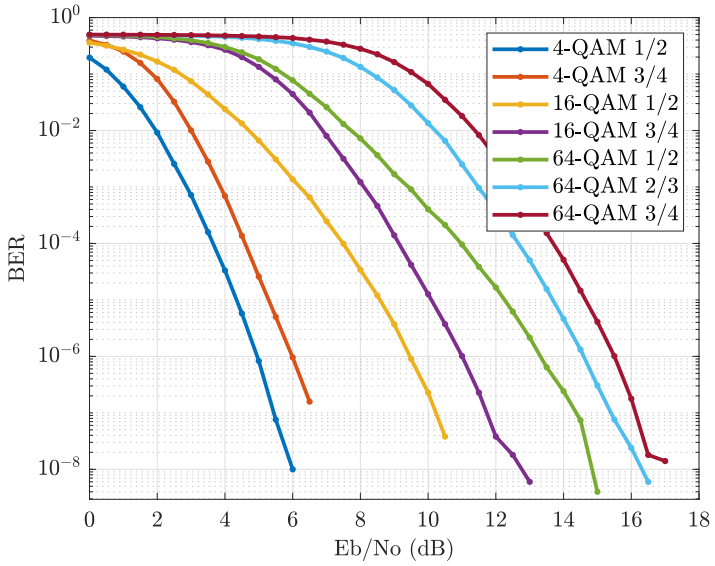

Figure 3.9: TBCC BER vs. E_b/N_0 over AWGN channel.

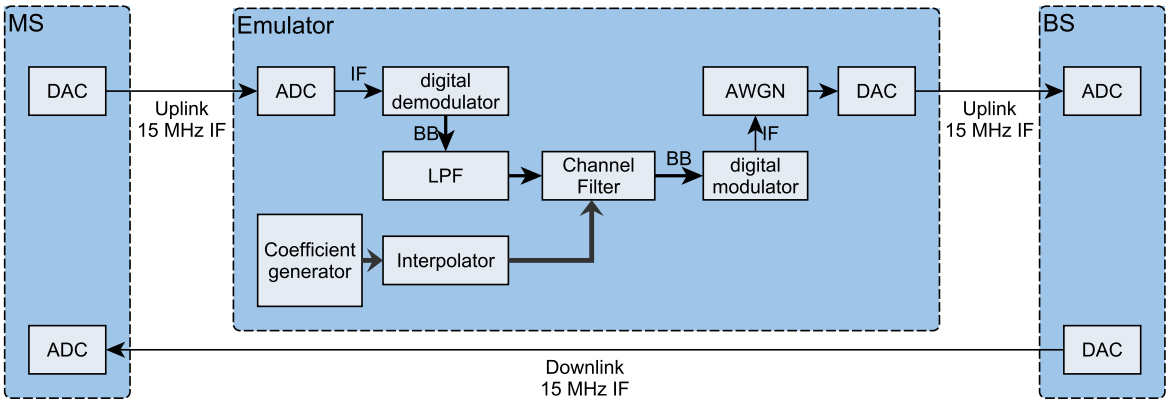

Figure 3.10: Block diagram of the OFDMA-TDD evaluation system configured to test the UL.

of 60 km/h or 120 km/h. The tapped delay line characteristics of these channels are shown in Table 3.5.

The Pedestrian A channel model only contains four paths with the last two being rather attenuated, providing low frequency selectivity but also low multipath diversity. This means that the channel equalization will be easier for this channel, but the probability of all paths being highly attenuated at the same time becomes higher. This can be seen in Fig. 3.11, where the power distribution is shown for a signal that is processed by each channel model. The output signal has higher probability of having very low power (-7 dB or less) with Pedestrian A than with the other channels. Pedestrian B and Vehicular A models provide richer multipath diversity and higher path delay spread than Pedestrian A. They have six paths with much longer delays than Pedestrian A, resulting in higher frequency selectivity, especially Pedestrian B channel.

Doppler spread emulation uses the Jakes Doppler power spectrum density assuming

Table 3.5: ITU-R M.1225 channel models.

	Pedestrian A		Pedestrian B		Vehicular A	
Path	Power (dB)	Delay (ns)	Power (dB)	Delay (ns)	Power (dB)	Delay (ns)
1	0	0	0	0	0	0
2	-9.7	110	-0.9	200	-1.0	310
3	-19.2	190	-4.9	800	-9.0	710
4	-22.8	410	-8.0	1200	-10.0	1090
5			-7.8	2300	-15.0	1730
6			-23.9	3700	-20.0	2510
Speed (km/h)	3		3		60, 120	

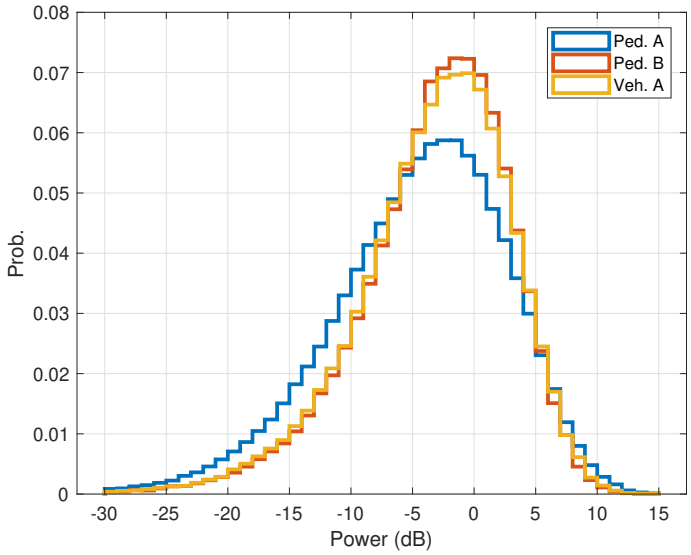

Figure 3.11: Histogram of the channel power gain for the ITU-R channels.

transmissions at 2.4 GHz. Note also that the maximum channel delay (3.7 µs) does not exceed in any case the default 1/8 cyclic prefix length (11.4 µs). Consequently, the system is immune to Inter-Symbol Interference (ISI).

These channels are supported by the implemented channel emulator. In order to obtain adequate performance metrics with respect to the average SNR, the AWGN generator included in the channel emulator is calibrated to match the SNR estimation obtained during the synchronization process.

3.6.3 Uplink Synchronization

The performance of the uplink timing-offset synchronization module was evaluated using the 3.5 MHz profile with 1/8 cyclic prefix (64 samples). The MS was configured to continuously

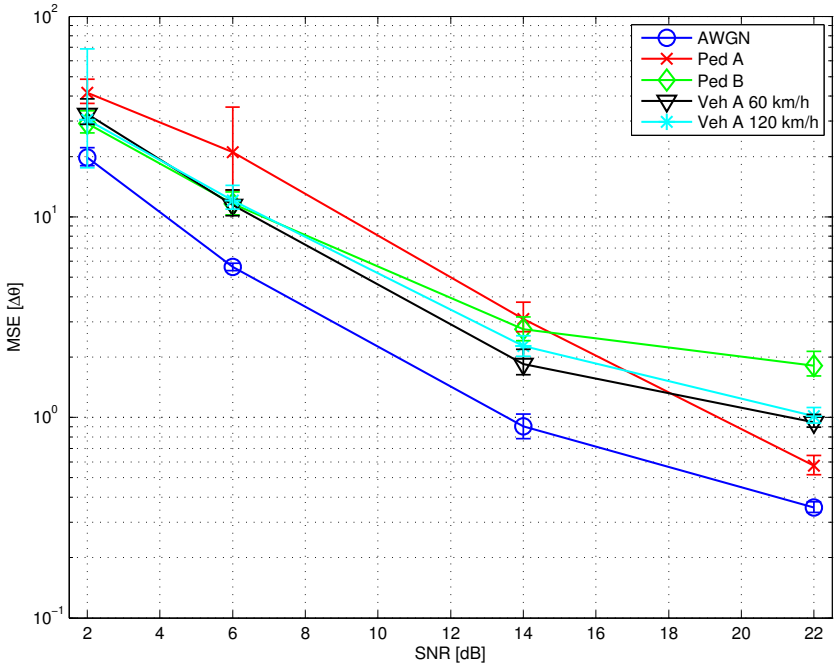

Figure 3.12: MSE of the time offset estimation in the uplink with respect to the average SNR.

send ranging codes in the uplink, and the time-offset estimations computed at the BS were stored. The result of this test is shown in Fig. 3.12 in which the mean squared error (MSE) of the time-offset estimations (expressed in number of samples) is shown with 90% confidence intervals computed using bootstrapping [EH94]. In this 3.5 MHz profile, each sample has a duration of 0.25 µs. It can be seen that the uplink timing-offset implementation is insensitive to the features of the different channel models and provides acceptable estimations in all cases, even at low SNR values. The worst results are obtained with Pedestrian A at 2 dB of average SNR, which achieves a standard deviation of just 6.4 samples.

3.6.4 BER and FER in ITU-R Channels

Several measurements were carried out over the ITU-R channels. In order to measure BER, a known structure for the subframes was used in the downlink and in the uplink. The purpose was to enable the measurement of BER even when the FCH or the DL-MAP messages could not be decoded. However, the undetected frames are ignored, i.e., BER calculation is not affected when the synchronization block fails to detect a preamble. The modulation and coding used in the following figures are QPSK and TBCC with 1/2 and 3/4 code rates.

Fig. 3.13 presents the coded BER for the uplink with the 8.75 MHz profile when the ITU-R channel models are employed. The lack of multipath diversity of Pedestrian A explains that this channel obtains the worst BER performance for both QPSK 1/2 and 3/4. The uplink channel equalization is able to correct the high selectivity of Pedestrian B as this channel achieves the best results. The fast fading of the Vehicular A channels affects the BER results, which are

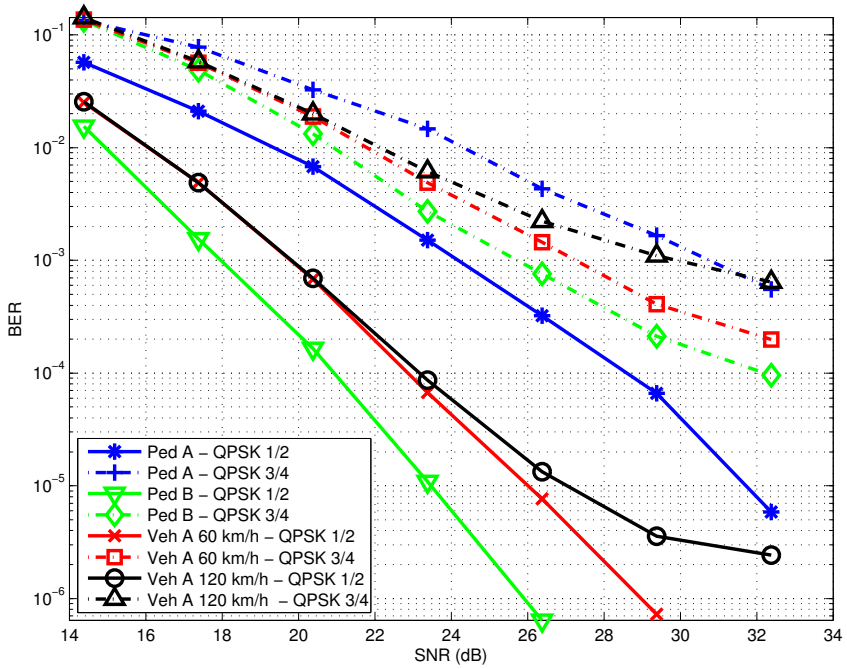

Figure 3.13: Coded BER over ITU-R channel using the 8.75 MHz uplink profile.

not so good as the Pedestrian B ones. The effects of the inter-carrier interference (ICI) caused by these channels are more evident at 120 km/h, as the curves seem to be approaching an error floor at high SNRs.

Finally, Figs. 3.14 and 3.15 show the frame error rate (FER) over the ITU-R channel models for the downlink and the uplink, respectively. The measured burst in the downlink occupies 15 subchannels along 18 OFDM symbols. This corresponds to a total of 6480 data subcarriers per downlink subframe. In the uplink measurement, the burst occupies the complete subframe with 10 080 data subcarriers per uplink subframe. The downlink FER results are heavily influenced by the frequency selectivity of Pedestrian B and Vehicular A channels. The downlink channel equalizer is not able to correct the highly attenuated subcarriers of these channels, generating some bit errors in each frame which the convolutional decoder is not always able to fix, especially at the 3/4 code rate. The additional noise added by the ICI of the Vehicular A channel at 120 km/h worsens the results even more. Pedestrian A channel obtains the best results as it has the lowest frequency selectivity and its low multipath diversity is not as influential as in the case of the BER, i.e., the high number of bit errors of Pedestrian A are clustered in fewer frames than in the other channels. The uplink FER results are better than the downlink ones. They are not so influenced by the frequency selectivity of the channels thanks to the higher pilot density in the WiMAX uplink frame structure, which allows for better channel tracking using the bilinear interpolation explained in Section 3.3.4.1. The results are consistent with the BER measurements (Fig. 3.13), with the exception of the Pedestrian A channel that improves its performance.

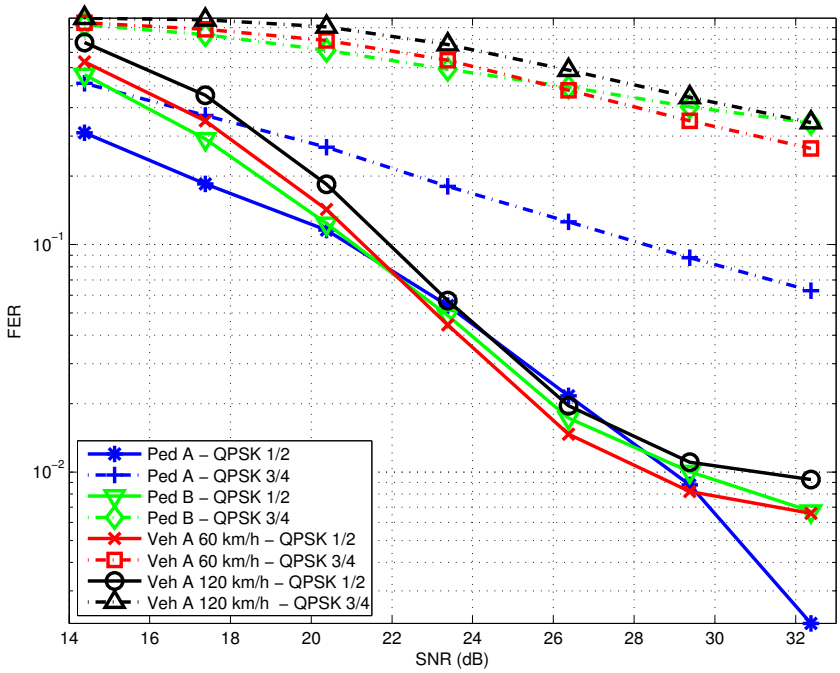

Figure 3.14: FER over ITU-R channel using the 8.75 MHz downlink profile. Bursts of 6480 bits for QPSK 1/2 and 9720 bits for QPSK 3/4.

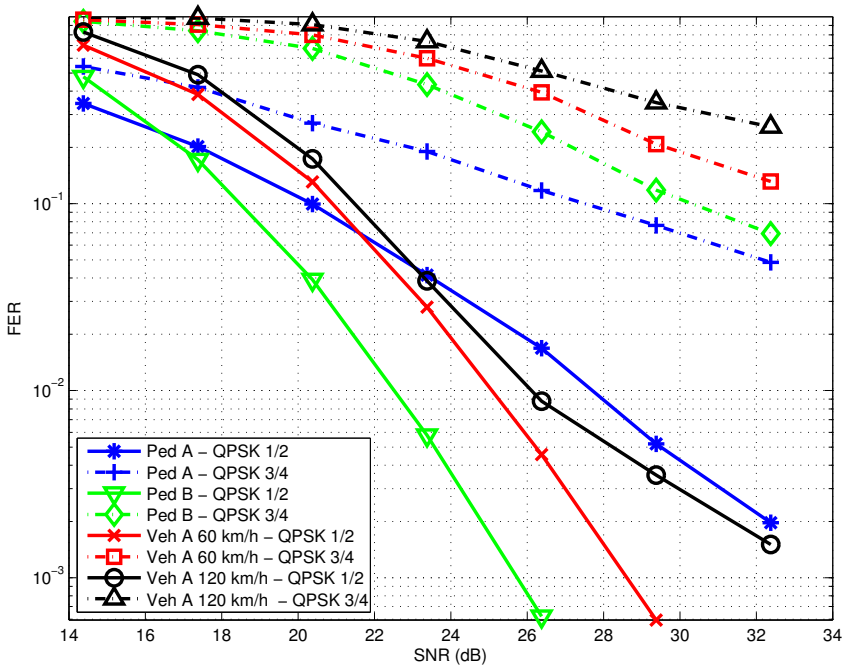

Figure 3.15: FER over ITU-R channel using the 8.75 MHz uplink profile. Bursts of 10 080 bits for QPSK 1/2 and 15 120 bits for QPSK 3/4.

Table 3.6: Throughput measurement configuration.

Parameter	Value	Parameter	Value
PHY	OFDMA	SNR values	14, 17, ..., 32
WiMAX Profile	8.75-MHz	Processed frames per SNR value	40 000
Duplexing mode	TDD	SDU size	1024 bytes
Cyclic prefix length	1/8	QPSK 1/2 max. UL throughput	2016 kbit/s
DL/UL symbols	25/18	QPSK 3/4 max. UL throughput	3024 kbit/s
Frame duration	5 ms		
Permutation schemes	DL/UL PUSC		
DL/UL-MAP MCS	QPSK 1/2	ARQ_WINDOW_SIZE	1024 blocks
Fragmentation	ON	ARQ_BLOCK_SIZE	32 bytes
Packing	ON	ARQ_RETRY_TIMEOUT	20 ms
CRC	ON	ARQ_BLOCK_LIFETIME	50 s
PDU size	max. 2047 bytes	ARQ_RX_PURGE_TIMEOUT	50 s
ARQ	ON	ARQ_SYNC_LOSS_TIMEOUT	OFF
ARQ feedback types	all	ARQ_DELIVER_IN_ORDER	ON

3.6.5 Throughput

Throughput measurements were performed over the same ITU-R channels, in this case affecting both downlink and uplink subframes at the same time. Therefore, the ARQ mechanism is correctly evaluated as ARQ feedback messages can also be corrupted. The channel emulator is shared in both directions in order to simulate the channel reciprocity characteristic of TDD systems. For each measurement, 40 000 frames were transmitted.

The complete configuration parameters of the experiments are shown in Table 3.6. During each measurement, SDUs of 1024 bytes are continuously added to the transmit queue. The PDUs are generated with the maximum possible size up to 2047 bytes. This minimizes the number of PDUs and the overhead introduced by the PDU header, but increases the error probability of the PDU. Furthermore, if some bits within the PDU are corrupted (detected with the CRC field), all ARQ blocks inside the PDU must be sent again and not only the corrupted part of the PDU.

Figs. 3.16 and 3.17 show the throughput values obtained with this configuration for both the downlink and the uplink. It can be seen that the QPSK 1/2 configuration almost achieves the maximum raw throughput of 2016 kbit/s [2]. There is some overhead added by the generation of PDUs and the unused burst space, which cannot always be completely filled, and some padding has to be added. In the uplink, the periodical addition of reserved ranging bursts also reduces the maximum achievable throughput. For QPSK 3/4, it is not possible to achieve the maximum

[2]This is the maximum raw throughput for the UL. The DL has a higher value but the throughput is limited by configuring an UGS service flow with this data rate. The same applies for QPSK 3/4.

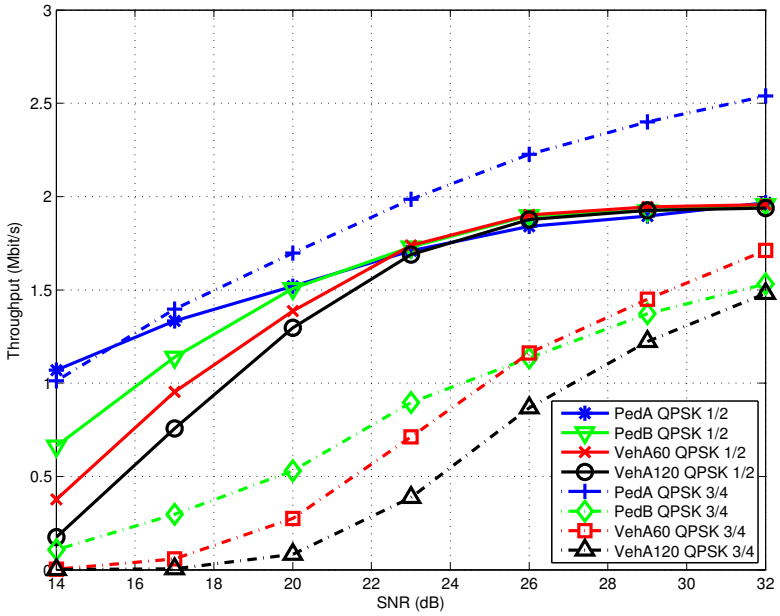

Figure 3.16: Throughput in the downlink.

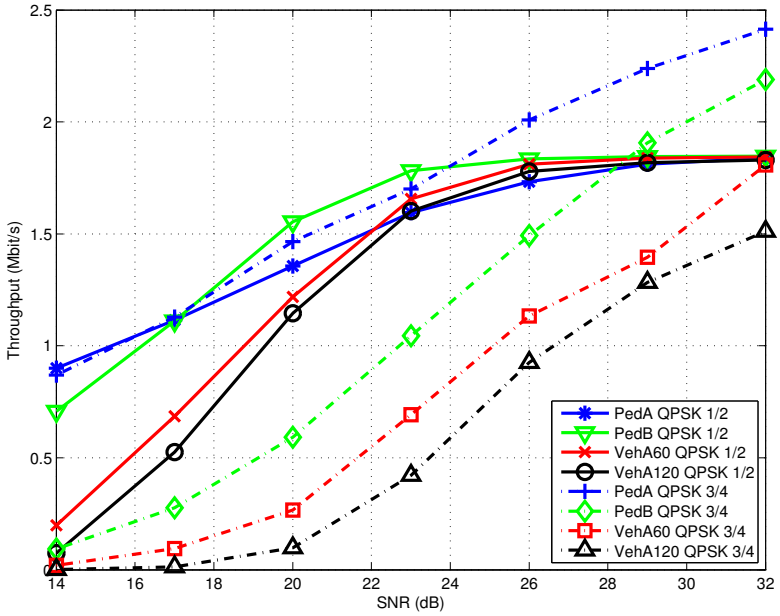

Figure 3.17: Throughput in the uplink.

throughput (3024 kbit/s) in the SNR levels tested in these scenarios since the highest measured throughput was 2.5 Mbit/s.

All the throughput values obtained are consistent with the FER measurements shown in Figs. 3.14 and 3.15. In the DL, the most favorable channel is Pedestrian A, which yields the highest throughput for all SNRs with QPSK 3/4. In the UL, Pedestrian A with QPSK 3/4 also obtains the best results except for the 18 to 24 dB SNR range, where Pedestrian B with QPSK 1/2 offers a higher throughput thanks to the low FER obtained.

These measurements also show the modulation and coding rate that should be selected for each channel. For the Pedestrian A channel, QPSK 3/4 configuration outperforms the QPSK 1/2 throughput at SNRs higher than 16 dB. Pedestrian B channel achieves better results using QPSK 1/2, except for SNRs higher than 29 dB in the uplink. Finally, the Vehicular A channel measurements also obtain higher throughput using the QPSK 1/2.

3.7 WirelessMAN-Advanced Air Interface

As shown in Section 2.4, the IEEE 802.16m standard introduces a completely new definition of MAC and PHY known as Advanced Air Interface (AAI). The proposed architecture needs some modifications to implement this new standard. The changes that affect the architecture are mainly in the PHY layer implementation, as the new MAC layer can be implemented in the same DSP as before.

To implement the new 20 MHz profile the FFT size needs to support 2048 subcarriers, and the DUC/DDC blocks have to support an additional up/downsampling factor of $25/7$. The new frame structure and the dynamic behavior of the subframes imposes the need to improve the *Frame Control* block to be more flexible.

The WiMAX Forum defines the minimum number of advanced base station (ABS) antennas as two, which leads to the need to replicate processing in transmit and receive chains only in the ABS.

To support the new extended length ranging preambles with reduced subcarrier spacing, the size of the FFT needs to be increased. Hence an adjustable FFT size in the corresponding processing blocks could be desirable.

Channel coding in 802.16m only requires the convolutional turbo code (CTC) and TBCC FEC schemes. It would be necessary to implement two encoding and decoding algorithms inside the FEC processing block. The mandatory HARQ processing can be addressed inside the *PHY Control* task.

The proposed architecture can be readily adapted to give support to an implementation of the AAI. As an example, an adaptation of the architecture is shown in Fig. 3.18, in which an ABS and advanced mobile station (AMS) are configured to support a 2×1 multiple-input-multiple-output (MIMO) scheme, which would require an increase of hardware resources to support the implementation of the new functionalities. As noted before, the *Frame Control*, *Synchronization*, and *FFT/IFFT* blocks must be enhanced to support the new subframe structure. The new subchannelization scheme can be implemented in the same DSP as the old *PUSC* blocks, as well as the channel equalization step. The ABS MIMO requirements impose the need to replicate the transmit and receive chains, forcing the increase of hardware resources in the FPGA and in the DSP modules, since they have to implement the new precoding techniques. In this case, we have concluded that a new DSP needs to be added into the ABS to accommodate the increase of the baseband processing needs. Also, the HARQ technique

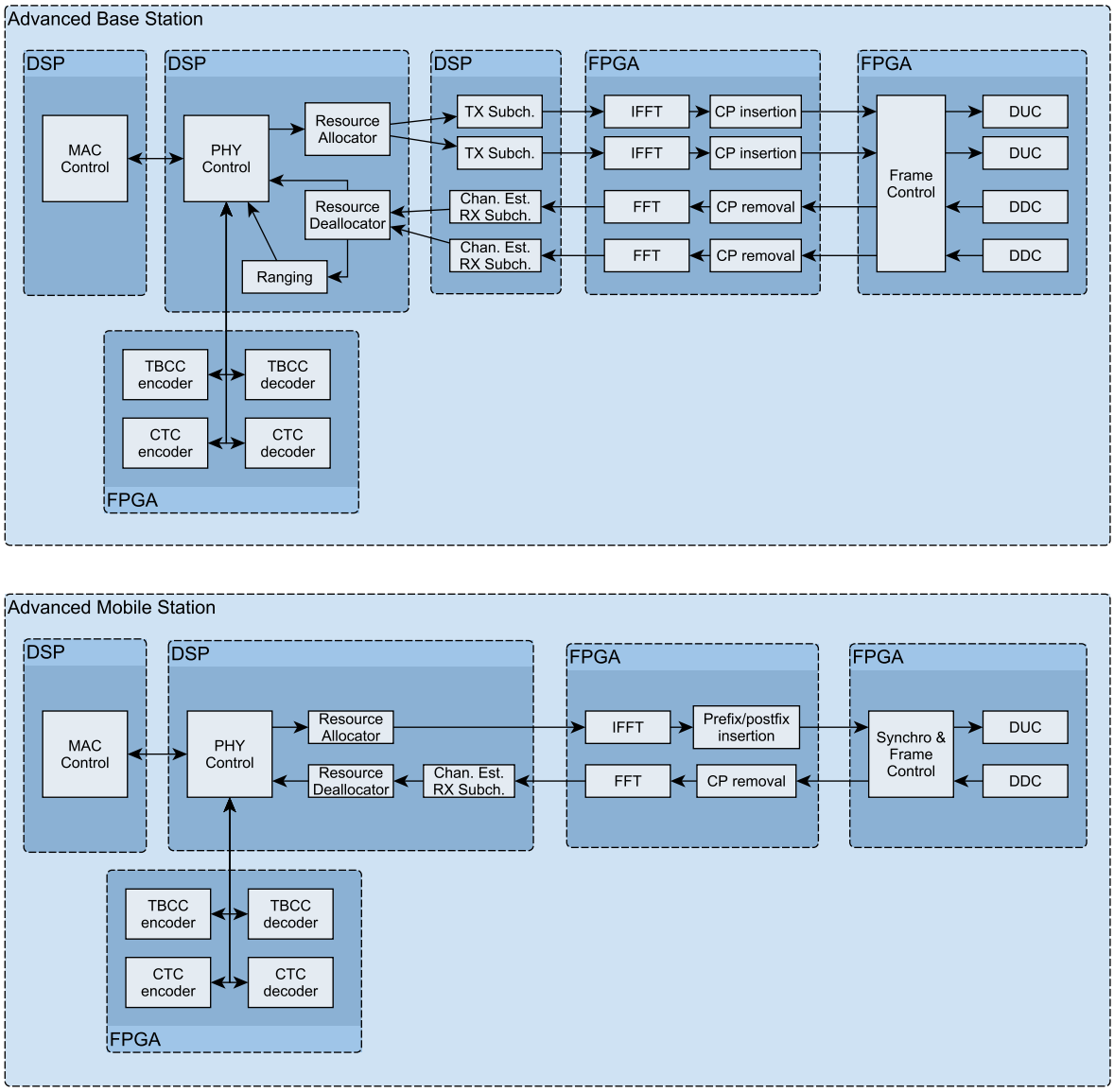

Figure 3.18: Proposed 802.16m architecture.

requires an increase in memory due to the need to store the received bursts. Finally, the new FEC schemes need to be implemented in a larger FPGA as the Virtex-II has not enough resources.

3.8 Conclusions

This chapter details a real-time implementation and validation of full-duplex OFDMA-TDD WiMAX transceivers that contain the complete PHY and MAC layers. The BS and MS transceivers are based on a cost-effective SDR hardware architecture made up of FPGA and DSP modules that allows us to implement all the mandatory functionalities of the WiMAX standard. A custom development methodology was followed and the different design decisions adopted were detailed. The final bidirectional implementation was successfully accomplished in

the selected hardware by making the most of the resources and distributing the tasks between the FPGAs and DSPs in a balanced way. The resource usage of each implemented task is shown, including the FPGA components usage and a static estimation of the most time-consuming processing in the DSP. The utilization of the proposed hardware architecture to implement the WirelessMAN-Advanced Air Interface is also discussed.

The implementation is validated in a repeatable and reproducible way by means of performance measurements carried out with the help of a real-time, custom-made channel emulator. The performance evaluation of the real-time implementations of both PHY and MAC layers is shown based on representative figures of merit such as bit and frame error rates or throughput and considering the reference scenarios recommended by the WiMAX Forum: Pedestrian A and B, and Vehicular A. These channel models are supported by the custom channel emulator.

Firstly, the implemented TBCC channel coding processing is validated using a custom design that allows us to obtain the BER performance under an AWGN channel independently of the rest of the system. Secondly, BER and FER measurements were carried out for both the uplink and the downlink considering the 8.75-MHz profile. Finally, throughput measurements including the MAC layer processing with the ARQ mechanism enabled are also provided with the aim of assessing the actual performance of the complete WiMAX system in realistic propagation conditions. The measurement results confirm that the proposed implementation is suitable for the scenarios modeled with the aforementioned channel models.

Chapter IV

System-Level Simulations of Communications in Transportation Systems

Modern railway transportation systems need a reliable communication infrastructure providing very high data rates and low latencies for applications such as communications-based train control (CBTC) or video surveillance. Before the deployment of a network infrastructure for these applications, it is important to perform network simulations in order to predict its performance under different situations and prevent possible problems.

To carry out these simulations it is common practice to use link-level and system-level simulators. To perform simulations of a complete system, it is more useful to carry out system-level simulations, in which the higher layer network protocols can be simulated using simplified models of the radio channel.

In this chapter, the suitability of different communication technologies for subway environments is evaluated. Long Term Evolution (LTE) and Wi-Fi deployments are simulated using tunnel propagation channels based on deterministic models and real channel measurements.

This chapter is mainly based on the following co-authored publication:

- Ángel Carro-Lagoa, Tomás Domínguez-Bolaño, José Rodríguez-Piñeiro, Miguel González-López, and José A. García-Naya. "**Feasibility of LTE for train control in subway environments based on experimental data**". *Proc. of 2019 27th European Signal Processing Conference (EUSIPCO)*. 2019, pp. 1–5.
  DOI: 10.23919/EUSIPCO.2019.8903070

This chapter is structured as follows. An introduction to the communications systems in subway scenarios is presented in Section 4.1. The most common services provided in subway scenarios are presented in Section 4.2 with their quality of service (QoS) requirements. The LTE and Wi-Fi modules of the ns-3 simulator are described in Section 4.3, including

the implemented modifications and enhancements needed to correctly simulate the subway scenario. In Section 4.4, a deterministic and a measurement-based propagation models for tunnel environments are presented. A deployment with three subway stations is simulated in Section 4.5 using the measurement-based channel model. In Section 4.6, a complete subway line deployment is detailed and several simulations are performed using the deterministic channel model. Finally, the conclusions are presented in Section 4.7.

4.1 Introduction

The railway industry is evolving their conventional signaling systems to communication-based systems demanding reliable and fault-tolerant infrastructures. Examples of these modern communication-based signaling systems are the CBTC system and the European Train Control System (ETCS). In this chapter, we will focus on the CBTC system as it is more common in subway environments.

CBTC systems require a communications infrastructure that gives support to their QoS needs, being a low latency the most critical one. Also, additional services are being deployed in public transportation systems that demand high data rates, e.g., closed-circuit television (CCTV). However, these throughput demands cannot be satisfied by legacy communication systems such as GSM for Railways (GSM-R). The selected communications system must be able to provide all these services fulfilling their QoS requirements.

In subway scenarios, IEEE 802.11 wireless local area network (WLAN) deployments are considered as a communication infrastructure for CBTC [FS17] [GRR17]. The main advantages of Wi-Fi are its low cost and the usage of the freely available industrial, scientific and medical (ISM) radio bands. However, the usage of this standard has several drawbacks as it was initially designed to replace the cables in local area networks. To support long-range and high-mobility scenarios, Wi-Fi deployments require several access points supporting the latest standard amendments such as the IEEE 802.11k/r/v. Nonetheless, interoperability among different manufacturers implementing these amendments is still unclear, as it is very common to use proprietary modifications of the standard [GRR17]. Additionally, managing the interference caused by other devices as well as that produced by neighbour access points is yet another issue.

The 3GPP LTE and the LTE-Advanced (LTE-A) standards are good alternatives for communications in subway environments. The disadvantages of LTE are its higher equipment cost and the licensing costs associated to the frequency bands. On the other hand, LTE provides mobility support, flexible QoS configuration, long range communications, etc. Also, LTE allows for sharing the deployed infrastructure with the passengers.

There are two ways of providing wireless coverage in tunnels: using radiating cable ("leaky feeder") or distributed antennas. Hybrid solutions are also very common [TOL15]. The leaky feeders are useful in complex environments as they provide uniform coverage of the area,

simplifying the deployment design [GRR17; HED09]. However, they are expensive to install and maintain, specially when used at frequencies higher than 2 GHz. In this chapter we will focus on antenna deployments because, according to [GUA+12], antennas are ten times cheaper to deploy than leaky feeder solutions and easier to maintain. The main drawback of antennas is the increased complexity in tunnel radio planning. Radio propagation inside tunnels depends very much on the characteristics of the tunnel, which makes measurement campaigns mandatory [TOL15].

In this chapter, we study the viability and performance of LTE and Wi-Fi for supporting the needed services in subway environments. We use Wi-Fi and LTE modules of the ns-3 network simulator to check if the QoS requirements of all the applications are met [HLR08] [PRO21] [PBM11]. Two channel models are used to correctly simulate the subway environment. On the one hand, a simplified channel model was developed from measurements carried out in the Madrid Metro [DOM+18]. On the other hand, a channel model based on modal-theory was enhanced to take into account the curves and slopes of the track.

Although previous works are focused on the simulation of subway scenarios with CBTC traffic, none of them uses a specific channel model for subway scenarios based on results from a measurement campaign. In [KHA+13], the OPNET simulator was used to study the LTE time-division duplexing (TDD) performance with different QoS configurations. However, the used channel model is unknown and only the uplink (UL) performance was considered. Zhao et al. [ZHA+14; ZHA+16] presented an integrated train ground communication system based on LTE TDD. They set up a testing environment, to verify that all the defined QoS requirements are fulfilled. The testing environment includes a commercial channel simulator to evaluate the system in an urban rail transit environment with speeds up to 200 km/h. A similar hardware setup is employed in [WAN+19] to perform a reliability analysis of the CBTC communications using a 1.4 MHz LTE network. Neglia et al. [NEG+16] evaluated the performance of CBTC in Wi-Fi deployments with an analysis of the probability of emergency brakes. They also implemented new modules for the ns-3 simulator, including a CBTC module, to validate their analysis with a Wi-Fi deployment and test the behavior of the handover process. Finally, in [WEN+15], the BRaVE railway simulator is integrated with the OMNeT++ network simulator to carry out CBTC simulations using a channel model based on [ZHA03].

4.2 QoS in Subway Communications

This section discusses the QoS requirements that the network infrastructure must meet for the correct functioning of the railway signaling protocols and other deployed services. Parameters such as communication latency or packet loss and their impact on the control protocols are considered.

The most common services deployed in a subway environment that use the train-to-ground connection are the following [ALL18; GRR17; KHA+13; ZHA+14]:

- Mission critical services.
  - CBTC: Signaling system to control and monitor the position and speed of the trains.
  - Voice communication: Public safety service that communicates the train drivers with the operational control center (OCC) controllers. Currently, this service is usually provided by a separate private mobile radio network such as Terrestrial Trunked Radio (TETRA) or Project 25. However, this service can be provisioned using the same common Wi-Fi or LTE infrastructure. Moreover, the LTE standard already includes public safety features.
- Applications for subway operator.
  - CCTV: On-board video surveillance of the train wagons. The video is sent from the trains to the OCC or the security center.
  - Platform TV: Real-time video surveillance of the platforms. This video stream is sent to the train cabin so the driver can see the platform before the train enters the subway station.
  - Maintenance: This service includes telemetry tasks to monitor the status of on-board sensors and equipment. Also, other maintenance operations can be considered such as on-board file update.
- Passenger services.
  - Passenger information: Two services are usually deployed to inform the passengers. The Passenger Information System (PIS) transmits multimedia messages for travelers, such as the next station on the line. The public announcement service is usually used by the train drivers to communicate with the passengers, but it can also be employed by the control center agents when the service supports using the wayside-to-train connection.
  - Internet on board: Provides connectivity inside the trains to give internet access to passengers. This can be provided by deploying Wi-Fi access points, or by enhancing the access to mobile operator services with repeaters when the penetration loss into the trains is too high [TOL15]. This service is not considered in this thesis.

It is very common that these services are deployed using different technologies with independent network infrastructures, specially in the case of mission critical applications. In this way, crashes and malfunctions in a network will only affect the services that make use of it, allowing the rest of the systems to continue working properly. However, the cost of maintaining all the different infrastructures can be very high and expensive. In this thesis we explore the feasibility of using a common technology for all these services. It is crucial to provide a redundant and reliable architecture that allows prioritizing mission critical services to ensure that their requirements are met.

The QoS requirements of these services differ depending on their configuration. In Table 4.1 the throughput requirements defined by different sources are shown. The throughput values are specified for each train in the downlink (DL) and UL direction. Some works do not consider

Table 4.1: Throughput requirements (for each train) in the literature.

Service	[ALL18]	[MB17]	[KHA+13]	[NOK16]	[ZHA+14]
CBTC (DL/UL)	150 kbit/s	100 kbit/s	4.8 kbit/s (DL) 8 kbit/s (UL)	50 kbit/s	200 kbit/s
Voice (DL/UL)	150 kbit/s	150 kbit/s	64 kbit/s	—	100 kbit/s
CCTV (UL)	2–6 Mbit/s	2–6 Mbit/s	2 Mbit/s	6 Mbit/s	1 Mbit/s
Platform TV (DL)	2 Mbit/s	2 Mbit/s	—	6 Mbit/s	—
Maintenance (DL/UL)	100–500 kbit/s	200–500 kbit/s	1 Mbit/s (DL)	50 kbit/s	100 kbit/s
Passenger info (DL)	100 kbit/s	100 kbit/s	64 kbit/s	50 kbit/s	2 Mbit/s

Table 4.2: Maximum delay (one-way) and packet loss rate requirements for CBTC in the bibliography.

	Max. delay (ms)	Packet error rate	Throughput (kbit/s)
[IEE04a]	500–2000	—	—
[GRR17]	800	—	10–50
[ALL18]	100	0.1%	150
[KHA+13]	50	0.1%	4.8–8
[NOK16]	75	0.1%	50
[ZHA+14]	150	—	200

all the services, but the table provides a general idea of the needed throughput for each service, being CCTV and Platform TV the most demanding services.

The CBTC traffic is the most prioritary in the subway enviroment. Although it has low throughput requirements, the maximum delay and packet error rate limits can be more demanding under high load situations. The IEEE standards 1474.1 and 1474.3 [IEE04a; IEE08] define functional requirements for CBTC systems and recommended practice. In [IEE04a, Annex C], the typical communication delay in the train-to-wayside link is defined within the range of 0.5 to 2 seconds. However, the maximum delay required in real CBTC systems is usually lower. These documents describe general guidelines, typical parameters and recommendations that cannot be used directly as requirements. In fact, the CBTC requirements are set by the supplier or the transport operator for each CBTC project.

Table 4.2 shows the defined CBTC requirements for several works in the bibliography. According to [GRR17], the required delay for each CBTC packet is less than 800 ms. In [ALL18], the typical maximum delay is 100 ms with an acceptable packet error rate of 0.1%. On the other hand, the requirements set in [KHA+13] are 50 ms of maximum delay and 0.1% of packet loss rate. In [NOK16], the requirements are 75 ms of delay and a packet loss rate of

0.1%. Finally, Zhao et al. [ZHA+14] indicate a 150 ms maximum delay requirement.

Given these diverse requirements, in this chapter we will consider an intermediate maximum delay of 100 ms and a packet loss of 0.1%. The QoS requirements of the remaining services are:

- Voice communication: As CBTC, voice over Internet Protocol (VoIP) requires low delay communications with low data rate. ITU-T G.114 [ITU03] recommends a maximum one-way delay ("mouth-to-ear") of 150 ms to ensure that the users experience transparent interactivity.
- CCTV and platform TV: These services require a high throughput but tolerate delays up to 500 ms.
- Maintenance: As these operations do not require real-time performance, they can be provided with low-priority or best-effort transmissions.
- Passenger information: If the PIS does not include infotainment messages, the throughput requirements will be low. Also, if voice announcement service is not provided, longer delays are tolerated and the requirements can be satisfied with a best-effort priority.

4.3 ns-3 System-Level Simulator

The ns-3 simulator is an open-source discrete-event network simulator for research and education. This software is not an independent progam but a collection of C++ libraries. To use the simulator, a main C++ program is created to define the simulation topology and configuration. This program uses the libraries provided by ns-3 to run the simulation. The main simulation program can also be implemented in Python, but some features are often lost.

The simulator is made up of a core library and several modules. The core library provides the basic functionality of the simulator defining classes to manage time, events, configuration, random variables, logging, etc. The ns-3 modules contain models of different protocols, devices or real-world phenomena that can be simulated. Some relevant modules of the simulator are:

- Network: Defines key concepts such as nodes, network devices (that can be attached to the nodes), packets, channels, etc.
- Mobility: This model allows for defining the position and motion of the nodes during the simulation. Custom mobility models can be added, such as a train mobility model.
- Internet: Implements the internet stack protocols: IPv4, IPv6, Address Resolution Protocol (ARP), User Datagram Protocol (UDP), Transmission Control Protocol (TCP), etc.
- Propagation: Includes several models of radio propagation loss such as the Friis free-space model, log distance propagation model, etc.
- Spectrum module: Provides support for modeling wireless transmissions using the power spectral density (PSD) representation of the signals. This module allows for implementing channel models that are frequency selective. Moreover, it provides support

Table 4.3: Standardized QCI characteristics [3GP14].

QCI	Resource Type	Priority	Packet Delay	PER	Example Services
1	GBR	2	100 ms	10^{-2}	Conversational Voice
2		4	150 ms	10^{-3}	Conversational Video (Live)
3		3	50 ms	10^{-3}	Real Time Gaming
4		5	300 ms	10^{-6}	Video (Buffered)
5	Non-GBR	1	100 ms	10^{-6}	IMS Signaling
6		6	300 ms	10^{-6}	Video (Buffered), TCP-based services
7		7	100 ms	10^{-3}	Voice, Video (Live), Gaming
8		8	300 ms	10^{-6}	Video (Buffered), TCP-based services
9		9			

for signal-to-interference-plus-noise ratio (SINR) calculation based only on the power received at each frequency band.

- Antenna module: Enables the use of antenna models with the desired radiation patterns.

The LTE and Wi-Fi modules are explained in detail in the following subsections.

4.3.1 LTE Module

The ns-3 LTE module was first published in 2011 and it has been actively developed and enhanced since then [PBM11; ZBM13]. Although the ns-3 LTE module only supports frequency-division duplexing (FDD) operation mode, the whole LTE protocol stack is implemented, including an Evolved Packet Core (EPC) model providing end-to-end Internet Protocol (IP) connectivity. The model includes design documentation [PRO21] and is open source, as the rest of the ns-3 simulator.

We had to implement some new features that were not present in the model, most of them related with the scheduling and the QoS. We detail these enhancements in Section 4.3.1.1.

In LTE, traffic packets are classified into different bearers based on each packet header. LTE defines the so-called QoS Class Identifiers (QCIs) to configure QoS requirements of the bearers. Each QCI defines a priority, a packet delay budget, and a tolerated packet error ratio (PER). Also, some QCIs support a guaranteed bit rate (GBR) for each bearer.

The standardized QCI characteristics in LTE Release 8 are shown in Table 4.3. More QCI values have been defined in the subsequent LTE releases to support new services such as mission critical push-to-talk voice. The first QCI values allow for creating GBR bearers with a minimum bit-rate that should be satisfied. The other classes do not have this minimum bit-rate and have less priority than the first 4 values, with the exception of QCI 5, which has the higher priority. The default bearer is configured with the QCI 9.

The ns-3 simulator allows us to use the nine QCI values defined in LTE Release 8. However, the provided QoS-aware schedulers only consider the assigned GBR value of each bearer and

ignore the remaining parameters. We have also enhanced the schedulers to take into account the priority of each bearer as explained in Section 4.3.1.1.

4.3.1.1 ns-3 LTE Scheduler Enhancements

The LTE module provides several scheduler implementations, such as the well-known proportional fair (PF) and maximum throughput (MT) opportunistic schedulers as well as other QoS-aware schedulers [ZBM13]. Only the DL scheduler is currently implemented in ns-3, whereas the UL employs a simple round robin (RR) scheduler. Also, the provided QoS-aware schedulers only prioritize some users over others, but do not consider different flows from the same user. In our scenario we need to prioritize the CBTC flows over the others, to minimize the delay of the CBTC traffic.

Given that all of our users have the same priority, our approach consists in modifying the PF scheduler to include a flow prioritization mechanism. First, a resource assignment to each user is performed by a fair algorithm. Then, these resources are shared between the different flows of each user taking into account the QoS requirements.

We also implemented the PF scheduler for the UL, taking into the account the additional restriction that the assignment of resource blocks (RBs) to each user equipment (UE) must be contiguous in frequency, as required by the single-carrier FDMA (SC-FDMA) modulation. We perform this assignment in an iterative way:

- Calculate the PF metric for each RB and UE that can transmit in that RB.
- Select the UE that has the best metric in more contiguous RBs.
- Assign some of the adjacent RBs to the UE depending on the UE data requirements.
- Go to the first step until no more RBs can be assigned.

We also implemented the riding-peaks algorithm with RB grouping [LEE+09], obtaining results equivalent to the previous method.

The LTE standard defines the logical channel prioritization (LCP) procedure that must be performed by the UEs to prioritize the logical channels (LCs) in a predictable way [3GP18]. We implemented this mechanism because the ns-3 implementation performed this process in a non-standard way using a RR algorithm. We also added the LCP procedure to the PF DL scheduler, thus providing the required QoS awareness.

The LCP mechanism is configured with the following parameters for each LC:

- *priority*: The LCs are served in this order. Higher priority values indicate lower priority.
- *prioritisedBitRate*: LCs will be able to transmit with this rate if higher priority LCs leave enough resources.
- *bucketSizeDuration*: Limits the amount of prioritized data the LCs can transmit continuously to avoid starving the lower priority LCs.

Fig. 4.1 shows an example of the operations performed by the LCP procedure with three LCs. A MAC protocol data unit (MPDU) is built in two steps: first, the *prioritisedBitRate* of each LC is served in priority order (operations 1, 2, and 3 in Fig. 4.1), and second, the MPDU

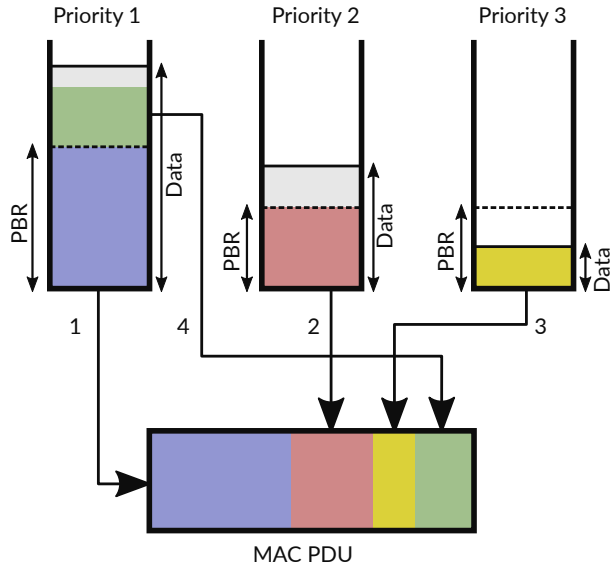

Figure 4.1: Logical Channel Prioritization.

is filled with the remaining data in the LCs, also in priority order (operation 4). The payload of each LC will be arranged contiguously inside the MPDUs.

The LCP parameters values are set by the Radio Resource Control (RRC) layer. The way the QoS parameters of a bearer are mapped to the LCP parameters is not standardized. Bouchemal et al. [BIT14] evaluated the effects of different configurations of these parameters, concluding that a correct configuration avoids starvation problems in low priority traffic. We configured this values to ensure that the required bit-rate of high priority LCs are always satisfied in our simulations. The parameters were assigned in the following way:

- The *prioritisedBitRate* is set to the GBR of the bearer. If the bearer does not have GBR, $(9 - priority) * 8000$ bits/s are used as *prioritisedBitRate*.
- The *bucketSizeDuration* parameter is assigned with the following expression: $300ms/packetDelayBudget$. The $packetDelayBudget$ is the allowed packet delay of each QCI as shown in Table 4.3.

4.3.2 Wi-Fi Module

Wi-Fi technology is defined in the IEEE 802.11 standard [IEE16] and has evolved over the years through various amendments. The most relevant for railway environments are:

802.11a (1999) operates in the 5 GHz band using an OFDM PHY with a maximum throughput of 54 Mbit/s. However, in real systems, this amendment usually achieves a data rate of around 25 Mbit/s.

802.11n (2009) improves the performance of previous amendments and has a theoretical peak rate of 600 Mbit/s thanks to the use of multiple-input-multiple-output (MIMO) transmissions and 40 MHz bands. It can work in the 2.4 GHz and 5 GHz ISM bands.

802.11ac (2013) works in the 5 GHz bands and improves performance by using MIMO with

more antennas, 80 MHz and 160 MHz channelization, and 256-QAM modulation.

802.11ax is still a draft [IEE20] but it is expected to be approved soon. This amendment will introduce significant changes to the PHY and MAC layers. It increases the number of OFDM subcarriers ($\times 4$), reducing the separation between them, and increasing the duration of the OFDM symbol. In addition, it uses orthogonal frequency-division multiple access (OFDMA) to reduce interference between stations. Several devices already support this amendment, including some industrial-grade equipment that has recently come onto the market.

802.11e (2005) adds QoS improvements by defining four types of traffic. Thus, some data flows can be prioritized and their latency reduced.

802.11f, 802.11k, 802.11r, and **802.11v** allow for reducing the roaming time between access points (APs) with different mechanisms.

802.11h (2003) allows for transmission in the U-NII frequency bands (5 GHz) that are also used by radar and satellite systems. The ammendment provides Dynamic Frequency Selection (DFS) and Transmit Power Control (TPC) mechanisms to avoid interference with other systems.

The Wi-Fi module of the ns-3 simulator has the following characteristics:

- The Wi-Fi devices can work in ad-hoc or infrastructure mode. In our case we will use the infrastructure mode that configures the devices as stations (STAs) or APs, according to Wi-Fi terminology.
- It supports several IEEE 802.11 physical layers: 802.11a, 802.11b, 802.11g, 802.11n, and 802.11ac. The 802.11ax version [IEE20] is still under development.
- When using 802.11n or 802.11ac, MAC service data units (MSDUs) and MPDUs can be aggregated to reduce overhead and improve the data rate [BHA+09].
- It implements the QoS defined in 802.11e with separate queues for each access category.
- It includes different rate control algorithms that allow for adapting the transmission rate to the radio channel or the number of interfering nodes.

However, the following shortcomings have been found in the Wi-Fi module:

- No handover mechanisms between APs are implemented. We had to modify the simulator and add support for fast handovers as shown in Section 4.3.2.1.
- Although the aggregation of MPDUs substantially improves the transmission rate, we have detected errors in the ns-3 implementation that cause long interruptions in transmissions in certain situations. This has forced us to disable this method and use the 802.11a standard instead of 802.11ac.

4.3.2.1 ns-3 Wi-Fi Fast Handover Support

In contrast to LTE, in Wi-Fi the mobile device (STA) decides the moment when the change of AP is made and which AP it decides to connect to. The handover mechanism we have implemented in the simulator assumes that the STAs know the details of the Wi-Fi deployment,

i.e., all STAs know their position and the distance to each AP. Moreover, they know the operating frequency (Wi-Fi channel) of each AP to avoid the need to scan all Wi-Fi channels before performing the handover. This information allows the STAs to perform the handovers with very short delay.

Three handover methods were implemented in the simulator:

- Passive channel scan (PassiveBeaconWait). The STA receives the beacons sent periodically by the APs. After some time (configurable), the STA connects to the AP which sent the beacon with the best reception SNR. This method is very slow because it depends on the beacon interval of the APs, which by default is 102.4 ms.
- Active channel scan (ActiveProbing). The STA sends special packets (probe requests) asking the APs on that channel to reply. After some time, the STA connects to the best AP or rescans the channel if no AP was found. The time it takes to perform the handover depends on the configured timeout, which by default is 50 ms.
- Direct connection without channel scan (FastHandover). The STA already knows which AP to connect to and connects to it without scanning. The only delay in this method is the time it takes for the AP to respond to the STA's association request. If there is no packet loss, the handover with this method usually takes no more than 1 ms.

During the handover process, the transmission queue of the STA is disabled. Therefore, the packets added to the queue during this process are lost. In addition, packets stored in the transmission queues of the previous AP are lost because they are not forwarded to the new AP to which the STA is connecting. In a real infrastructure it is possible that the access points are able to forward these packets to the next AP.

4.4 Tunnel Propagation Models

The radio propagation channel in tunnels is very different from the other channels present in high-speed train (HST) scenarios such as viaduct, cutting, open space, etc. Conventional channel models are suitable for most HST scenarios, but cannot be used in tunnel scenarios [LIU+17]. In [WAN+16] a study is made of the different works in the modeling and characterization of the channels for HST, noting the special properties of tunnel propagation channels.

Radio propagation in tunnels is characterized by the waveguide effect that shows up from certain distances. However, the propagation model depends largely on the physical characteristics of the tunnel such as its dimensions, shape, and the material and roughness of the walls. In addition, the presence of curves and underground stations, as well as the dimensions of the train wagons, significantly modify the radio channel.

Furthermore, the location of the antennas in the tunnels and in the trains is a very important factor in the received signal quality. Normally, the antennas are placed on top of the wagons, as close as possible to the front of the train to have a better line of sight with the wayside antennas.

These antennas should be placed as far as possible from the tunnel walls [HKJ14] [SA10], although it is common to place them on the side of the tunnel to facilitate maintenance.

This high number of factors makes it very difficult to simulate radio coverage inside a tunnel. For this reason, it is highly recommended to perform measurement campaigns before a deployment [TOL15] to adjust the selected channel model and the radio propagation can be predicted accurately.

In the literature there are many articles focused on the study of the radio channel propagation model in tunnels (see [HKJ14; FOR+13; LIU+17] and their references). Most of them focus on the frequencies commonly used in standards such as Global System for Mobile Communications (GSM), Universal Mobile Telecommunications System (UMTS), Wi-Fi and LTE. In general, channel models can be classified into two groups: deterministic and empirical. On the one hand, deterministic channel models simulate the behavior of electromagnetic waves to predict the power and delay when they reach the receiver. These models can be based on solving Maxwell's equations, on analysis of the waveguide effect, or on ray tracing methods (geometric optics model). On the other hand, empirical models are based on the analysis of measurements obtained in tunnels. From these collected data, they try to generalize the behavior of the channel with mathematical expressions whose parameters depend on the scenario.

An interesting deterministic channel model is described in [SA10] because it produces realistic results and it does not require as many calculations as other models. This work proposes a hybrid model for rectangular tunnels (known as multimode model) that enhances the waveguide model using the geometric optics (GO) model to calculate the contribution of each propagation mode. This way, this model can be used both for short and long distances, i.e., near and far propagation regions of the tunnels.

Empirical channel models are based on the results obtained in measurement campaigns. They try to explain and generalize the results by using other deterministic channel models or by performing a linear fitting of the measurements and providing the obtained path loss coefficients. These models usually divide the path loss curve into two or more regions and provide the mechanisms to calculate the position of the breakpoints. Several two-slope channel models have been proposed [ZH97; ZHA03; BCA07; DOM+18] where they only consider the near and far regions, while other works use more breakpoints and can combine different deterministic channel models [HKJ10; GUA+12; GUA+13].

Usually, the articles in the literature only consider the channel in straight sections of tunnels. In [AI+16], the additional signal loss caused by curved sections is analyzed for different frequencies, radius of curvature and antenna polarization. With these results it is possible to simulate the presence of curves avoiding the need to use more complex models.

In the following subsections two channel models suitable for system level simulators are described. On the one hand, a deterministic channel model is developed combining several models found in the literature to provide maximum flexibility when modeling a tunnel environment. On the other hand, a measurement based channel model is detailed bringing

realistic results but only for deployments that match the measurement campaign environment.

4.4.1 Deterministic Channel Model

The channel model used is based on the multimode model [SA10] for rectangular tunnels. This model obtains very realistic results when compared to a measurement campaign in a straight tunnel with low roughness (1 cm) for 450, 900 and 2100 MHz frequencies [DUD+07]. This is a waveguide based channel model that provides analytical expressions for the received power and can be used in the near and far propagation regions of the tunnel.

The waveguide effect only shows up when the cross-sectional dimensions of the tunnel are several times larger than the signal wavelength. Also, the waveguide effect works as a high pass filter, as only the signals with frequencies higher than the cut-off frequency will pass through the tunnel.

In this waveguide models, the electromagnetic waves in the tunnel are represented as the sum of multiple propagation modes with different field distribution and attenuation coefficients. The propagation modes are solutions to the wave equations or the forms of the waves that can be propagated inside the tunnel. There is a cut-off frequency for each mode in the rectangular tunnel waveguide:

$$f_{m,n}^{\text{cutoff}} = \frac{1}{2\sqrt{\mu_0 \varepsilon_0}} \sqrt{\left(\frac{m}{w}\right)^2 + \left(\frac{n}{h}\right)^2}$$

where w and h are the width and height of the tunnel; μ_0 and ε_0 are the vacuum permeability and permittivity physical constants; m and n are the mode numbers in the horizontal and vertical directions. The signals with lower frequency than $f_{m,n}^{\text{cutoff}}$ will not be able to propagate in that mode.

We define a coordinate system centered in the rectangular tunnel with the axes x and y as the horizontal and vertical directions, respectively. The z-axis goes through the center of the tunnel, starting in the transmitting antenna position, i.e., the transmitter antenna is located at $(x_0, y_0, 0)$.

The transmitted signal has a central frequency f_0, so only modes with lower cut-off frequency will contribute to signal propagation. The tunnel has the following electrical parameters:

- ε_v, ε_h and ε_a : relative permittivity for vertical/horizontal walls and the air in the tunnel.
- σ_v, σ_h and σ_a : conductivity of the vertical/horizontal walls and the air.

The received signal power at the point (x, y, z) according to the multimode model [SA10] for horizontally polarized antennas is:

$$P_r(x, y, z) = P_t G_t G_r \left(\frac{1}{E_0} \sum_{m,n} C_{mn} \cdot E_{m,n}^{\text{eign}}(x, y) \cdot e^{-(\alpha_{mn} + j\beta_{mn}) \cdot z} \right)^2 \tag{4.1}$$

where P_t, G_t and G_r are the transmission power and the transmission and reception antenna gains, respectively; E_0 is the field at the transmitter; C_{mn} is the mode intensity on the excitation

plane; $E_{m,n}^{\text{eign}}$ is the field distribution of each mode; α_{mn} and β_{mn} are the attenuation and phase shift coefficients. The results for vertically polarized antennas can be obtained by simply swapping the x and y axes.

$E_{m,n}^{\text{eign}}$ can be approximated in the form of eigenfunctions:

$$E_{m,n}^{\text{eign}}(x,y) = \sin\left(\frac{m\pi}{w}x + \varphi_x\right)\cos\left(\frac{n\pi}{h}y + \varphi_y\right)$$

where $\varphi_x = (m \mod 2)\pi/2$ and $\varphi_y = (n+1 \mod 2)\pi/2$.

The α_{mn} and β_{mn} coefficients are obtained with the expressions:

$$\alpha_{mn} = \frac{2}{w}\left(\frac{m\pi}{wk}\right)^2 \text{Re}\,\frac{\overline{k_v}}{\sqrt{\overline{k_v}-1}} + \frac{2}{h}\left(\frac{n\pi}{hk}\right)^2 \text{Re}\,\frac{1}{\sqrt{\overline{k_h}-1}}$$

$$\beta_{mn} = \sqrt{k^2 - \left(\frac{m\pi}{w}\right)^2 - \left(\frac{n\pi}{h}\right)^2}$$

where the constant k is the wave number in the tunnel space obtained as $k = 2\pi f_0\sqrt{\mu_0\varepsilon_0\varepsilon_a}$. $\overline{k_v}$ and $\overline{k_h}$ are the relative electrical parameters for vertical and horizontal tunnel walls and are obtained as:

$$\overline{k_v} = k_v/k_a \qquad k_v = \varepsilon_0\varepsilon_v + \frac{\sigma_v}{j2\pi f_0}$$

$$\overline{k_h} = k_h/k_a \qquad k_h = \varepsilon_0\varepsilon_h + \frac{\sigma_h}{j2\pi f_0}$$

$$k_a = \varepsilon_0\varepsilon_a + \frac{\sigma_a}{j2\pi f_0}$$

To obtain C_{mn}, the mode intensity on the excitation plane, a field analysis with the GO model is performed in [SA10] and the sum of rays is converted to the sum of modes. The final expression is:

$$C_{mn} = \frac{4E_0\pi}{wh\sqrt{1-\left(\frac{m\pi}{wk}\right)^2 - \left(\frac{n\pi}{hk}\right)^2}} E_{m,n}^{\text{eign}}(x_0,y_0)$$

Note that since this expression is plugged in Eq. (4.1), the E_0 constant can be ignored.

This model can also be applied to tunnels with different cross sections by calculating the equivalent rectangular tunnel. Given a tunnel with an arched cross section with radius a and flat base L, there are several methods that obtain the equivalent rectangular tunnel dimensions (width w and height h). A simple method or "rule of thumb" is described in [BCA07]:

$$w = L$$
$$h = \sqrt{4a^2 - w^2}$$

However, we use the method proposed in [MAH10; EME17] that uses perturbation theory to ensure that the behavior of the first modes is very similar in the original and equivalent tunnels.

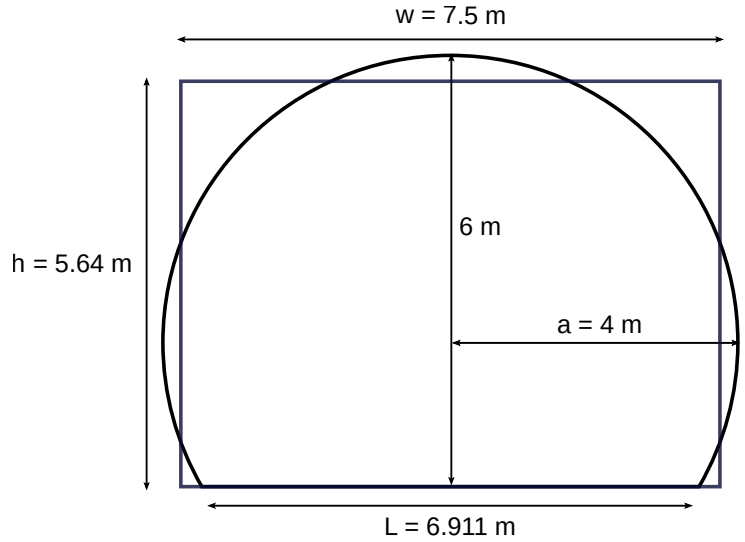

Figure 4.2: Example of arched tunnel cross section with radius of 4 m, height of 6 m, and a flat base of 6.911 m. The equivalent rectangular tunnel (blue) has 7.5 m of width and 5.64 m of height.

The dimensions are calculated as follows:

$$\begin{aligned} \xi &= \arcsin \frac{L}{2a} \\ C &= (1 + \cos \xi)/2 \\ R &= 1.145 C^n \\ area &= R((\pi - \xi)a^2 + (L \cdot a/2)\cos \xi) \\ h &= \sqrt{area \cdot C} \\ w &= area/h \end{aligned}$$

where n is a tuning factor for best fitting, with a recommended value of $n = 0.33$, and R is the ratio between the rectangular area and the arched cross section area. An example of an arched tunnel and the obtained equivalent rectangular dimensions is shown in Fig. 4.2. The "rule of thumb" method provides a result with only 4.03 m of height.

The model considers that the tunnel has an ideal rectangular cross section with no roughness and the walls are perfectly vertical. However, propagation losses due to the roughness and tilt of the walls should also be considered. These losses are modeled in [ELS75] and corrected in [ZH97]:

$$\begin{aligned} L_{\text{roughness}}(\text{dB}) &= 8.686\pi^2\gamma^2\lambda(\frac{1}{w^4} + \frac{1}{h^4})z \\ L_{\text{tilt}}(\text{dB}) &= \frac{17.372\pi^2\theta^2}{\lambda}z \end{aligned}$$

where $L_{\text{roughness}}$ and L_{tilt} are the roughness and tilt losses in dB; γ and θ are the root-mean-square roughness and tilt of the tunnel walls, respectively; z is the distance in meters between the transmitter and receiver along the z-axis; and $\lambda = c/f_0$ is the wavelength. Wall roughness

Table 4.4: Multimode channel model parameters for Figs. 4.3 and 4.4.

Parameter	Value
Tx. power	0 dBm
Antenna gains	0 dBi
Tunnel cross section	Arc shaped
Tunnel radius	4 m
Tunnel base	6.9 m
Equiv. rect. tunnel dims. (w, h)	7.5 m, 5.64 m
ε_v, ε_h and ε_a	5, 5 and 1
σ_v, σ_h and σ_a	0.01, 0.01 and 0
x_0, y_0	3.25, 0.18
x, y	1.87, 0.18

has a greater effect when using low frequencies, while tilt has higher impact when using high frequencies.

We also need to consider the insertion loss (or coupling loss) of an antenna in the tunnel. This loss affects both the transmitting and the receiving antennas and is constant along the entire line as it only depends on the positions inside the tunnel cross section. The coupling loss for an antenna with position (x, y) in the tunnel cross section is modeled in [ELS75; ZHA03] as:

$$L_{\text{coupling}}(\text{dB}) = 10\log_{10}\left(\frac{2\pi wh}{\lambda^2 G}\cos^{-2}\left(\frac{\pi x}{w}\right)\cos^{-2}\left(\frac{\pi y}{h}\right)\right)$$

where G is the antenna gain. The coupling loss is higher the closer the antennas are to the walls, but Zhang points out that the equation becomes inaccurate when the antenna is very close to the tunnel walls. For this reason we use this equation assuming a minimum distance of 50 cm between antennas and tunnel walls.

We use the coupling loss to normalize the received power in the model in the following way: we ensure that the received power of the first mode ($n = m = 1$) for $z = 0$ corresponds to the coupling loss of the transmitting and receiving antennas. This normalizes the received power the same way as in [ZHA03].

Fig. 4.3 shows an example of the model output for the parameters in Table 4.4. The figure shows the fast fading behavior of the channel with deep fades of the signal, specially the first kilometer, and how this channel is better than the free space model for long distances. The first mode corresponds with the waveguide model developed by Emslie et al. [ELS75]. The higher order modes lose strength with the distance and only the lower order modes remain for long distances. The coupling loss for the transmitter and receiver antennas is $53.8 + 43.2 = 97$ dB. It can be seen how this value was used to normalize the received power as it is the starting value for the first mode.

The channel behavior for different frequencies is shown in Fig. 4.4. The figures show the

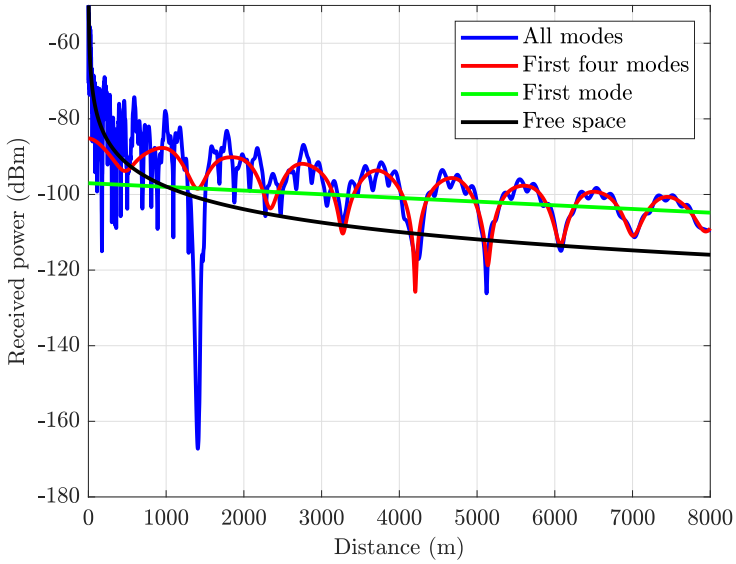

Figure 4.3: Received power with the multimode channel model using horizontally polarized antennas and central frequency 1869.9 MHz. The remaining parameters are shown in Table 4.4. The free-space path loss channel $L(\text{dB}) = 20\log_{10}(4\pi z/\lambda)$ is also plotted as a reference.

effect of the roughness and tilt loss. In these examples, the roughness loss is almost unnoticeable while the tilt loss is notable, specially for long distances and high frequencies.

This channel model can be enhanced by taking into account the curves of the track and their impact on the channel. The model proposed in [AI+16] is very useful for this purpose as it provides the additional propagation loss in a curve regarding the expected received power in the straight tunnel. They study the measurements obtained in different curved sections of tunnels and compare them with ray tracing simulations of the straight tunnels, ensuring that their simulations provide realistic results for both the straight and curved sections of the tunnels. This extra propagation loss model only requires the knowledge of the curve radius, the signal frequency, the polarization of the antennas, and the tunnel cross section type. With these parameters, the model provides the extra loss of the curve in decibels per 100 m. For example, for a 300 m radius curve this model indicates that there is an extra loss of 5.5 dB/100 m for 1869.9 MHz and 6.6 dB/100 m for 5.5 GHz.

Finally, the channel is also affected by changes in the slope of the tunnel, but no model has been found in the literature that takes these changes into account. Therefore, these variations have been modeled as curves using the previous extra loss model [AI+16]. All slope changes are considered to be curves with a radius of 500 m, allowing to calculate the size of the attenuated tunnel section.

4.4.2 Channel Model Based on Measurements

In this subsection we develop a simplified channel model suitable to perform LTE system level simulations from a previous measurement campaign [DOM+18]. Such a measurement

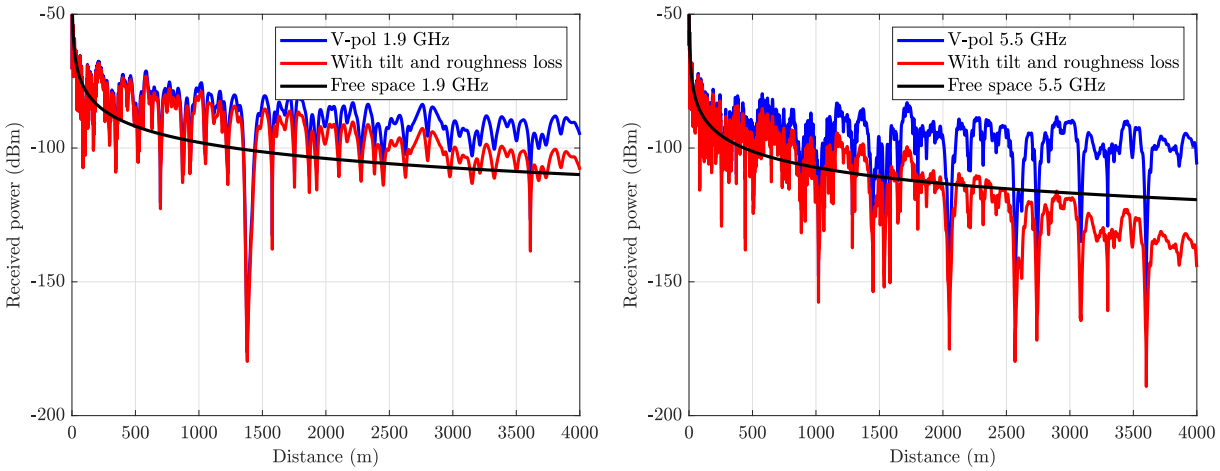

(a) Frequency of 1.9 GHz. Roughness loss of $1.80 \cdot 10^{-4}$ dB/100 m. Tilt loss of 0.326 dB/ 100 m.

(b) Frequency of 5.5 GHz. Roughness loss of $6.11 \cdot 10^{-5}$ dB/100 m. Tilt loss of 0.958 dB/ 100 m

Figure 4.4: Influence of central frequency in roughness and tilt loss with vertically polarized antennas. $\gamma = 0.01$ and $\theta = 0.1°$. The remaining parameters are shown in Table 4.4.

campaign was conducted in a modern subway station and its entrance tunnel in the Madrid Metro as shown in Fig. 4.5. An LTE Evolved Node B (eNodeB) transmit antenna was placed at the center of the station platform and two receivers were used to characterize the eNodeB-train and eNodeB-mobile links. This model will only consider the eNodeB-train link where two external antennas were placed on the train front window.

The so-called GTEC Testbed [DOM+16] was employed for the generation, transmission, acquisition and processing of LTE signals. This testbed was designed considering the requirements to carry out measurement campaigns in HST environments [ROD+13]. The testbed nodes are small and light, robust, and with low-power consumption. Moreover, they can perform MIMO 2x2 measurements in frequencies from 70 MHz to 6 GHz with a maximum bandwidth of 56 MHz.

As shown in Fig. 4.5, a testbed node was placed at the subway station in the role of an eNodeB to cyclically transmit an LTE signal with a bandwidth of 10 MHz (50 RBs) at a carrier frequency of 2.6 GHz, while the receiver node was connected to the train antennas to store the received signals.

The eNodeB employed a vertically polarized 90° sector antenna and transmitted with a power of 18.5 dBm. At the receiver, two vertically polarized 30° sector antennas were attached to the train front window.

During the measurements, the eNodeB was placed at the middle of a 100 m length station. The signal was acquired from an approaching train, starting the measurements at a distance of 145 m from the eNodeB. Once the train passed the middle of the station the line-of-sight (LoS) component was lost and the signal-to-noise ratio (SNR) of the received signals decreased quickly. Hence, for this model, we only considered the measurements up to the middle point

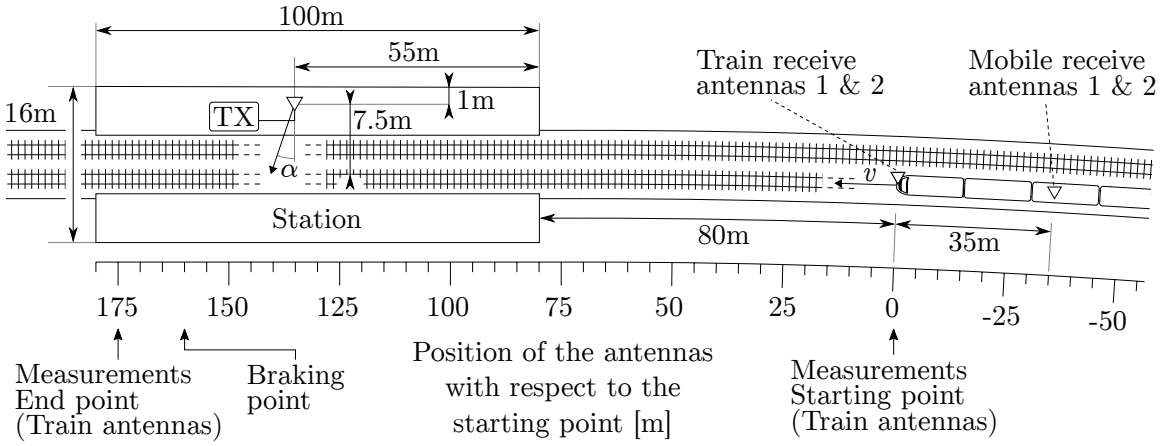

Figure 4.5: Schematic of the measurement scenario at "La Almudena" subway station, Madrid Metro, Spain. Reprinted from Domínguez-Bolaño et al., "Measurement-Based Characterization of Train-to-Infrastructure 2.6 GHz Propagation Channel in a Modern Subway Station", ©2018 IEEE.

of the station. The considered measurement trajectory can be divided into a tunnel section of 90 m, and a station section of 55 m.

By only using the measurements from tunnel and station sections, we are assuming that the train antennas are bidirectional, i.e., they receive the signal from the front and rear with the same strength, and there is no SNR loss when the train passes in front of the eNodeB.

From the measurement campaign results, we obtained a path loss model and a fading model suitable for the system level simulator. These models focus on the simulation of LTE deployments and only depend on the distance between the eNodeB and the UE. Also, to simulate FDD transmissions, we need to consider different channel realizations for the DL and UL, as the UL carrier frequency is different from that of the DL. In the measurement campaign, the same carrier frequency was used for both receive antennas. Thus, we decided to use the measurements from antenna 1 for the DL and those from antenna 2 for the UL.

4.4.2.1 Path Loss Model

The signal propagation characteristics change when the train moves from the tunnel to the station. Hence, in the previous work [DOM+18], a log-distance path loss model with two breakpoints was proposed. Note that for obtaining this model, the impact of the antenna radiation patterns was not removed from the measurements. The proposed model is defined as:

$$\mathrm{PL}(d) = \begin{cases} b_1 + 10\gamma_1 \log_{10}(d), & d_0 \leq d \leq d_1 \quad \text{(station)} \\ b_2 + 10\gamma_2 \log_{10}(d), & d_1 \leq d \qquad\quad \text{(tunnel)}, \end{cases} \tag{4.2}$$

where d_0 is the distance from the eNodeB to the starting point of the measurements, d_1 is the estimated distance where the propagation characteristics change. For the station and the tunnel section, respectively, b_1 and b_2 are the intercepts, and γ_1 and γ_2 are the path loss exponents. The

Table 4.5: Path loss estimated parameters using Eq. (4.2).

Antenna	γ_1	γ_2	b_1	b_2	d_1
1	-0.709	1.773	79.905	41.816	34.270
2	-0.329	2.037	74.801	36.433	41.865

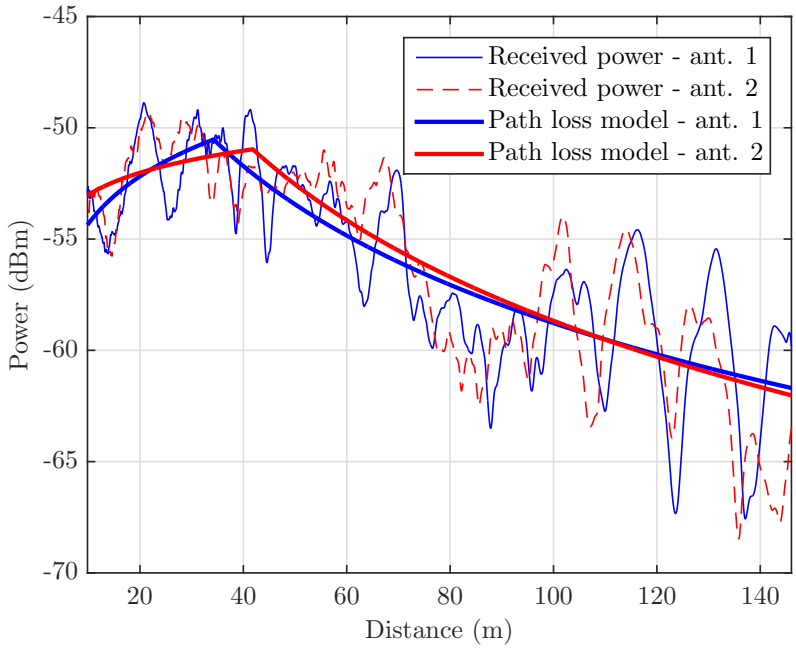

Figure 4.6: Received signal power (smoothed) vs distance and the corresponding path loss model estimation.

path loss exponents, the intercepts, and the distance d_1 are estimated jointly by a least-squares fitting.

The results obtained are shown in Table 4.5. Note that in this scenario the receive power does not only depends on the distance, but also on the relative angles of the transmit and receive antennas due to the directivity of the antennas used. Because of this, the estimated values for d_1 (34.270 and 41.865 m) does not match the actual distance to the tunnel (55 m).

Fig. 4.6 shows the received power at each antenna and the estimated path loss model applied to the transmit power. Note that the path loss exponents are negative in the first section due to the directivity of the receive antennas and their relative angles with respect to the transmit antenna.

The log-distance path loss propagation model can be implemented in the ns-3 simulator configuring the `ThreeLogDistancePropagationLossModel` path loss

Table 4.6: Path loss model configuration using Eq. (4.3).

Antenna	L_0	d_0	d_1	d_2	n_0	n_1	n_2
1	90.78	0.0292	34.27	∞	-0.709	1.773	-
2	80.14	0.0239	41.87	∞	-0.329	2.037	-

model [PRO21], which is defined with respect to the distance d as follows:

$$\mathrm{PL}(d) = \begin{cases} 0 & d < d_0 \\ L_0 + 10n_0 \log_{10}(\frac{d}{d_0}) & d_0 \leq d < d_1 \\ L_0 + \beta_{1,0} + 10n_1 \log_{10}(\frac{d}{d_1}) & d_1 \leq d < d_2 \\ L_0 + \beta_{1,0} + \beta_{2,1} + 10n_2 \log_{10}(\frac{d}{d_2}) & d_2 \leq d, \end{cases} \tag{4.3}$$

where $\beta_{i,j} = 10n_j \log_{10}(d_i/d_j)$; d_0, d_1 and d_2 are the distance fields; n_0, n_1 and n_2 are the path loss exponents; and L_0 is the path loss at d_0. This formulation is slightly different and the parameters in Table 4.5 had to be adapted. The converted parameters are shown in Table 4.6.

4.4.2.2 Fading Model

The ns-3 simulator includes a fading model based on traces of PSD values with RB granularity. This model was modified so that it does not depend on simulation time but on the distance between transmitter and receiver. The channel traces are extracted from the recorded data and are processed to remove the large-scale fading (i.e., the path loss term), hence the average power of the traces is one for all the path traveled by the train. This way, the path loss model can be applied to these traces during simulation. Fig. 4.7 shows the processed traces for the antenna 1. The fades in the signal are more deep in the time than in the frequency dimension.

In the measurement campaign, data for the tunnel environment was acquired only for the last part of the tunnel environment, before entering the station, with a maximum distance of 145 m. We need to extend these traces to perform simulations with trains that are farther away in the tunnel. In order to do so, we follow a simple approach: when the distance between the UE and the eNodeB exceeds the maximum distance in the measurement data, we repeat cyclically the traces of the initial 55 m of the tunnel section. This repetition is performed reading in reverse order the traces to avoid introducing discontinuities. Note that, as explained before, a path loss depending on the distance is still applied.

Fig. 4.8 shows the DL SINR for an UE moving from an eNodeB station to another and performing a handover. The combined path loss and fading effects can be seen with the eNodeB transmit power being fixed at 18.5 dBm. Also, the noise figure of the receiver is set to 2.07 dB to match the results obtained in the measurements. Notice that the UL SINR results would be different as the power control mechanism would allow for changing the transmit power between -40 and 23 dBm.

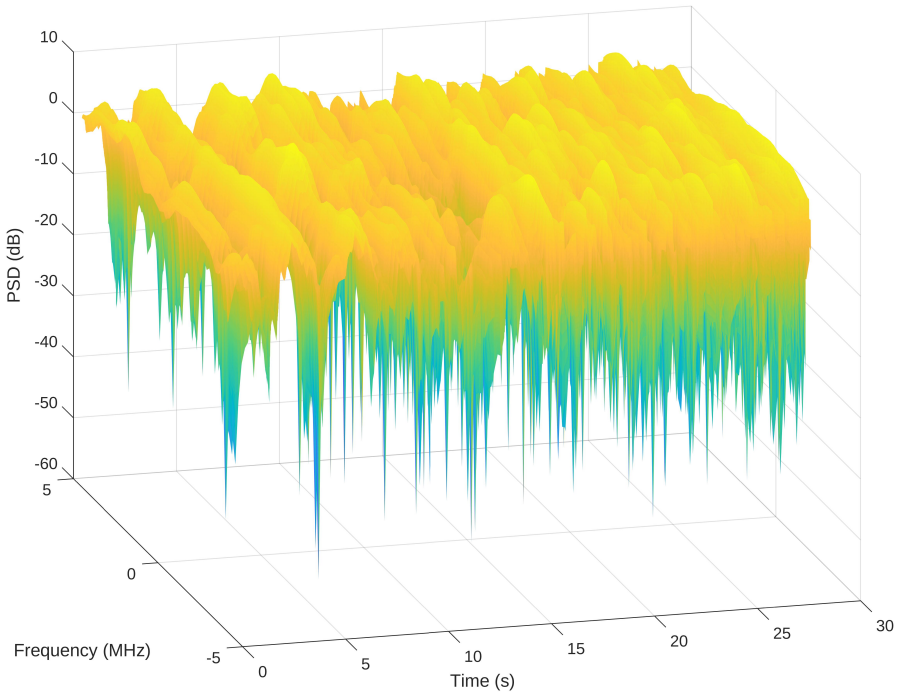

Figure 4.7: Channel PSD with the path loss model removed for antenna 1.

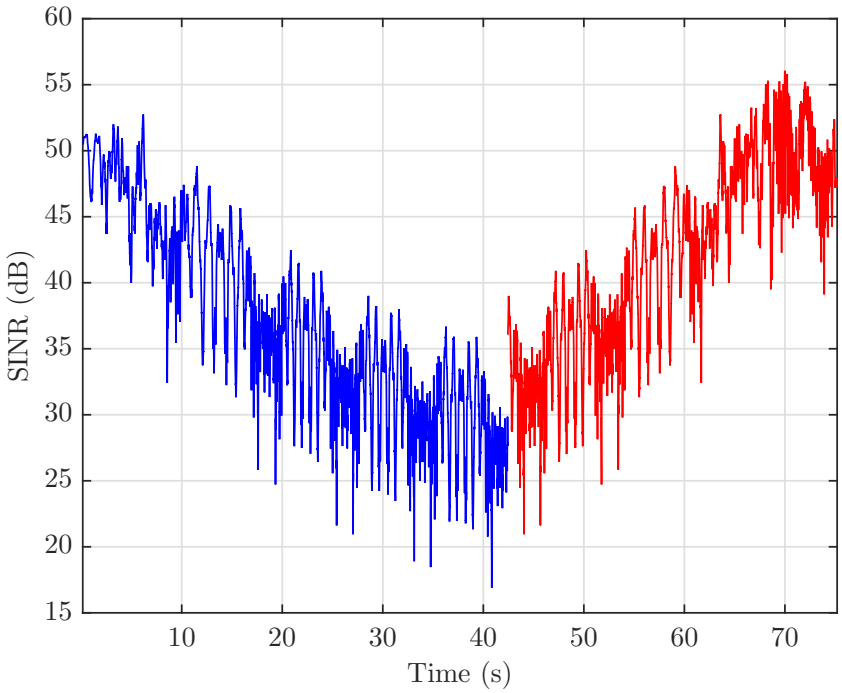

Figure 4.8: DL SINR versus time for an UE performing a handover. Blue and red lines represent the SINR for the first and second eNodeBs, respectively. The distance travelled by the UE is 1130 m.

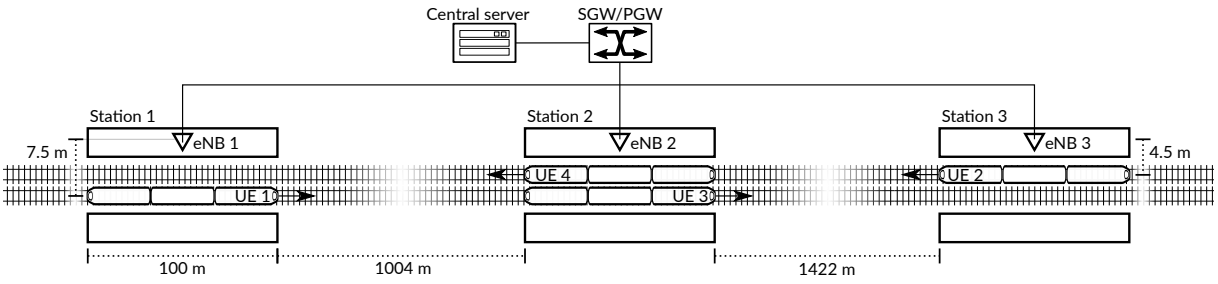

Figure 4.9: Stations and LTE deployment with the trains placed at their initial positions.

4.5 LTE Three-Stations Deployment

In this section, we consider a scenario to test the measurement based channel model of Section 4.4.2 with a 10 MHz FDD LTE deployment. The scenario has three identical and consecutive subway stations with a separation of 1104 and 1522 m, respectively. These are approximately the distances between "La Almudena" station of the Madrid Metro (where the measurement campaign was conducted [DOM+18]) and the adjacent stations "La Elipa" and "Alsacia". We consider the same transmitter setup for all the stations, with the eNodeBs located at the center of each platform and connected between them through an X2 interface to allow the handover process. A central server is connected to the simulated packet data network gateway (PGW) node of the EPC with a point-to-point connection at 100 Gbit/s and without delay. This central server will send all the DL packets and receive the UL packets.

Fig. 4.9 shows the stations and LTE deployment. Four trains and two parallel tracks are considered in the simulation scenario. Two trains move on one track departing from the first and second stations. The other two move on the other track in opposite direction departing from the second and third stations. This way, the second station will have two trains leaving and two trains arriving.

We model a train trip by setting waypoints at different positions with a given velocity, i.e., train acceleration is constant between two waypoints. Each train performs the following steps to travel between stations:

- The train starts from the station and accelerates to a speed of 19.44 m/s ($\approx$ 70 km/h).
- The speed is maintained until the train approaches the destination station.
- The train decelerates to 5.55 m/s ($\approx$ 20 km/h).
- Inside the station, the train maintains the speed before stopping at the end of the station.

A constant acceleration of 1 m/s^2 is considered between waypoints regardless of whether the train accelerates or brakes.

Table 4.7: Applications configuration for the three-stations deployment. The throughput values are all constant, except for the video stream where the mean bitrate is indicated, and the voice stream which has silence periods.

Application	DL (kbit/s)	UL (kbit/s)	Packet Size (bytes)	QoS priority	Transport protocol
CBTC	4.8	8	200	1	UDP
CCTV	0	2000 (mean)	variable	9	UDP
VoIP (G.711)	68.8 (max)	68.8 (max)	172	2	UDP
File update	1000	0	256	9	TCP

4.5.1 QoS Configuration

The different applications considered for this scenario with their assigned data rates and QoS priorities are shown in Table 4.7. This configuration is mostly based on [KHA+13] and it does not consider all the applications shown in Section 4.2, i.e., the platform TV and passenger info applications are not defined.

The CBTC application is configured to send packets of 200 bytes every 333 ms for the DL and 200 ms for the UL. The maximum priority is considered for this application, which implies that the QCI 5 will be used for this flow, as shown in Table 4.3.

The CCTV application is configured to send a video with subway train surveillance footage from the trains to the control room. To simulate this video source, we transmit traces of this video footage encoded according to H.264 with an average bit-rate of 2000 kbit/s. These traces contain the size and timestamp of each packet so the exact behavior of the video flow can be simulated. These traces are generated using a maximum transmission unit (MTU) of 1450 bytes, taking into account the way I, P and B-frames are sent through the network. The same trace file is sent cyclically, but each flow selects the starting point randomly. The lowest priority is assigned to this application, so it does not affect the CBTC and VoIP flows.

The voice application is configured with the G.711 codec parameters, i.e., 50 packets per second are sent with a size of 160 bytes plus 12 bytes for the RTP header. Also, the duration of active and silence periods is modeled using exponential distributions. The active period has a mean duration of 175 ms, whereas the silence period distribution has a mean of 325 ms [BIT14]. QCI 1 (with priority of 2) is assigned to VoIP application and the EPS bearer is configured with the needed GBR.

Finally, the maintenance file update application simulates a constant transmission of data to the trains with a data rate of 1000 kbit/s. This data transmission does not affect the other applications as the lowest priority is assigned to this flow.

All the applications use Unacknowledged Mode (UM) Radio Link Control (RLC) to avoid

the use of the automatic repeat request (ARQ) mechanism. However, hybrid automatic repeat request (HARQ) was enabled for all the transmissions as it only adds a delay of 24 ms in the worst case. Also, the RLC-UM buffer size was set to 1 MiB to avoid packet drops in the simulations.

4.5.2 Frequency Reuse

As shown in Fig. 4.8, there is a high channel variability in the tunnel, even when the receiver is very far away from the eNodeB. Hence, the UEs may receive very high interference from vicinity stations, degrading its SINR and increasing the probability of undesired handovers. Also, the eNodeB will see the interference of the UEs at cell edge. Therefore, using Inter-Cell Interference Coordination (ICIC) techniques is required to mitigate these problems.

We considered the *Hard Frequency Reuse* ICIC technique for this scenario, which is already implemented in the ns-3 simulator. This is the technique that best reduces the interference between eNodeBs and UEs at the expense of a reduced bandwidth. This technique splits the bandwidth in sub-bands and assigns each sub-band to a cell, so transmissions in each cell only use the assigned sub-band. In our case, the 50 RBs are divided into sub-bands of 16, 16 and 18 RBs that are used by the first, second and third eNodeBs, respectively.

However, even with this technique, there is a residual interference affecting the DL signal, as some LTE physical channels have to be transmitted at fixed frequency positions. When the UEs are at the cell edge, we found that the Physical Control Format Indicator Channel (PCFICH) and Physical Downlink Control Channel (PDCCH) signals could not be decoded due to the high interference of the eNodeBs in several subframes. The loss of these control channels causes that the complete subframe in the DL transmission is lost. In addition, the scheduling information for an oncoming UL subframe is also lost.

4.5.3 Handover Customization

The LTE handover process is controlled by the source eNodeB and assisted by the UE, which sends measurement reports to the source eNodeB to decide whether a handover should be performed. Large SNR variations at the cell edges, as those shown in Fig. 4.8, can provoke ping-pong handovers as the conditions for the handover can be met too often, yielding multiple handovers instead of a single one. We have decided to use the *Strongest cell* handover algorithm implemented in the ns-3 LTE module, which is based on [DIM+09]. This algorithm has the following parameters that help to avoid ping-pong handovers:

- **Hysteresis**: The difference in dB between the Reference Signal Received Power (RSRP) of the source and destination cells. We use the default value of 3 dB.
- **Time-to-trigger**: The hysteresis condition should be satisfied during this time before the handover is triggered. We increased the default value from 256 ms to 640 ms.

A high time-to-trigger parameter helps to avoid the ping-pong handovers but delays the handover process. If the handover is delayed too long, a radio link failure can be triggered, increasing the delay of the handover process and the probability of packet loss [ZHA+12]. We incremented the time-to-trigger value as it was required to avoid the ping-pong handovers but also avoiding radio link failures in all the simulations.

4.5.4 Simulation Results

The duration of the simulations is 110 s, which gives enough time to the trains to reach the next station and start the trip to the next one. The trains travel a total distance of about 1300 m or 1510 m, depending on their route.

The transmit power of the eNodeBs was set to 18.5 dBm and the noise figure of both the eNodeBs and UEs was set to 2.07 dB to match the configuration of the measurement campaign described in the Section 4.4.2.

4.5.4.1 Throughput

We performed a simulation to obtain the achievable throughput of each UE over time. We configured two custom traffic sources for each UE to saturate both the DL and UL with packet sizes of 1000 bytes. The applications in Table 4.7 were not configured.

Fig. 4.10 shows the results of this throughput simulation. UEs 1 and 2 start with the complete bandwidth of their cells to end the simulation sharing the second cell. The opposite happens to UEs 3 and 4. This behavior can be seen more clearly in the DL figure as the UL is using the power control mechanism which strives to adapt the transmission power to the fast fading channel. We can see how the PF scheduler in the second cell is assigning the resources to the UEs in a fair way. Also, the differences in the peak throughput are explained by the unequal division of RBs between the cells, as explained in Section 4.5.2.

The average PER obtained in the simulation is $1.1 \cdot 10^{-2}$ for the DL and $2.5 \cdot 10^{-4}$ for the UL. This difference is a consequence of the interference problems in the DL control channels, which can be mitigated with the enhanced PDCCH (ePDCCH) channel used in LTE-Advanced. This enhanced control channel is more flexible in the time-frequency allocation, allowing the eNBs to coordinate between them and minimize the interference in this channel.

4.5.4.2 Packet Delay

This simulation uses the configuration shown in Table 4.7. Fifty runs of the simulation were performed with different random seeds to obtain averaged results. This modifies the behavior of the traffic sources for each run. Also, the distances between the stations and the initial positions of the trains are also modified by a random offset of ± 10 m, i.e., an $U(-10, 10)$ distribution is used to modify the positions. This is needed as the channel model is deterministic and only

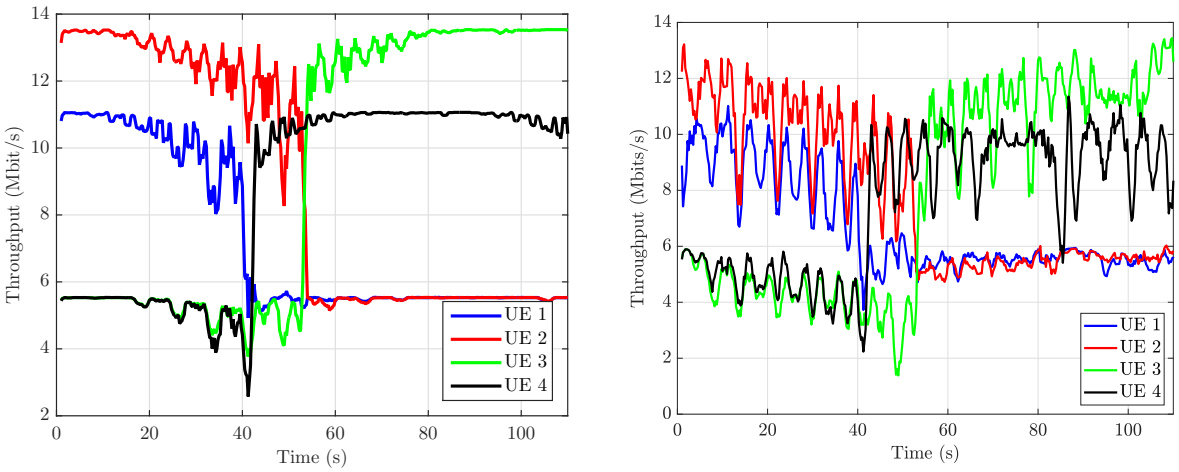

(a) DL throughput.

(b) UL throughput.

Figure 4.10: Throughput for the different UEs for DL and UL. Smoothing of 1 second.

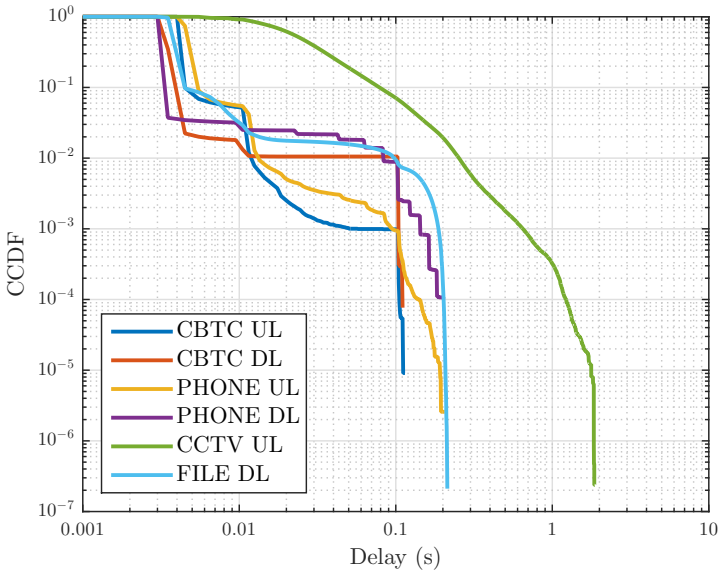

Figure 4.11: CCDF of packet delay for different flows.

depends on the distance. Otherwise, the trains would experience the same channel realizations at the same time instant in all the simulations and the interference between eNodeBs would also be the same.

In Fig. 4.11, the complementary cumulative distribution function (CCDF) of the packet delay for the different flows is shown. The maximum delay for the CBTC traffic slightly exceeds 100 ms with a probability of 10^{-4} and so we can consider that the delay requirements are fulfilled. Also, VoIP traffic has a maximum delay of 200 ms with low probability. The only problematic case is the CCTV traffic, which has a delay of 1 s with a probability of 10^{-4}. This is because the UL channel model is more challenging than that of the DL (has a slightly higher path loss exponent) and the data rate peak values of the CCTV flows cannot be satisfied at some

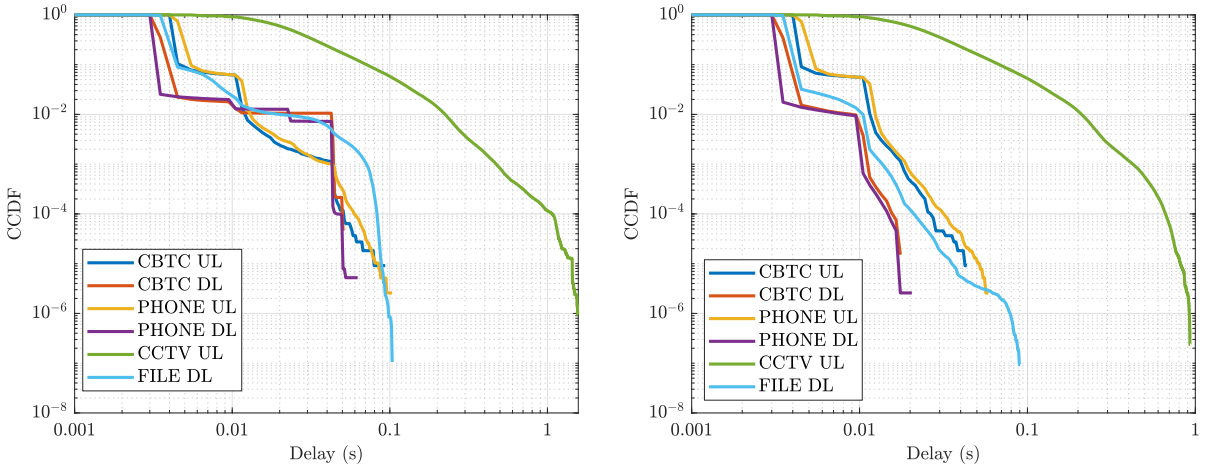

(a) CCDF of packet delay with *t-Reordering* timer set to 40 ms.

(b) CCDF of packet delay with control channel errors disabled. *t-Reordering* timer set to 40 ms.

Figure 4.12: CCDF of packet delay with different configurations.

time instants.

Focusing on the CCDF of the CBTC DL traffic shown in Fig. 4.11, the horizontal line with a 10^{-2} probability indicates that no packets arrived with a delay between 11 and 111 ms, but some outliers arrived with a delay of 111 ms. The reason for these outliers is a delay due to the packet reordering mechanism at the RLC layer. When a packet is lost and the next packet arrives, the *t-Reordering* timer at the RLC layer starts to wait for the lost packet as it could arrive out of order. Only when the timer expires the packet is considered lost and the delayed packet is sent to the upper layer. In the ns-3 simulator, this timer is fixed to wait 100 ms, which explains the delay of the outliers. In Fig. 4.12a, the CCDF of the delay is shown with this timer set to 40 ms, which is a more appropriate value for these simulations as the delay of all the prioritary flows is reduced and the PER is not affected.

We can disable the errors in the DL control channels to simulate that the ePDCCH channel used in LTE-Advanced is activated. Fig. 4.12b shows the delay in this case, with no errors in control channels and only errors in data channels. The delay is clearly reduced for all the applications, being CCTV the only one that exceeds 100 ms. As explained before, the achievable throughput is not enough in some instants, specially the short periods when three UEs are connected to the eNB 2 at the same time. Regarding PER, this enhancement significantly reduces the number of lost packets, achieving an average PER of $4.20 \cdot 10^{-5}$ for the DL and $5.58 \cdot 10^{-4}$ for the UL.

4.6 Complete Subway-Line Deployment

In this section we consider a complete subway-line based on the line 3 of Bilbao Metro. We use the deterministic channel model explained in Section 4.4.1 to perform simulations considering

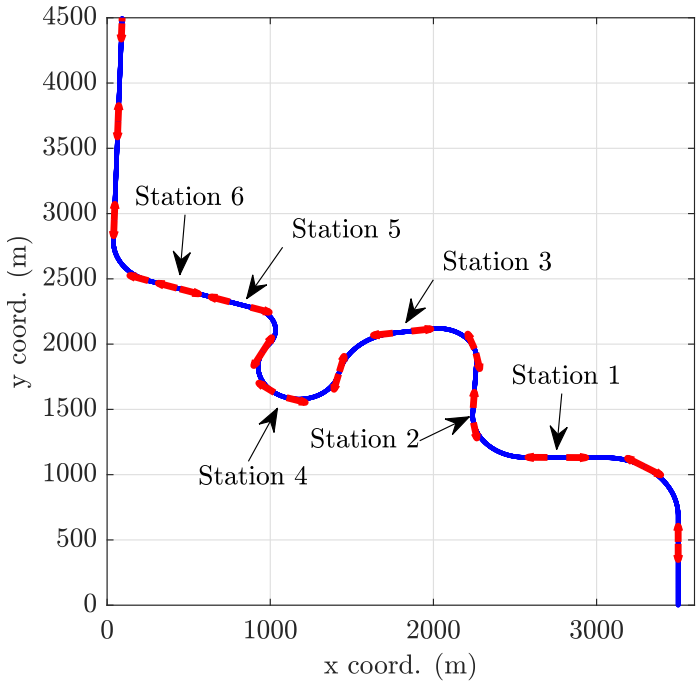

Figure 4.13: Simplified map of the subway line. The red arrows indicate antenna positions. The locations of the six stations are also shown.

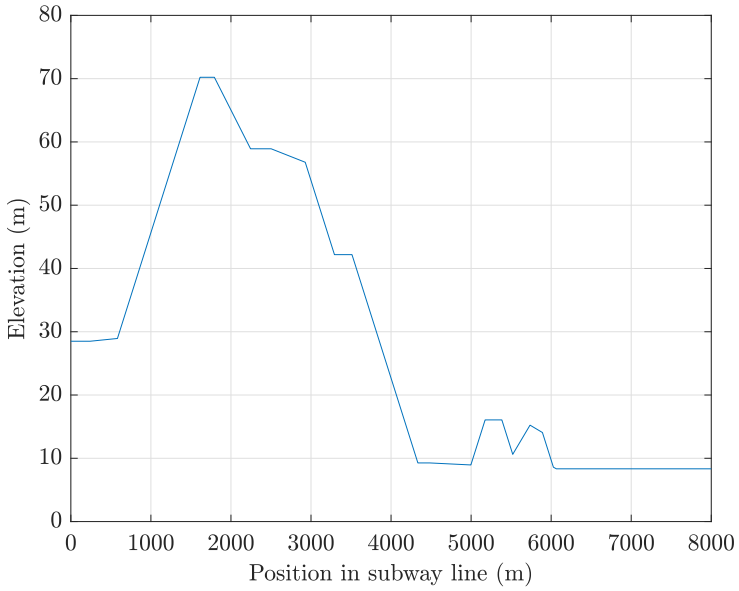

Figure 4.14: Elevation of the subway line.

LTE and Wi-Fi deployments. The complete line is 8 km long with several stations, curves, and slope changes. Fig. 4.13 shows a simplified map of the line with circular curves with radius between 170 and 445 m. The positions in meters of the six stations from the line starting point are 1632, 2330, 3358, 4375, 5255 and 5770. The proposed initial deployment is also shown, with directive antennas located near emergency exits and stations, facilitating installation and maintenance.

We perform LTE and Wi-Fi simulations in this scenario to compare their performance. The considered properties of the deployment are the following:

- Tunnel:
  - Smooth concrete walls with low tilt. We consider that the root-mean-square roughness and tilt are $\gamma = 0.01$ and $\theta = 0.1°$as in Fig. 4.4.
  - Arched cross section with a diameter of 8 m and a height of 6 m, as shown in Fig. 4.2.
  - A simplified version of the tunnel made up of straight lines and circular curves (Fig. 4.13) is used for the generation of the propagation channel as explained in Section 4.4.1.
  - The elevation along the subway line shown in Fig. 4.14 is also considered for the propagation channel.
- Antennas:
  - Tunnel antennas are assumed to be directional with 11.6 dBi and front-to-back-ratio of 25 dB. This is assumed for both LTE and Wi-Fi deployments.
  - Tunnel antennas are deployed in pairs to cover both directions.
  - Tunnel antennas are placed 0.38 m from the walls at a height of 3 m.
  - Train antennas are assumed to be omnidirectional with a gain of 7.5 dBi for LTE and 8.5 dBi for Wi-Fi.
  - Trains only have one antenna installed at the front.
  - All antennas are assumed to be configured with vertical polarization.
- Signal characteristics:
  - 20 MHz bandwidth for both LTE and Wi-Fi.
  - LTE uses the central frequencies 1774.9 MHz (UL) and 1869.9 MHz (DL). EARFCN 1849.
  - Wi-Fi can use all the available 5 GHz channels.
  - The transmission power used in LTE and Wi-Fi is not the same due the different regulations. In LTE we use 34 dBm of transmission power and in Wi-Fi we use 20 dBm of effective isotropic radiated power (EIRP), i.e., we have to take into account the antenna gains to not exceed the EIRP limit.

These parameters are the same as the used for the generation of Fig. 4.4. The only differing parameters are the transmission power and the defined antenna gains for LTE and Wi-Fi. Also, the figure does not show the propagation channel for all the central frequencies as only the LTE DL (1869.9 MHz) and the 5.5 GHz Wi-Fi channel are shown.

Fig. 4.15 shows the simulation setup with the six considered stations and ten trains. The wayside infrastructure is not shown as it is distributed along all the line. There is a unique central server that sends and receives all the DL and UL packets. The simulation starts with the trains inside the stations, with two trains in stations 2–5 and one train in stations 1 and 6. The trains' routes are simulated in the same way as in Section 4.5.

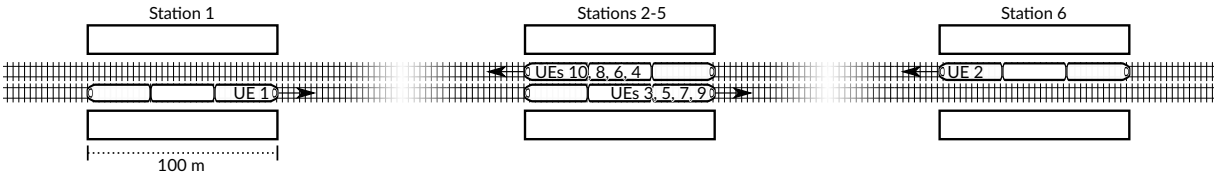

Figure 4.15: Starting position of the trains in the simulations.

4.6.1 Channel Model for LTE Deployment

This section shows the radio propagation in the tunnel for the LTE deployment taking into account the models described in Section 4.4.1. The deployment uses FDD with transmission frequencies 1869.9 MHz and 1774.9 MHz for the DL and UL, respectively.

The propagation channel for one wayside antenna can be easily obtained using the multimode channel model and considering the coupling loss, roughness loss and tilt loss, as shown in Fig. 4.4. Additionally, the effect of curves and slope changes are calculated for each antenna depending on the position. This will provide us the received power from each antenna along all the tunnel positions.

Cellular network technologies are usually deployed inside tunnels using distributed antenna systems (DASs) to ensure the coverage along all the tunnel [LIU+17; TOL15]. The usage of DASs allows for deploying cells that cover more distance, minimizing the interference between them and avoiding an excessive number of handovers inside the tunnel. A DAS allows for configuring several distant antennas as only one cell, transmitting the same signal in a coordinated way that minimizes the interference between antennas. More details about DAS usage in cellular networks can be found in [TOL15; HEJ14].

Fig. 4.16 shows the received power from wayside antennas along a segment of the tunnel. It can be seen how the signal from one antenna (red) will experience high interference from the remaining antennas (blue) if they transmit independent signals in the same frequency. If a DAS is configured with these antennas, all the antennas will transmit the same signal at (nearly) the same time. This way there will be no interference in the receiver and only an artificial multipath channel will be perceived by the receiver. The complexity of the multipath channel will depend on the separation of the antennas and the synchronization between the antennas. So, the size of each configured cell in the tunnel is limited by the distance between the DAS antennas as timing issues may arise [TOL15, Chapter 11].

We assume that the transmission of the same signal by the different antennas is always constructive unless the delay exceeds the cyclic prefix (CP), which would create inter-symbol interference. This assumption can be unrealistic in some cases as shown in [HSI+11], where a 0 dB echo channel with a delay of half of the CP seriously degrades the throughput in a WiMAX system. However, we consider that these situations are very uncommon in this scenario and they would further complicate the study unnecessarily.

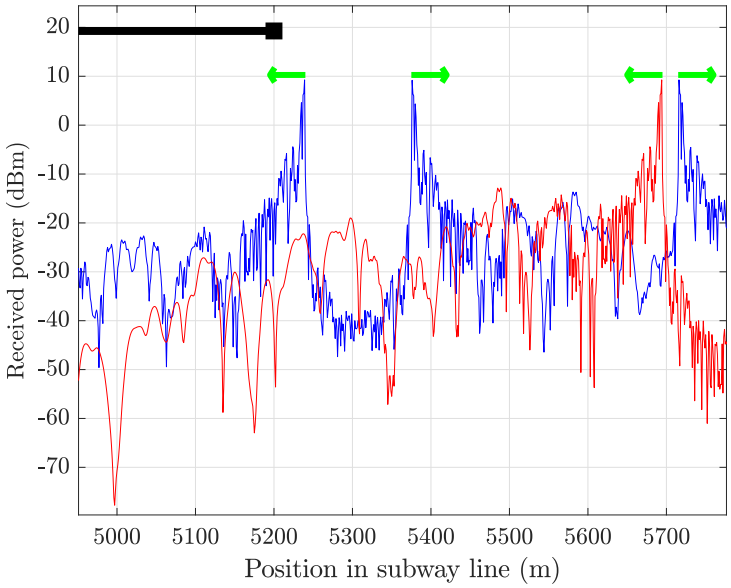

Figure 4.16: DL received power in a subway segment from one antenna (red). The sum of the received power from the remaining antennas is shown in blue. The green arrows indicate the position of tunnel antennas. The black line indicates a curved segment.

In LTE, the normal CP length is 4.7 μs although an extended CP length can be configured with 16.7 μs. Fig. 4.17 shows the received power and interference in the line if we consider that all the antennas are used in a DAS. The interference calculation is idealized as only signals with delay higher than 4.7 μs are considered interference. Also, a perfect DAS synchronization is assumed. The perceived interference is very low along all the line except in positions 6000 and 8000, as the last three antennas pairs are too separated.

If only one cell is configured, the system capacity will be very limited and radio resources will be underused. Very distant trains could use the same time-frequency allocation as they will not interfere between them but the one-cell configuration does not allow it. A better solution that increases the total throughput is to group the antennas into three cells using DASs . These three cells will combine DAS with ICIC techniques to minimize interference in cell limits and increase system capacity [WAN+16]. The lower size of the configured DAS will help with the potential timing issues and the artificial multipath channel will be weaker.

The received power from each cell is shown in Fig. 4.18. Frequency reuse techniques should be used to mitigate the high interference in the cell edges. The central cell is smaller in size because the deployment is configured so each cell serves two subway stations. This configuration will be used in the LTE simulations.

To include this channel model in the simulator we had to implement a new propagation model in ns-3. This propagation model indicates to the simulator the received signal strength for each communication between the devices and the base stations (eNB) based on their position on the metro line and the frequencies used. This model uses two files generated offline for each eNB, one for the DL and other for the UL. Each file contains the propagation losses at each

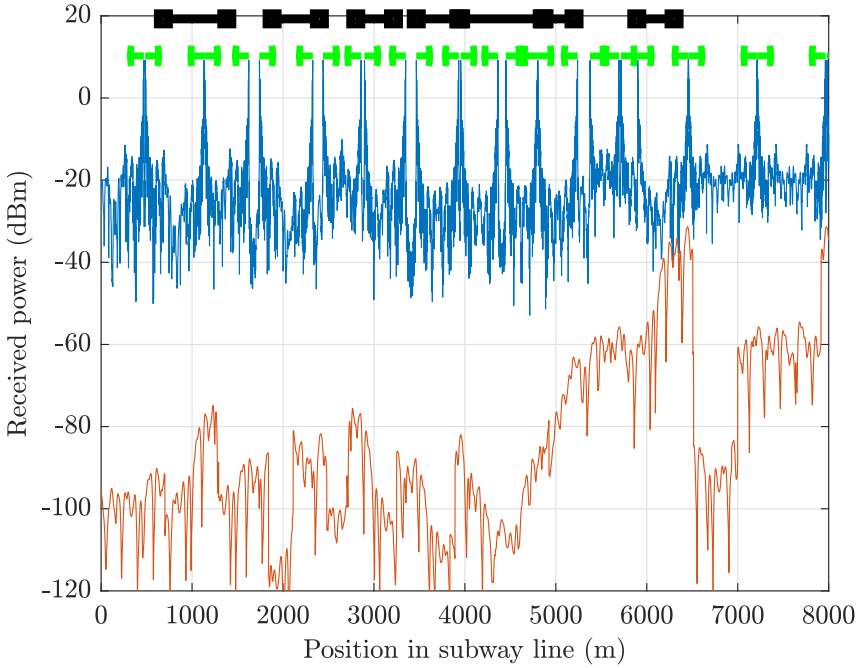

Figure 4.17: DL received signal power along the line if all the antennas are part of a DAS and transmit the same signal at the same instant (blue). The received power of the signal with a delay higher than the CP length is shown in red as it is considered interference. The green arrows indicate the position and orientation of tunnel antennas. The black lines indicate the curves.

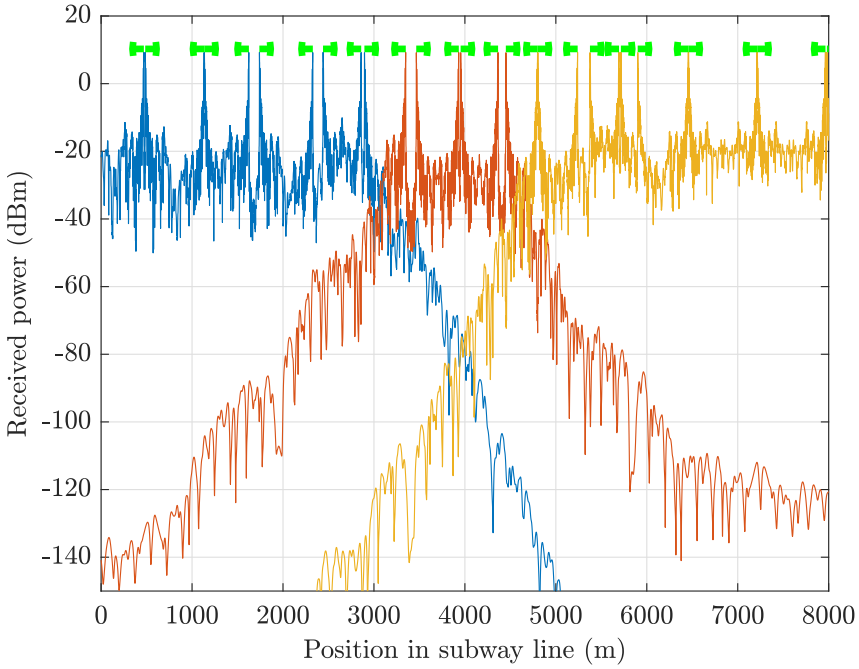

Figure 4.18: DL received signal power from each cell along the line. DAS are used to configure three cells. The green arrows indicate the position and orientation of tunnel antennas.

position in the tunnel and for each physical resource block (PRB). Furthermore, this model allows for the calculation of interference between devices: on the one hand, each UE receives the signal from the eNB to which it is connected in addition to interference from the rest of eNBs and, on the other hand, each eNB receives the signal from all the UEs connected to the station and the interference generated by the UEs connected to other stations.

4.6.2 Channel Model for Wi-Fi Deployment

This section shows how radio propagation is for a Wi-Fi deployment taking into account the models described above. The deployment to be simulated will use one access point for each antenna deployed in the tunnel. In addition, the 5 GHz band will be used because it has a greater number of independent channels than in the 2.4 GHz band, thus reducing interference.

A significant limitation of Wi-Fi is that the transmission power allowed is quite low. The EIRP values defined in Europe[1] for the 2.4 and 5 GHz bands are:

- 2400–2483.5 MHz: 100 mW.
- 5150–5250 MHz: 200 mW. Restricted to indoor.
- 5250–5350 MHz: 100 mW. Restricted to indoor. DFS usage is required to avoid interfering with radar systems.
- 5470–5725 MHz: 500 mW. DFS usage is required.
- 5725–5875 MHz: 25 mW. Restricted band for short range devices (ETSI EN 300 440-1).

To simplify the analysis we will assume that the transmission power of all Wi-Fi devices is 100 mW (20 dBm). In addition, it should be noted that antenna gain also influences EIRP calculation, forcing a reduction of the transmission power to avoid exceeding the limit. Therefore, antenna gain only increases the signal reception power but not the transmission power.

The simulations will use 20 MHz Wi-Fi channels to maximize the number of available channels and minimize the interference between APs and STAs. In addition, in the case of Wi-Fi, using channels with higher bandwidth would reduce the received signal quality because the same transmission power is distributed over a higher band, reducing the power transmitted by subcarrier and, therefore, the SNR. In this subway scenario we use 20 MHz channels to maximize the coverage distance and minimize the number of APs needed. Moreover, this configuration is able to provide the required throughput for the applications when a minimum SNR is guaranteed.

In contrast to LTE deployment, the low transmission power makes the initially proposed antenna deployment unfeasible. Fig. 4.19 shows the SINR obtained along the line with the antennas deployed for LTE. It can be seen that the SINR is very low at too many points along the line.

[1] https://eur-lex.europa.eu/legal-content/EN/TXT/HTML/?uri=CELEX:32005D0513&from=EN

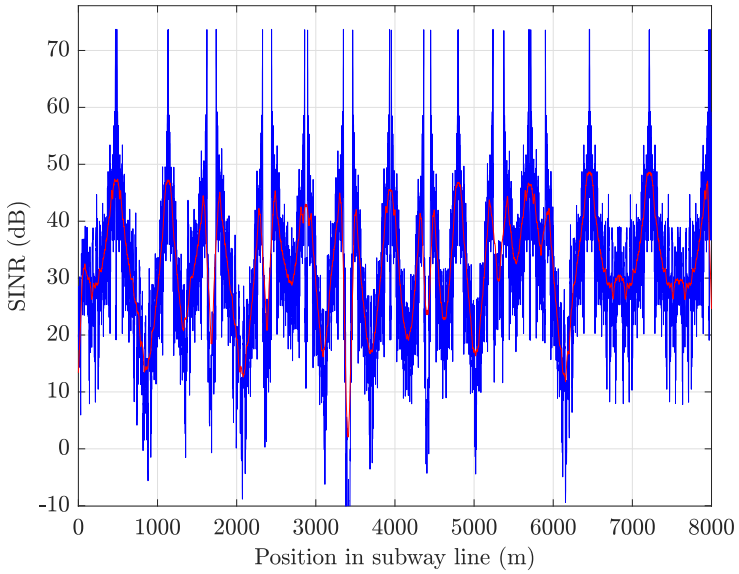

Figure 4.19: SINR along the line in Wi-Fi deployment using the same antenna positions as in the LTE deployment (blue). The red line is the smoothed SINR.

The noise floor used for the SINR calculation is obtained with the expression:

$$P_{\text{noise}}(\text{dBm}) = -174 + 10\log_{10}(\text{BW}) + \text{NF}$$

where BW is the signal bandwidth and NF is the receiver noise figure . This expression assumes a thermal noise of -174 dBm/Hz. The obtained noise floor for this Wi-Fi case is -93.99 dBm as the bandwidth is 20 MHz and the receiver noise figure is 7 dB.

To ensure that the SNR does not fall below 10 dB at any point, access points should be placed every 400 m or less. Fig. 4.20 shows the SNR for an antenna located at the beginning of the curve with the highest attenuation (7.65 dB per 100 m). It can be seen that the SNR is not lower than 10 dB until 200 m. If the antennas are placed at 400 m, the train could change the access point at 200 m to remain connected with good signal reception.

Therefore, a Wi-Fi deployment will be simulated with two directional antennas every 400 m to provide coverage of the entire line. In total there will be 38 access points on the line (19 pairs of APs) with one directional antenna each. The first AP will be at position 400 m and the last one at position 7600 m. Every 400 m there will be two access points, each with a directional antenna pointing in opposite directions. Fig. 4.21 shows the power received along the line with this deployment and the interference between the access points when using 8 different Wi-Fi channels. This way the APs interfere with a separation of 1600 m allowing interference to stay below the noise floor and obtaining an SINR higher than 10 dB for all the line.

To simulate this Wi-Fi deployment is necessary to develop a new propagation model in ns-3. This new propagation model takes into account the Wi-Fi channel used and the distance between the devices. It uses a file for each Wi-Fi channel containing the propagation loss as a function of the distance. The model also calculates propagation losses due to curves and slope

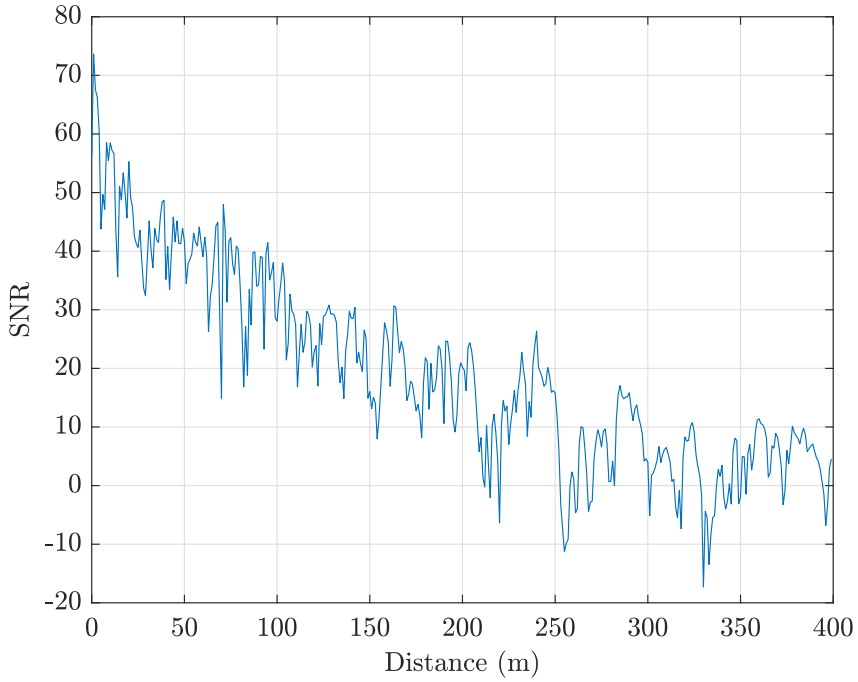

Figure 4.20: SNR vs. distance for a Wi-Fi signal in the curve with the highest attenuation.

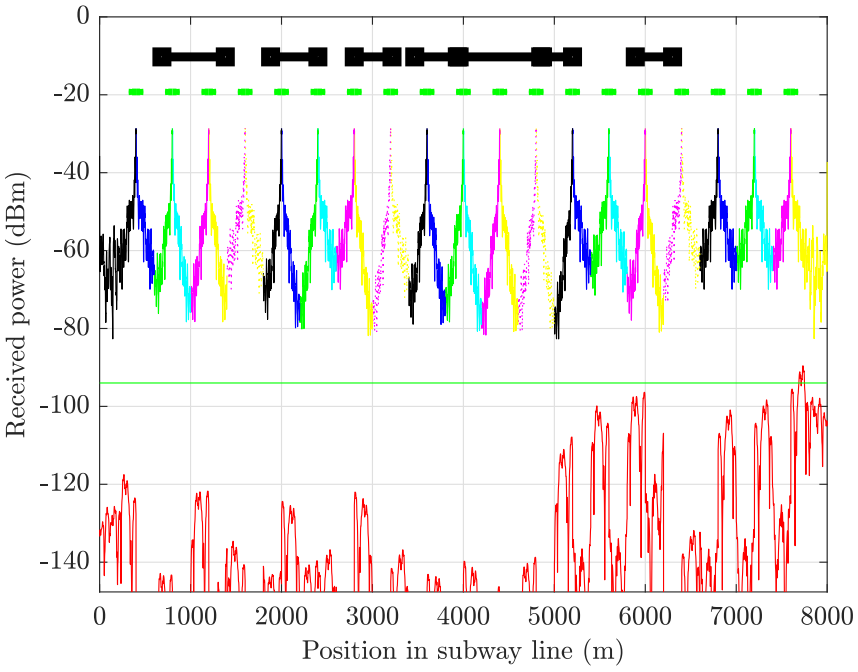

Figure 4.21: Reception power for a Wi-Fi deployment with APs every 400 m configured to use eight different Wi-Fi channels. The received power is shown in different colors depending on the used channel. The interference between APs is shown in red. The -93.99 dBm noise floor is represented with the green horizontal line. The black and green lines at the top indicate the curves and the APs positions, respectively.

Table 4.8: Applications configuration for the complete subway-line deployment. The throughput values are all constant, except for the video streams where the mean bitrate is indicated, and the voice stream where the active period bitrate is shown.

Application	DL (kbit/s)	UL (kbit/s)	Packet Size (bytes)	QoS priority	Transport protocol
CBTC	100	100	200	Very high	UDP
CCTV	0	6 ×1000 (mean)	variable	Best effort	UDP
Platform TV	2 ×1000 (mean)	0	variable	Best effort	UDP
VoIP (G.711)	68.8 (max)	68.8 (max)	172	High	UDP
Maintenance	200	200	200	Best effort	UDP
Passenger info	100	0	256	Best effort	UDP

changes, taking into account the positions of the devices within the line. This calculation is performed in simulation time and is necessary because the files only depend on the distance and not on the position of the devices in the subway line.

Finally, the wayside antennas were configured in the simulator with a radiation pattern that applies the considered front-to-back-ratio of 25 dB.

4.6.3 QoS Configuration

The different applications considered for this scenario with their assigned data rates and QoS priorities are shown in Table 4.8. This configuration considers all the applications analyzed in Section 4.2. The selected data rates are based on Table 4.1, resulting in a more demanding configuration in terms of throughput with respect to the configuration used in the three-stations deployment (Table 4.7). The total throughput required for each train is 2.47 Mbit/s for the DL and 6.37 Mbit/s for the UL, not taking into account the overhead caused by the headers of the different protocols.

All the applications are simulated using UDP as transport protocol. This allows us to calculate the packet loss in each application more easily. Although, another protocol such as TCP may be used in real implementations.

The CBTC application is configured to send packets of 200 bytes every 16 ms, for both UL and DL.

Each video stream sent by the CCTV and platform TV applications is generated using a video file trace with an average bitrate of 1 Mbit/s. The throughput requirements of the video changes with time as the bitrate fluctuates between 0.4 Mbit/s and 1.7 Mbit/s. The CCTV application sends six video streams while the platform TV application sends two. The video

traces are generated the same way as in Section 4.5.1.

The voice application is configured with the G.711 codec parameters, the same way as in Section 4.5.1, with the same active and silence periods.

The maintenance application has a data rate of 200 kbit/s in DL and UL for telemetry tasks and does not include the file update service. The passenger information application has a low bitrate to support the PIS and the public announcement service.

Regarding the QoS, it has been decided to give priority to CBTC and VoIP traffic, leaving the rest of the services with best effort priority. This ensures that these two applications have the minimum delay. Video streams could be given a slightly higher priority, but this could seriously impact the remaining applications due to the high throughput requirements of video streams.

In the LTE case, these priorities are mapped into the QoS classes shown in Table 4.3. CBTC traffic is assigned to the class with the highest priority (QCI 5 "IMS signaling"). VoIP traffic is assigned to the next class in priority (QCI 1 "conversational voice"). All other applications use the default best effort class with the lowest priority (QCI 9).

For Wi-Fi, priorities are mapped onto the access categories defined in IEEE 802.11e. CBTC and VoIP will use the voice category (AC_VO), which has the highest priority and lowest delay. The remaining applications will use the best effort category (AC_BE).

4.6.4 LTE Simulations

The ns-3 simulator provides a highly detailed simulation of the behavior of an LTE network. However, there are certain features of LTE-Advanced systems that cannot be simulated such as the ePDCCH. The PDCCH is a channel that contains the control information needed to decode the rest of the data for each subframe. In the first LTE releases, this channel is always transmitted in the same time slots and at the same frequencies, causing quite a lot of interference between cells. The ePDCCH is more flexible and allows for minimizing the interference on this critical data between the different stations. In order to simulate this expected behavior in a real system, errors in the control data have been disabled, so it is assumed that base stations will coordinate to avoid interference in these data.

As explained in Section 4.6.1, the LTE deployment is configured with three eNBs, each one using a DAS to connect to all its assigned antennas. The three cells cover the subway line positions 0–3000, 3000–4600 and 4600–8000, respectively. This way, each eNB provides coverage to two metro stations.

As in the three-stations deployment, all the applications use UM RLC to avoid the use of the ARQ mechanism, but HARQ is enabled for all the flows.

The eNBs transmit with a power of 34 dBm. UEs use power control and their transmit power ranges between -40 dBm and 23 dBm. The default value for the noise figure is used, so 5 dB and 9 dB are considered for the eNBs and UEs, respectively.

LTE is designed to use a frequency reuse factor of one, i.e., all the cells (or sectors) use

the same carrier frequency to maximize the usage of spectral resources. This design requires the use of ICIC techniques such as fractional frequency reuse (FFR), where each cell uses a subset of all the available subchannels to communicate with some users (usually the cell-edge users). The simulator also allows for the use of different FFR mechanisms explained in the ns-3 documentation[2]. We will perform simulations with three FFR configurations: FFR disabled (NoFR), hard frequency reuse (HFR), and a custom dynamic FFR scheme (DFR):

NoFR FFR is disabled. The three cells are allowed to use all the available spectrum.

HFR The hard FFR method distributes the usable spectrum in several sub-bands which are assigned exclusively to each cell. This way, there is no interference between adjacent cells. This method was also used in the three-stations deployment (Section 4.5.2).

DFR This is a custom FFR method based on the soft frequency reuse (SFR) algorithm. The previous methods are static, as the spectrum sharing does not change with time. This scheme is dynamic as it adjusts the sub-band size of each cell depending on the number of users in the cell. The number of assigned RBs per user is configured depending on the QoS needs and the total number of UEs (which are fixed in our use case). This way, when a UE performs handover, the cells adapt their used sub-band to provide enough bandwidth for the users, trying to avoid interference with other cells. Like in other FFR methods, the UEs are also classified into cell-center or cell-edge. This way, the UEs near the cell center are allowed to transmit in all the assigned sub-band, but the cell-edge UEs are restricted to use a smaller sub-band to avoid interference in the cell edge. Moreover, different power levels can be used to communicate with cell-center or cell-edge UEs. UE measurements are used to classify the UEs into cell-center or cell-edge. In our case, we only use the Reference Signal Received Quality (RSRQ) measurement.

The HFR method is already implemented in ns-3 for a cellular deployment with reuse factor of 3. Given the unusual cell placement in the tunnel, we adapted this algorithm to use a reuse factor of 2, so more bandwidth can be used by each cell. This way, the first and last cell can use the same sub-bands since they are far away from each other and the interference is very low (see Fig. 4.18). The DFR algorithm was also customized to define only two sub-bands.

4.6.4.1 Throughput and PER with One Train

These first simulations allow us to obtain the PER and the throughput under ideal conditions, with only one train leaving from the first station.

To obtain the throughput, a single traffic flow is transmitted in each direction (DL, UL) with 80 Mbit/s and a packet size of 1000 bytes. These flows will saturate the communications allowing us to obtain the maximum achievable throughput. In order to calculate the PER, it is necessary to reduce the bitrate so no packets are lost due to network saturation, i.e., packets

[2]Fractional frequency reuse documentation in ns-3 LTE module: https://www.nsnam.org/docs/models/html/lte-design.html#supported-fr-algorithms

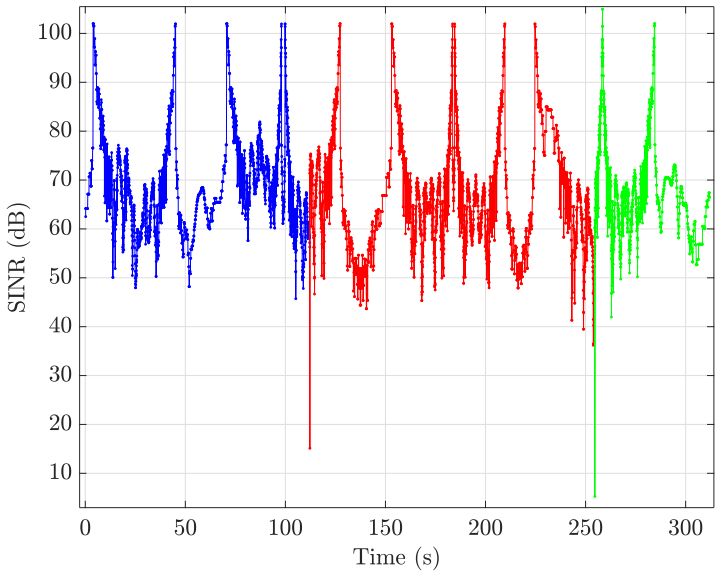

Figure 4.22: DL SINR during the train trip in LTE deployment. The colors indicate which cell the train was connected to.

Table 4.9: Throughput and PER with one train in LTE deployment.

	DL	UL
Throughput (Mbit/s)	75.37	74.84
PER	$5.76 \cdot 10^{-5}$	$2.77 \cdot 10^{-5}$

dropped due to overflow in transmission queues. Therefore, we opted to configure 25 Mbit/s in each direction.

The simulation has a duration of 300 s, in which the train departs from the first station (1732 m) and arrives at the fifth station (5355 m), stopping at intermediate stations.

Fig. 4.22 shows the SINR on the DL during the simulation. It can be seen that the SINR is very high because there is no interference as the base stations only transmit data when they are connected to the UE. Only two SINR drops are perceived when the handover process is performed.

The obtained throughput and PER are shown in Table 4.9. As expected, the throughput obtained is 75 Mbit/s and corresponds to the theoretical maximum for LTE with 20 MHz bandwidth and 64-QAM modulation. During the handover process some packets were lost which makes the PER not zero, but still very low.

4.6.4.2 Throughput and PER with Ten Trains

We repeat the previous simulations with ten trains distributed as shown in Fig. 4.15. Interference will arise in these simulations as the trains will be connected to different cells. The three FFR configurations are evaluated in this subsection: NoFR, HFR and DFR.

Table 4.10: Total throughput and PER with ten trains in LTE deployment.

	NoFR		HFR		DFR	
	DL	UL	DL	UL	DL	UL
Throughput (Mbit/s)	204.3	185.2	107.7	105.1	144.4	132.2
PER	$4.50 \cdot 10^{-4}$	$1.65 \cdot 10^{-3}$	$1.72 \cdot 10^{-5}$	$1.91 \cdot 10^{-4}$	$1.08 \cdot 10^{-4}$	$8.25 \cdot 10^{-4}$

In these simulations, the flows in each direction are configured with 38 Mbit/s to saturate the cells and calculate the maximum achievable throughput. To correctly calculate the PER, the flows are configured with 7 Mbit/s for NoFR and DFR simulations, and with 5 Mbit/s for HFR.

The simulations have a duration of 140 seconds. The obtained averaged results for 50 runs of the simulations are shown in Table 4.10. Each run of the simulation has a different random seed, modifying the behavior of the traffic sources, the distances between the stations and the initial positions of the trains.

The NoFR simulations achieve more total throughput than the simulations of the previous section. This is because the three eNBs are serving the trains simultaneously. However, the interference between the cells increases the packet loss.

In HFR simulations, the total throughput is reduced because each cell has one half of the assigned spectrum, but it should be enough to fulfill the application requirements. The achieved error rate is very low because there is no interference between cells.

Finally, DFR obtains intermediate results compared to NoFR and HFR. The obtained throughput is higher than in HFR simulations and the error rate is lower than in NoFR. This dynamic FFR method provides more bandwidth to each cell only when needed (depending on the number of users) to increase the achievable throughput without introducing too much interference. The DFR algorithm was configured to assign 20 RBs per user for each cell of the 100 RBs available. This way, two neighboring cells can interfere each other only when they have three or more cell-edge users each (assuming there is no interference between cell-edge and cell-center users). Also, when five or more users are in a cell, all the available bandwidth can be used by the cell-center users. Fig. 4.23 shows the number of users assigned to a cell during the simulation, which is usually three or four and never higher than five. Using a more conservative configuration of 15 RBs per user reduces PER to $1.77 \cdot 10^{-5}$ and $4.27 \cdot 10^{-4}$ for DL and UL, respectively.

4.6.4.3 Packet Delay

These simulations have a duration of 140 seconds with ten trains and the traffic configuration of Table 4.8. This implies that with ten trains a total bitrate of 24.7 Mbits/s on the DL and 64 Mbit/s on the UL will be required on average. The delay distribution for each application is shown in Figs. 4.24 and 4.25 for each FFR configuration. Fifty runs with different random

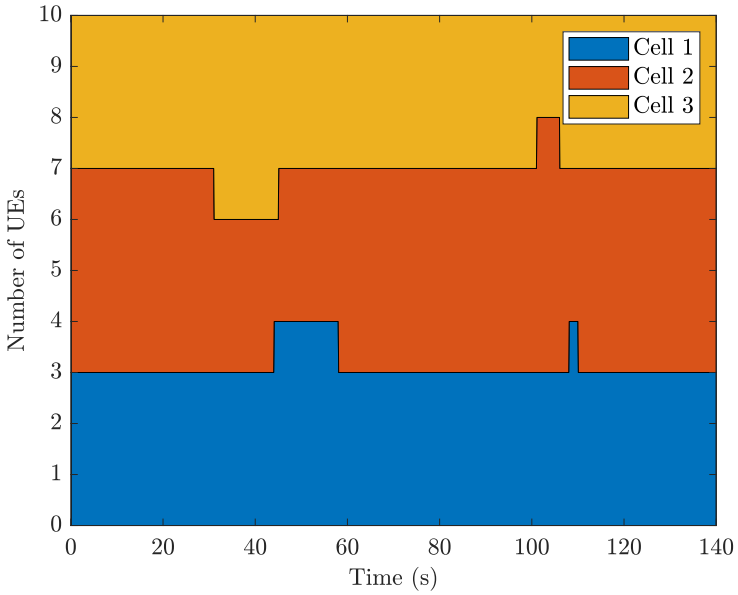

Figure 4.23: Number of UEs assigned to each cell during a simulation with ten trains in LTE deployment.

seeds were performed for each configuration.

The results of the NoFR configuration are shown in Fig. 4.24 where the priority applications (CBTC and PHONE) have a low delay. The DL applications without priority (INFO, TVPLAT and MAINT) have a slightly higher delay that almost reaches 100 ms. This is because there is enough capacity in the DL to transmit all its information during all the simulation. UL applications without priority (CCTV and MAINT) suffer longer delays due to the high throughput requirements of CCTV traffic, but these delays of 300 ms are perfectly acceptable. The mean PER for the CBTC application is $1.65 \cdot 10^{-3}$ for the DL and $1.35 \cdot 10^{-3}$ for the UL. These values are slightly higher than the required 0.1% packet loss.

Fig. 4.25a shows the delay using HFR. In these simulations, the DL flows have lower delay than the NoFR simulations thanks to the very low PER. However, the UL applications suffer longer delays because the variable throughput demands of CCTV flows cannot be met during the whole simulation. This has a small impact on the prioritized applications in the UL such as CBTC, which exceeds 100 ms delay with a very low probability ($5 \cdot 10^{-6}$). The CCTV and MAINT UL traffic experienced delays higher than 500 ms with a probability of $9 \cdot 10^{-4}$, with a maximum delay of 1.2 seconds. The packet loss requirement for the CBTC application was fulfilled in these simulations, obtaining a mean PER of $1.9 \cdot 10^{-5}$ and $2.10 \cdot 10^{-4}$ for DL and UL, respectively.

Fig. 4.25b shows the delay using DFR. The results obtained are analogous to those in Fig. 4.24 (NoFR), except that the delay of UL applications is higher. However, the delay requirements of CBTC and CCTV are still satisfied. A very small number of CBTC and PHONE UL packets were received with more than 100 ms that results in a very low probability of $7 \cdot 10^{-7}$ and $2 \cdot 10^{-6}$, which is still acceptable. Regarding CBTC PER, in contrast to the NoFR results, the 0.1% packet loss requirement was satisfied with a mean PER of $4.8 \cdot 10^{-5}$ and $6.11 \cdot 10^{-4}$

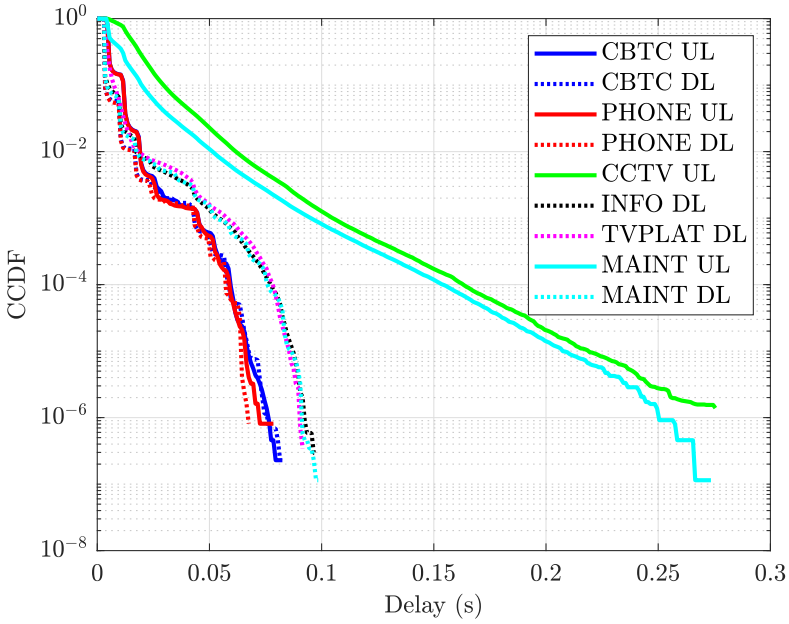

Figure 4.24: CCDF of packet delay for each application with FFR disabled (NoFR) in LTE deployment.

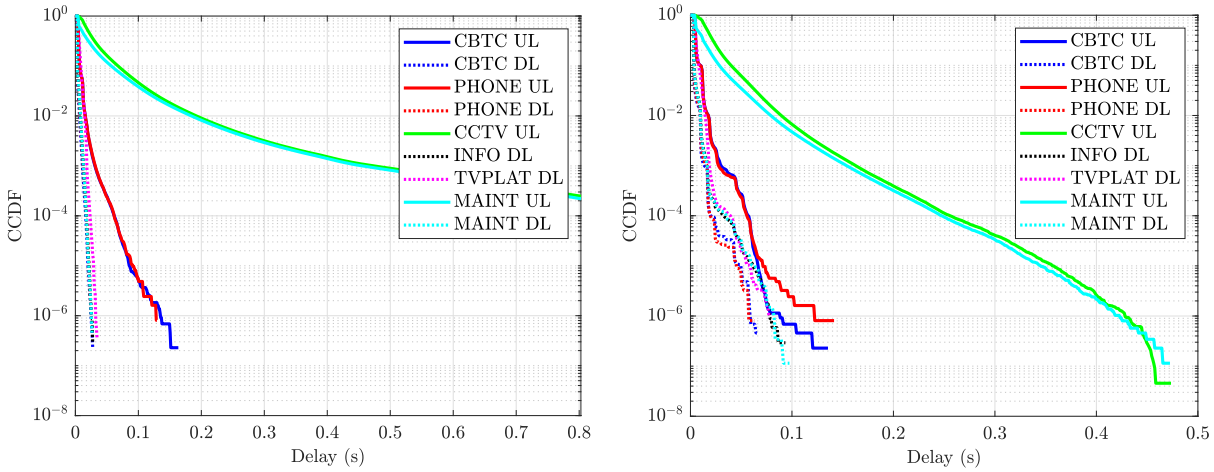

(a) Packet delay using HFR configuration.

(b) Packet delay using DFR configuration.

Figure 4.25: CCDF of packet delay for each application using FFR in LTE deployment.

for DL and UL, respectively.

4.6.5 Wi-Fi Simulations

The simulations are performed with the deployment described in Section 4.6.2: 19 pairs of APs separated every 400 m and using eight different Wi-Fi channels in the 5 GHz. As explained in Section 4.3.2, 802.11a is used to avoid some bugs in the 802.11ac implementation of ns-3.

To evaluate the impact of the handover delay, we perform simulations using two of the handover methods explained in Section 4.3.2.1: ActiveProbing (with 20 ms delay) and FastHandover. The STAs are configured to check which is the closest AP every 100 ms and perform a handover if necessary. This handover will be done by switching directly to the Wi-Fi channel used by the destination access point.

The simulated backbone is very simple and contains a switch that interconnects all APs with the central server via 10 Gbit/s Ethernet connections. IP routing is assumed to be perfect and is done without any delay when the handovers are performed. In addition, all devices have the MAC addresses of the other devices preloaded in their ARP cache, avoiding the delays produced by the ARP protocol.

The simulator allows for the use of several rate control algorithms. Due to the high variability of the channel during the trains' route, it is very important to select an algorithm that adapts quickly to these changes in order to take advantage of the moments with high SNR and avoid losing packets when the SNR drops quickly. The Collision-Aware Rate Adaptation (CARA) algorithm [KIM+06] has been selected because it provides the best results in the simulations.

Wi-Fi QoS mechanisms are activated in the simulations. Each access category has a separate queue. Each of these queues cannot transmit data until the other higher priority queues are empty. In some cases this priority queueing mechanism can cause lower priority queues to go unattended for a long time, but in our case the higher priority flows require low throughput.

An FqCoDel[3] queue has also been configured for each queue of the Wi-Fi device so that, within the same queue, one type of traffic cannot block the correct operation of the rest. Packets are classified within each queue according to their destination (IP and port) and are assigned an equivalent priority within their queue.

As for LTE, three types of simulations are performed: with a single train to measure throughput and PER without interference, with all ten trains to measure throughput and PER, and the final simulation with all applications to measure the delay.

4.6.5.1 Throughput and PER with One Train

These simulations obtain the PER and throughput under ideal conditions, with a single train leaving from the first station.

[3] https://www.nsnam.org/docs/release/3.29/models/html/fq-codel.html

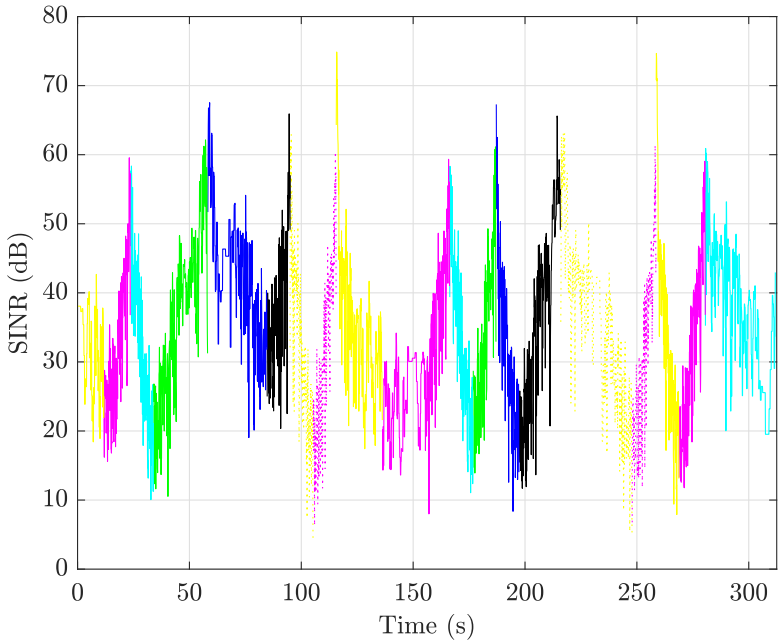

Figure 4.26: DL SINR during the train trip in Wi-Fi deployment. The color indicates the Wi-Fi channel used. Each AP is configured with one of the eight channels considered in the deployment.

Table 4.11: Throughput and PER with one train in Wi-Fi deployment.

	ActiveProbing		FastHandover	
	DL	UL	DL	UL
Throughput (Mbit/s)	11.34	11.60	11.35	11.59
PER	$1.89 \cdot 10^{-3}$	$1.80 \cdot 10^{-3}$	$8.32 \cdot 10^{-4}$	$4.69 \cdot 10^{-4}$

The throughput calculation is performed with a single flow in each direction (DL, UL) at 90 Mbit/s, with a packet size of 1000 bytes. The PER simulations use 5 Mbit/s flows. The simulation has a duration of 300 seconds.

Fig. 4.26 shows the DL SINR during the simulation. It can be seen that the maximum and minimum values in the graph correspond to Fig. 4.21 and the SINR is almost always higher than 10 dB.

Table 4.11 shows the throughput and PER results for the two handover mechanisms.

The PER is low in both cases, although the FastHandover mechanism obtains better results because it performs the handover process faster. In fact, in these simulations no packets are lost in Wi-Fi transmissions thanks to the Wi-Fi retransmission mechanism that allows for sending the same frame up to 7 times while the receiver does not confirm its reception. In addition, CARA algorithm uses more robust transmission rates when it is necessary to retransmit frames. This ensures that no packets are lost at the cost of lowering the transmission speed. In the simulations, packet loss occurs in the following situations:

Table 4.12: Throughput and PER with ten trains in Wi-Fi deployment.

	ActiveProbing		FastHandover	
	DL	UL	DL	UL
Total throughput (Mbit/s)	101.01	109.85	101.07	109.93
PER - 2.5 Mbit/s	$1.59 \cdot 10^{-3}$	$1.52 \cdot 10^{-3}$	$4.40 \cdot 10^{-4}$	$3.55 \cdot 10^{-4}$
PER - 5 Mbit/s	$4.86 \cdot 10^{-3}$	$1.77 \cdot 10^{-3}$	$3.73 \cdot 10^{-3}$	$6.09 \cdot 10^{-4}$

- During handover process:
  - The STA is disconnected and any attempt to send an IP packet from the STA is discarded.
  - When the STA disconnects from an AP, the packets that are still in the AP queues are discarded.
- When the achieved throughput is too low and the transmission queues are filled. In these simulations, no packet loss has been detected for this reason.

The throughput results are not affected by the handover mechanism used. Moreover, the total obtained throughput (DL + UL) is close to the actual throughput usually obtained with 802.11a (around 25 Mbit/s).

4.6.5.2 Throughput and PER with Ten Trains

The above simulations are repeated to calculate the PER and achievable throughput with ten trains distributed over the stations as shown in Fig. 4.15. The flows of each train are configured in the same way as the previous subsection, but the PER is also obtained using flows of 2.5 Mbit/s. The simulations are now 140 seconds long. Fifty runs of each configuration are performed to obtain averaged results.

Table 4.12 shows the results of PER and throughput. As in the previous simulations, packet loss occurred only during the handover process and no packets were lost in Wi-Fi transmissions. This causes the PER results to be affected by the configured transmission bitrate: the higher the transmission rate, the higher the number of packets lost during the handover, specially the packets discarded in the AP queues, which will be more filled. This explains that the PER obtained with 2.5 Mbit/s is lower than with 5 Mbit/s, more notably in the DL.

The throughput obtained by each train is slightly lower than in the one-train simulations (Table 4.11). No degradation due to possible interference is observed, and no AP is overloaded by the simultaneous connection of several trains. It is also observed that the UL obtains a better bitrate than the DL. This is because the UL obtains a longer transmission time than the DL when two trains are connected to the same AP: each device transmits for 1/3 of the time and therefore the UL transmits 2/3 of the time and the DL only 1/3 of the time. This situation is rare and only occurs during 9% of the simulation time. In addition, the AP antennas have more gain that the

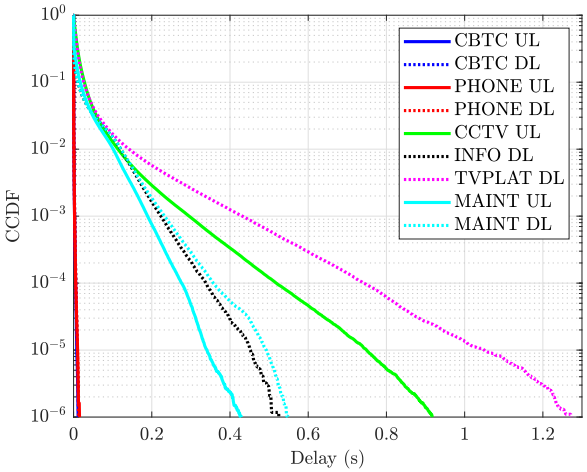

(a) Packet delay using ActiveProbing mechanism.

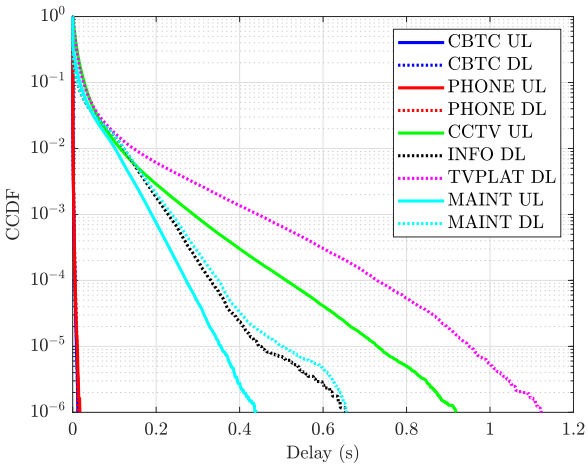

(b) Packet delay using FastHandover mechanism.

Figure 4.27: CCDF of packet delay for each application in Wi-Fi deployment.

trains antennas. This allows for receiving with higher quality in the UL than in the DL. In this case, the gain of the antennas only benefits the reception of the signal and not the transmission power, which is limited by the maximum allowed EIRP.

These results demonstrate that the use of 8 Wi-Fi channels is enough in this scenario to avoid interference between the different access points.

4.6.5.3 Packet Delay

As in the previous subsection, these simulations have a duration of 140 seconds with ten trains, and fifty runs of each configuration were performed with different random seeds. These simulations use the traffic configuration of Table 4.8. Therefore, the deployment shall provide a rate of 2.47 Mbits/s on the DL and 6.37 Mbit/s on the UL for each train. In view of the previous simulations, the average bitrate achieved should be enough, although there can be instants when the throughput is not enough for some trains.

Fig. 4.27 shows the delay distribution of each application for the ActiveProbing and FastHandover mechanisms. The two figures are very similar because, in these simulations, the handover process causes packet loss and does not add delay to the transmitted packets. As explained in Section 4.3.2.1, the STA transmission queues are disabled during handover and the new packets are discarded instead of being added to the queues. The packets in the AP queues are also lost because they are not forwarded to the new AP.

The delay of CBTC traffic is minimal and does not exceed 10 ms. The same applies to the VoIP traffic. The QoS mechanism of Wi-Fi, in which data from the highest priority queues is always sent first, gives maximum priority to this critical services.

The delay of the remaining applications depends on their throughput requirements. Video applications have the longest delay, and exceed the 500 ms with a probability of 10^{-4} and $6{\cdot}10^{-4}$ for CCTV and TVPLAT traffic, respectively. The delay of CCTV traffic is lower than that of

Table 4.13: PER for each application with ten trains in Wi-Fi deployment.

	ActiveProbing		FastHandover	
	DL	UL	DL	UL
CBTC	$1.49 \cdot 10^{-3}$	$1.49 \cdot 10^{-3}$	$2.91 \cdot 10^{-4}$	$2.86 \cdot 10^{-4}$
CCTV	-	$3.13 \cdot 10^{-3}$	-	$1.88 \cdot 10^{-3}$
Platform TV	$4.33 \cdot 10^{-3}$	-	$3.28 \cdot 10^{-3}$	-
VoIP	$1.51 \cdot 10^{-3}$	$1.52 \cdot 10^{-3}$	$2.91 \cdot 10^{-4}$	$3.04 \cdot 10^{-4}$
Maintenance	$2.27 \cdot 10^{-3}$	$2.34 \cdot 10^{-3}$	$1.04 \cdot 10^{-3}$	$1.14 \cdot 10^{-3}$
Passenger info	$2.23 \cdot 10^{-3}$	-	$1.03 \cdot 10^{-3}$	-

TVPLAT, although its throughput requirements are higher. This is because, on the one hand, the balance between DL and UL traffic in Wi-Fi is adapted to the needs of the devices and, on the other hand, as there is a greater transmission of data in the UL, it is more common for the APs to find the channel occupied when they want to transmit, having to wait for another opportunity to transmit the DL data.

As in the previous subsection, the obtained PER is different for each configuration. Moreover, the PER also depends on the application throughput and priority, as the low priority queues will be more full with data. Table 4.13 shows the PER of each application for each configuration. The 0.1% packet loss requirement of CBTC traffic was satisfied only in the FastHandover simulations.

4.7 Conclusions

This chapter evaluates the suitability of different communication technologies for subway environments. LTE and Wi-Fi deployments were simulated using tunnel propagation channels based on real channel measurements and deterministic models.

The services deployed in subway environments and their communication requirements were detailed. It was concluded that the CBTC service requires a maximum packet delay of 100 ms and a PER of 0.1%. The VoIP service also requires a low packet delay (150 ms) but the remaining services tolerate higher delays. The video surveillance applications (CCTV and platform TV) have a variable bitrate that demands high data rates from the network infrastructure at specific times.

The LTE and Wi-Fi modules of the ns-3 simulator were enhanced to match the subway scenario conditions and to optimize the performance of typical applications. A QoS-aware LTE scheduler was implemented to allow for prioritizing different flows from the same user while performing a fair resource assignment between users, both in DL and UL. An idealized Wi-Fi handover mechanism was implemented assuming that the train devices know their positions and the APs deployment details, allowing for very fast handovers.

A deterministic and a measurement-based propagation models for tunnel environments were developed. The deterministic channel model combines several works found in the literature, taking into account the dimensions and section of the tunnel and also considering the curves and slope changes of the tunnel. The model based on real channel measurements allows us to perform the simulations with the exact behavior as in the measurement campaign and it also extrapolates the channel data allowing for simulations with longer distances. These channel models are suitable for the system-level simulator, but they have some limitations:

- They do not take into account the alterations caused by obstacles such as the trains. However, these obstacles do not significantly affect the simulations given the small size of the trains compared with the tunnel size.
- The presence of metro stations that modify the tunnel section is not considered in the deterministic channel model.
- Only the received power for each frequency band is considered in the simulator. The Doppler effects produced by the high velocity of trains is not taken into account. It is assumed that the receiver is able to correct the frequency offset caused by the Doppler shift, whereas the inter-carrier interference (ICI) produced by the Doppler spread in the OFDM signal is very low.

We evaluated the suitability of LTE and Wi-Fi in subway environments by performing system level simulations in two scenarios with the propagation models developed. The three-stations deployment was designed to match the conditions of the measurement campaign for the channel model: an eNB at the center of each station configured to use a 10 MHz FDD LTE system. Several LTE deployment parameters were customized, including frequency reuse and the handover algorithm, to ensure the correct operation of the network, minimizing the interference and avoiding ping-pong handovers. From the obtained results, it can be concluded that the QoS requirements of the configured applications were satisfied. Only the CCTV flows have problems to maintain the packet delay below 500 ms, exceeding this value with a probability of $6 \cdot 10^{-4}$.

The complete subway-line deployment was used to test the deterministic channel model and to compare the two technologies most used in real systems: a DAS based LTE network and a custom Wi-Fi solution. The distinct characteristics of these solutions such as the frequency of operation or the power limitations lead to very different deployments: the LTE network uses three DASs with the original antenna positions, but a deployment with antennas every 400 m was needed for Wi-Fi.

For both LTE and Wi-Fi simulations, it was necessary to improve and adapt the ns-3 simulator in order to obtain results close to what would be obtained with commercial equipment. The aspects that most differ from a real deployment are the following:

- Only one antenna is installed in each train. However, two antennas are usually placed at the front and rear of each train. This adds more connection reliability and redundancy as two transceivers are used. Interference will also be reduced if the installed antennas are

directional.

- The deployment only allows for single-input and single-output (SISO) communications. Real deployments could install more antennas in the wayside or in the trains so MIMO could be used. The simulator allows for MIMO techniques by configuring several spatial streams and by applying a gain to the received signal SINR. The simulator assumes that there is no spatial correlation between the antennas, but measurements have shown that the correlation can be high, specially at long distances [MAS+12].
- LTE:
  - The simulator does not support all the features that can be expected from a modern LTE system. To correct this, it is assumed that there are no errors in the control data (PDCCH).
  - The performance of DAS is idealized: it is assumed that the transmission of the same signal by different antennas will always be constructive as the delay does not exceed the cyclic prefix. However, the effects on the propagation channel can degrade the system performance in some cases.
- Wi-Fi:
  - The 802.11a version of Wi-Fi is used. Although performance would be higher if 802.11ac were considered, the errors in the ns-3 implementation forced us to use 802.11a.
  - The handover mechanism is idealized. Trains are able to perform this transition at the right time to the right AP and with very low delay. In addition, they do not need to exchange authentication information because the simulator does not implement Wi-Fi security protocols. However, some commercial Wi-Fi solutions for subway environments perform proprietary modifications to the standard similar to these to achieve handovers with very low delay.

Even taking into account the possible inaccuracies of the simulator, the results obtained are relevant and give an idea of the capacity of the simulator and its versatility to evaluate different deployments.

LTE and Wi-Fi performance has been evaluated in terms of throughput, packet loss and delay. In both cases the requirements defined in Section 4.2 are met:

- Delay: With both LTE and Wi-Fi, the restriction that the delay is always less than 100 ms for CBTC traffic is fulfilled. In Wi-Fi the CBTC and VoIP delay is extremely low. All other flows have an acceptable delay.
- PER: The CBTC 0.1% packet error rate limit is fulfilled with both technologies. However, a FFR configuration is needed for LTE and the FastHandover method is needed for Wi-Fi simulations. If other flows need error-free communications, they can use protocols such as TCP, but with a negative impact on delay.

Chapter V

Conclusions and Future Work

This work studied the design and real-time implementation of physical (PHY) and medium access control (MAC) layers of 4G communication systems as well as their applicability in rail transport systems. On the one hand, base and mobile station transceivers were implemented using Mobile WiMAX standard as an orthogonal frequency-division multiple access (OFDMA) reference system. This implementation was carried out in a software-defined radio (SDR) architecture based on reconfigurable hardware. On the other hand, several simulations were performed to evaluate the applicability of Long Term Evolution (LTE) communication networks in rail transport systems, focusing on subway scenarios. Special attention was given to radio propagation modeling in tunnels and to the quality of service (QoS) requirements of the applications used in subway environments. Wi-Fi networks solutions were also studied as they are very common in these environments.

This chapter presents the main conclusions of this work and proposes future study lines.

5.1 Conclusions

The first two chapters of this thesis were focused on the design and implementation of PHY and MAC layers of OFDMA-based communications systems. Chapter 2 described how these systems work using the IEEE 802.16e standard (Mobile WiMAX) as reference system. A detailed description of the PHY and MAC layers was presented, focusing on the mandatory features specified by the WiMAX Forum. The PHY layer has a flexible OFDMA frame structure that allows for sharing radio resources efficiently among different users. The ranging process allows the different mobile stations (MSs) to synchronize in time and frequency with the base station (BS) so their transmissions can be correctly decoded minimizing interference between MSs. The connection-oriented MAC layer define the packet format and the mechanisms to fill PHY layer bursts. The MAC layer also provides automatic repeat request (ARQ) functionality, which can be enabled for each transport connection. Regarding QoS, several parameters are defined for each service class that can be used by the scheduler to prioritize the different

connections. The scheduling is centralized in the BS, as it determines the resources granted to each MS. This information is packed in the downlink map (DL-MAP) and uplink map (UL-MAP) management messages in each frame.

The design and real-time implementation of Mobile WiMAX transceivers was presented in Chapter 3. The MAC and PHY layers of the mobile and the base stations were implemented allowing for real-time bidirectional communications using time-division duplexing (TDD). The BS and MS transceivers are based on a cost-effective SDR hardware architecture made up of field programmable gate array (FPGA) and digital signal processor (DSP) modules that provide all the processing power needed to implement the mandatory functionalities of the WiMAX standard.

A custom development methodology was followed for the implementation of the PHY layer. This methodology is appropriate for heterogeneous hardware setups where different tasks need to be distributed into the modules depending on their requirements and complexity. The necessary resources for the operation of each processing block of the system in real time are estimated to appropriately place these blocks in the hardware architecture. The defined FPGA task template was very helpful, as it provides a communication protocol between tasks and a configuration mechanism. The defined PHY and MAC service access points (SAPs) also aided in determining the responsibilities for each layer and the way in which they interact.

The relevant details of the design and implementation of the PHY and MAC layers were pointed out. The tasks related with signal filtering, fast Fourier transform (FFT), synchronization and channel coding were implemented in the FPGAs, while the remaining tasks were implemented in the DSPs, including channel equalization and ranging processing. The resource usage in the final implementation was shown, including the FPGA components used and the estimated execution time of each DSP task per OFDMA frame. It is worth noting the high amount of FPGA resources required for the synchronization task in the MS. Moreover, channel estimation and equalization are the most computationally intensive tasks in the DSP. The utilization of the proposed hardware architecture to implement the WirelessMAN-Advanced Air Interface was also discussed. The modifications in the hardware architecture required to implement the evolved version of the standard, known as WirelessMAN-Advanced Air Interface (802.16m), were also proposed.

Validation and performance evaluation of the transceivers was also carried out with the help of a custom-made channel emulator. The correct implementation of the channel coding processing was verified in terms of bit error ratio (BER) performance under an additive white Gaussian noise (AWGN) channel. The expected results for the convolutional decoder with 3 soft-bits were achieved. A 10^{-6} BER was obtained for QPSK 1/2 and 64-QAM 3/4 at 5 and 15,5 dB of E_b/N_0, respectively.

The developed channel emulator was used to test the complete system in the scenarios recommended by the WiMAX Forum: Pedestrian A and B, and Vehicular A at 60 and 120 km/h. The timing-offset estimation error of the uplink (UL) synchronization task was first measured

using the 3.5 MHz profile. The implemented algorithm is not excessively impacted by the effects of the channels. The worst results were obtained for the Pedestrian A channel at 2 dB of average signal-to-noise ratio (SNR), achieving a standard deviation of 6.4 samples (1.6 µs), which is a relatively small offset compared with the 64 samples of the cyclic prefix. Moreover, these small errors are further reduced thanks to the iterative mechanism used by the ranging process, i.e., the procedure is repeated until the BS considers that the estimated offset is small enough.

BER, frame error rate (FER) and throughput measurements were performed for both DL and UL using the channel emulator. Regarding BER and FER results, Pedestrian A channel obtained the worst bit error rates, but has good results in terms of FER. This is because this channel has an almost flat frequency response and the received frames are either error-free or contain many errors, which has strong impact on BER performance but not on FER. The rest of the channels have higher frequency selectivity and it can be seen that the results in the UL are better than in the DL due to the higher density of pilots and to the fact that the channel estimation in the UL is done in time and frequency. The results of the Vehicular A channel clearly show the influence of high speeds on the results, which are more affected by inter-carrier interference (ICI) at higher speeds.

The MAC layer processing with the ARQ mechanism was enabled during the throughput measurements, showing the actual performance of the complete WiMAX system in realistic propagation conditions. The maximum allowed protocol data unit (PDU) size was used (2047 bytes) to minimize the header overhead. The obtained results are consistent with the previous FER measurements, achieving the maximum throughput with the QPSK 1/2 configuration. For Pedestrian A channel, it is always better to use QPSK 3/4. For Pedestrian B channel, higher transfer rates are obtained using QPSK 1/2, except for SNRs higher than 29 dB in the UL. Finally, the frequency selectivity and ICI of the Vehicular A channel causes that QPSK 3/4 is not able to outperform the QPSK 1/2 results with these measurement configuration.

The results could be improved if smaller PDUs were used, especially in the Pedestrian B and Vehicular A channels, where the QPSK 3/4 results are not able to surpass the maximum QPSK 1/2 throughput. Furthermore, the better performance obtained with the UL indicates that the DL results could also be improved. The DL channel equalizer only performs a linear interpolation in the frequency domain and ignores that the channel coherence time is usually longer than several OFDM symbols. The implementation does not take advantage of the DL cluster structure (shown in Fig. 2.3) and does not use the pilot subcarriers of the adjacent OFDM symbols. Finally, if adaptive modulation and coding (AMC) techniques were implemented, the system would track the channel conditions to dynamically select the best modulation and code rate for each frame, obtaining much better throughput results.

Chapter 4 evaluated the applicability of different radio communication technologies in rail transport systems considering the reliability and safety requirements of these systems and focusing on subway environments. The most common services deployed in subway scenarios

that use train-to-wayside radio communications were studied. The configuration and QoS requirements of these services were analyzed based on different works found in the literature. On the one hand, the communications-based train control (CBTC) signaling system is the most important mission critical service and requires a reliable low-latency radio link with high availability. On the other hand, the service that demands more throughput is the video surveillance system, but the delay and packet error rate requirements are not so stringent.

LTE and Wi-Fi deployments were simulated using the ns-3 system-level network simulator in order to evaluate and select the most appropriate system configuration for the environment. The ns-3 network simulator was enhanced to match the subway scenario conditions developing tunnel propagation channels based on deterministic models and real channel measurements. Moreover, the LTE scheduler was enhanced to allow for the prioritization of critical services, and an idealized custom fast handover mechanism was implemented in the Wi-Fi module.

A review of the radio propagation models for tunnel environments was performed to propose two different models. On the one hand, a deterministic channel model was developed that combines several works found in the literature allowing for the definition of complex scenarios, including curved tunnels and different tunnel cross sections. On the other hand, a channel model based on measurements was developed using the results of a measurement campaign performed in a modern subway station, with the transmitting antenna placed at the center of the station and an approaching train. Two different scenarios were defined to test the developed propagation models.

An LTE three-stations deployment was simulated assuming that an eNodeB was placed in the center of each subway station. This way, the channel model based on measurements could be used to perform realistic LTE simulations. Three LTE cells were configured with a bandwidth of 10 MHz in frequency-division duplexing (FDD) mode and using hard frequency reuse to minimize interference. The handover algorithm was also configured to avoid ping-pong handovers. The configured applications included the CBTC service and a CCTV stream of 2000 kbit/s sent by each train. The obtained results showed that the QoS requirements were satisfied. However, the CCTV traffic experienced delays longer than one second with a probability of 10^{-4}. The delay results were improved by reducing the delay added in the Radio Link Control (RLC) layer when packets are lost.

The main issue found in this LTE deployment was the high interference in the downlink control channel, which was always transmitted in the same time slots and frequencies. The enhanced control channel defined in LTE-Advanced allows for minimizing the interference in control data, but the ns-3 simulator does not support this feature. However, we can disable errors in the control data and assume that the eNBs are able to coordinate to avoid interference in this channel. Additional simulations were performed disabling control data errors to verify the high impact of this interference in the results.

A complete subway-line scenario based on a real deployment (line 3 of Bilbao Metro) was also simulated. The deterministic channel model was used in these simulations to evaluate two

common technologies in subway: a distributed antenna system (DAS) based LTE network and a custom Wi-Fi solution. All the defined applications in Section 4.2 were configured in the simulations. These solutions resulted in very different deployments. The LTE deployment used the initially proposed antenna positions configured as three independent DASs, and each one of the DAS is connected to an eNodeB. In the Wi-Fi deployment, a maximum separation of 400 m was needed because the deterministic channel model predicted SINRs lower than 10 dBs for longer distances, being the 20 dBm of EIRP the most limiting factor.

The LTE and Wi-Fi performance obtained in the simulations was evaluated in terms of throughput, packet loss and delay. The defined scenario consisted of 10 trains, each requiring 2.47 Mbits/s on the DL and 6.37 Mbit/s on the UL. The Wi-Fi deployment needed more antennas than the LTE deployment (38 vs 29), but the availability of several channels in the 5 GHz band allowed for performing a deployment with low interference between all the APs. Moreover, this solution provided a high throughput as, most of the time, the APs are connected to only one train which does not have to contend with any other train for transmission opportunities. The frequent handover between APs was not a problem in these simulations as the custom methods implemented in the simulator (Section 4.3.2.1) are idealized and work very well. In LTE, a total bandwidth of 40 MHz was available (20 MHz for DL and 20 MHz for UL) which provided a maximum throughput of 75 Mbit/s in both directions, assuming single-input and single-output (SISO) communications. The high throughput needed in this scenario could not be provided using the hard frequency reuse technique. Simulations without frequency reuse and with dynamic frequency reuse were performed to show how to satisfy the throughput requirements.

LTE and Wi-Fi performance were evaluated in terms of throughput, packet loss and delay. In both cases the defined requirements were met thanks to the custom modifications for subway environments. Both technologies achieved a delay lower than 100 ms for CBTC traffic, especially in Wi-Fi, where the CBTC and VoIP delay is extremely low. The low priority flows experience tolerable delays. Regarding packet error ratio (PER), the 0.1% limit is not exceeded when a custom fractional frequency reuse (FFR) configuration is applied in LTE, or the FastHandover method is used in Wi-Fi simulations. The remaining flows experience similar PER but, if needed, they can use protocols such as Transmission Control Protocol (TCP) to avoid packet loss, although increasing the delay.

There are some differences between the performed simulations and real deployments that may affect the accuracy of the obtained results. Two antennas are usually placed at the front and rear of each train, but the simulations were performed with only one antenna on each train. Moreover, the simulator does not support the latest Wi-Fi and LTE features, forcing the use of the 802.11a version of Wi-Fi, and to assume that there are no errors in LTE control channels. Also, the Wi-Fi handover mechanism is idealized and performed with very low delay, which is not commonly found in commercial Wi-Fi solutions. Finally, the radio propagation in the real scenarios may differ from the channel model used. However, the propagation model can be

adapted to measurements made on the metro line to obtain more realistic results.

Even taking into account the possible inaccuracies and thanks to the adaptations made to the simulator, the obtained results predict the behavior of the different technologies appropriately and show the versatility of the simulator to evaluate different deployments.

5.2 Future Work

This dissertation focused on both real-time implementation and simulation of different communication systems. In the following subsections we point out some interesting research lines based on this work.

5.2.1 Real-time Hardware Architecture

The implemented WiMAX transceivers could be enhanced in several ways:

Improve current implementation The downlink channel equalization could perform a bilinear interpolation similar to the method used in the uplink or other method that takes into account the channel estimation of previous symbols. This should enhance the results obtained with the ITU-R channels. The ranging algorithms could also support the detection of several users and periodic ranging could be implemented. The downlink synchronization method could also use the timing information of the previous frames to refine its predictions and filter out possible false positives using less resources.

Evaluate the impact of using smaller bursts and packets Sending smaller packets will reduce the PER but the packet header overhead will be increased. Depending on channel state, it can be better to send several concatenated packets in a burst than one big packet. Furthermore, using several smaller bursts instead of one big burst will also reduce the packet error rate. This is because if a packet header is corrupted, the remaining packets of the burst will also be lost, as the start position of the next packet is unknown. It would be useful to find out the burst and packet size selection that optimizes the throughput, depending on the channel model and SNR.

AMC The used modulation and coding are currently fixed in the initial configuration. The scheduler in the base station could automatically select the appropriate values. The uplink modulation and coding can be selected according to the received signal quality in the base station. The downlink rate adaptation can be performed based on the received signal strength indication (RSSI) and carrier-to-interference-and-noise ratio (CINR) reports sent by the mobile stations.

New features Implement hybrid automatic repeat request (HARQ) as the standard supports both chase combining and incremental redundancy for tail-biting convolutional code (TBCC) and convolutional turbo code (CTC). Peak-to-average power ratio (PAPR) reduction techniques could also be added.

MIMO support Only SISO is currently supported. Supporting multiple-input-multiple-output (MIMO) would improve the performance of the transceivers, but it would require a more complex and sophisticated design. Additional hardware resources that provide the required processing power would be needed in the PHY layer.

Implement other OFDMA based standard

Other communication systems could be implemented using the hardware architecture as a base. The required changes in the architecture to support the 802.16m Advanced Air Interface (AAI) were already analyzed in Section 3.7. The implementation of 5G new radio (NR) could also be studied as it is also based on OFDMA with cyclic prefix. The support of the different numerologies (subcarrier spacing, cyclic prefix, and FFT size) is a challenging task that would need several changes in the FPGA processing tasks, specially if single-carrier FDMA (SC-FDMA) is also implemented. The channel coding tasks should also support the low-density parity check (LDPC) and polar codes. Most likely, to maintain the SDR design philosophy, the use of newer and more powerful hardware will be required.

5.2.2 Wireless Communications in Transportation Systems

There are multiple research lines related with the simulation of wireless communications and transportation systems:

Enhance and publish the ns-3 simulator modifications The modifications performed in the ns-3 simulator models can be published so these new features are available to other researchers. The developed LTE scheduler provides the ability to prioritize between traffic flows of the same user, and can be further improved and combined with other QoS-aware schedulers besides the proportional fair scheduler. The Wi-Fi roaming mechanism can be enhanced to work in a more realistic way, so it can be used in other applications and scenarios.

Infrastructure shared with passengers An agreement between a railway operator and a mobile operator could allow for using a public mobile network to carry train signaling data (or other services). Alternatively, the railway operator may want to offer internet access to passengers inside trains and stations. In both cases, the deployed infrastructure would be shared with the passengers. An analysis can be performed addressing potential security issues and the impact on the mission critical services. The scheduler should be able to guarantee the QoS requirements even when a high number of passengers overloads the network.

Simulations with 5G and Wi-Fi 6 The latest 3GPP and IEEE 802.11 standards can provide remarkable advantages and performance improvements when compared with the current technologies. The ns-3 simulator is progressively being improved to support the features of these new standards. This will enable the simulation of transportation scenarios with

these new technologies, evaluating their advantages and performance gain.

5G NR-U: 5G in unlicensed spectrum Several initiatives and amendments were proposed in the last few years to support the usage of LTE/5G in unlicensed spectrum such as LTE-Unlicensed (LTE-U), LTE Licensed Assisted Access (LTE-LAA), MulteFire and 5G new radio unlicensed (NR-U). Only MulteFire and NR-U allow the deployment of standalone private networks with no need to use licensed spectrum. NR-U, based on LTE-LAA and MulteFire, is going to be included in 3GPP Release 16 and will allow the use of the 5 GHz and 6 GHz unlicensed bands.

Tunnel channel model The developed deterministic channel model for tunnels can be improved to model the effects of obstacles such as trains or to take into account the presence of stations. Moreover, the multimode model can be replaced with more flexible or precise methods such as ray-tracing or vector parabolic equation. The increase in capacity when using several antennas could also be studied using the results of works that characterize the MIMO channel in tunnel environments. Finally, ns-3 simulator could also be improved to take into account the performance degradation produced by the high velocity of the trains.

Train-to-train communications Train-to-train communications is an active research area. The trains have more autonomy as they can communicate with the nearby trains to know their position and velocity, allowing them to make decisions without the need of a central coordinator. Several channel models and measurements have been published for this kind of communications in different frequencies. These works can be used with our simulator to compare the classical centralized control systems with this new proposal.

Appendix I

Resumen de la Tesis

Los sistemas de comunicaciones inalámbricos han evolucionado mucho desde la aparición de la primera generación de tecnología celular en los años 80. Las siguientes generaciones han mejorado de forma significativa las tasas de datos, la eficiencia espectral, la seguridad y la cobertura. Las últimas generaciones (4G y 5G) utilizan una capa física (PHY) basada en modulaciones multiportadora para transmitir datos con un gran ancho de banda. Estas modulaciones subdividen la señal en varios canales que son transmitidos en paralelo, permitiendo corregir los efectos de los canales de propagación radio de forma más sencilla. OFDM con prefijo cíclico es la modulación más utilizada y estudiada de las modulaciones multiportadora. Es la modulación utilizada en estas últimas generaciones debido a su alta eficiencia espectral y baja complejidad de implementación gracias al algoritmo *fast Fourier transform (FFT)*. Además, se utiliza OFDMA como mecanismo para el reparto del los recursos radio disponibles entre los diferentes usuarios, que se puede realizar tanto en tiempo como en frecuencia. Esto aporta una gran flexibilidad que permite adaptarse tanto a los requisitos de calidad de servicio (Qos) de los usuarios como al estado del canal radio.

En entornos de investigación, para probar y verificar el rendimiento de los sistemas de comunicaciones es habitual recurrir a la utilización de bancos de pruebas (*testbeds*) o simulaciones. Sin embargo, no es habitual considerar las restricciones de procesado necesarias para lograr el funcionamiento en tiempo real del sistema. La implementación en tiempo real del sistema permite evaluar su rendimiento en condiciones realistas, teniendo en cuenta las limitaciones de la implementación y el uso de algoritmos de baja complejidad.

Las implementaciones comerciales de estos estándares utilizan chips dedicados o ASICs para reducir al mínimo las necesidades de energía del dispositivo. Estas implementaciones son muy eficientes, pero muy inflexibles y no permiten modificar las formas de onda o protocolos utilizados. Los sistemas de radio definida por software (SDR) sustituyen estos elementos ad-hoc por módulos software ejecutados por procesadores más genéricos como DSPs. Esta idea ha ganado interés gracias al aumento de la potencia de cálculo de los procesadores y a los avances en la computación heterogénea.

El primer objetivo de esta tesis es estudiar el diseño y la implementación de las capas

de acceso al medio (MAC) y PHY de un sistema de comunicaciones basado en OFDMA utilizando una arquitectura SDR compuesta por DSPs y FPGAs. Tanto WiMAX como LTE fueron las dos tecnologías candidatas a convertirse en el estándar 4G mundial. Aunque LTE fue la seleccionada, Mobile WiMAX es una tecnología similar, basada en una capa física OFDMA y con mecanismos avanzados de QoS, siendo interesante su estudio y evaluación de rendimiento. Por este motivo, esta tesis se centra en la implementación y evaluación de Mobile WiMAX.

Las tecnologías 4G y 5G son tecnologías muy interesantes para las comunicaciones tren-tierra en entornos ferroviarios. Los sistemas de control y señalización ferroviaria dependen de un sistema de comunicaciones inalámbrico tren-tierra que les permita transmitir su posición y recibir las indicaciones y limitaciones de velocidad de forma continua. De esta forma, estos sistemas supervisan la conducción del tren y activan el freno de emergencia cuando no se cumplen las condiciones de seguridad. También permiten la conducción automática de los trenes, sin la intervención del conductor. Los sistemas de control más utilizados actualmente son *European Train Control System (ETCS)*, que está orientado al transporte de media y larga distancia, y *communications-based train control (CBTC)*, más utilizado en el transporte metropolitano. ETCS actualmente utiliza GSM para ferrrocarriles (GSM-R) para las comunicaciones y está planeado sustituirlo por un estándar basado en 5G. CBTC, en cambio, no requiere una tecnología de comunicaciones específica. Lo habitual es utilizar soluciones propietarias basadas en la tecnología IEEE 802.11 (Wi-Fi) por permitir la utilización de bandas ISM. Sin embargo, LTE y su evolución 5G se adaptan mejor a los entornos de metro que Wi-Fi: tienen mayor alcance y eficiencia espectral, soportan mejor la movilidad e incluyen mecanismos de QoS robustos.

El segundo objetivo de este trabajo es evaluar la aplicabilidad de LTE y Wi-Fi en los sistemas de transporte ferroviario utilizando un simulador de red adaptado a entornos de metro. Los simuladores de red son muy útiles para probar distintas configuraciones de las redes y optimizar su rendimiendo en diferentes escenarios. Permiten estudiar el comportamiento esperado de la red en entornos complejos donde es muy difícil realizar pruebas reales. Por esta razón, el modelado y la simulación de despliegues de redes de metro es muy útil, ya que ayuda en la planificación de la red y permite comprobar si se cumplen los requisitos de los distintos servicios desplegados.

Para que los resultados de las simulaciones sean realistas se deben utilizar modelos de propagación radio apropiados. Existen múltiples factores que afectan a la propagación radio dentro de los túneles: sus dimensiones y forma, la posición de las antenas, la frecuencia de transmisión utilizada, el tamaño de los trenes, etc. Es necesario realizar campañas de medición antes de un despliegue para ajustar correctamente el modelo de canal utilizado y predecir la cobertura en el túnel con precisión. Es importante que el simulador de redes permita utilizar mediciones obtenidas en campañas de medida además de utilizar modelos teóricos de propagación en túneles.

A.1 Implementación SDR de las capas PHY y MAC de Mobile WiMAX

WiMAX es un estándar de comunicaciones inalámbricas desarrollado para proporcionar acceso inalámbrico de banda ancha a larga distancia. El término WiMAX fue adoptado por el WiMAX Forum, una organización creada para promover la interoperabilidad de los estándares de comunicaciones IEEE 802.16. En esta memoria nos hemos centrado en la implementación del modo TDD de Mobile WiMAX, definido en el estándar 802.16e, y que utiliza OFDMA para soportar múltiples usuarios en entornos de movilidad.

La mayoría de trabajos existentes que evalúan el rendimiento de WiMAX se centran en la simulación de sistemas WiMAX, pruebas en exteriores con equipamiento WiMAX comercial, o implementaciones en tiempo real parciales del estándar que solo evalúan comunicaciones unidireccionales.

La capa física de Mobile WiMAX tiene un estructura de trama flexible dividida en ráfagas. Sólo el preámbulo y las ráfagas *frame control header (FCH)* y *downlink map (DL-MAP)* tienen una posición fija dentro de la trama. Se pueden utilizar diferentes estructuras de símbolo OFDMA en la trama, permitiendo una disposición contigua o distribuida en frecuencia de las portadoras de cada usuario. Sin embargo, el WiMAX Forum solo exige la implementación de la estructura de símbolo denominada *partial usage of subchannels (PUSC)*. Los mensajes de gestión DL-MAP y *uplink map (UL-MAP)* especifican la estructura de símbolo a utilizar así como las posiciones, tamaños y configuración de las ráfagas de la trama.

La sincronización en tiempo y frecuencia en el enlace descendente (DL) se realiza utilizando el preámbulo transmitido por la estación base. También es necesario sincronizar las estaciones móviles para que sus transmisiones lleguen correctamente a la estación base. Para este fin, se reservan regiones dentro de las tramas (regiones de *ranging*) en las que las estaciones móviles pueden transmitir códigos de *ranging*, que la estación base procesa para informar a las estaciones móviles de las correcciones que deben realizar.

La capa MAC WiMAX proporciona una interfaz entre las capas superiores y la capa física, y está dividida en tres subcapas: convergencia, común y de seguridad. La subcapa de convergencia clasifica los paquetes de capas superiores (como IP o Ethernet) para poder ser transmitidos por una conexión y los transforma en *MAC service data units (MSDUs)*. Estos MSDUs son procesados por la capa común para generar *MAC protocol data units (MPDUs)* utilizando los mecanismos de fragmentación (división de paquetes grandes en varios de menor tamaño) y empaquetado (unión de varios paquetes en uno). Las ráfagas de la capa física contienen estos MPDUs. La capa MAC de WiMAX también se encarga gestionar las diversos flujos de información de cada usuario y proporciona mecanismos de control de errores como *automatic repeat request (ARQ)*, que son muy interesantes para poder evaluar el rendimiento real del sistema.

Con respecto a la QoS, la MAC define varias clases de servicio con distintos parámetros (p.

ej., latencia máxima) que pueden ser configurados para cada conexión. Estos parámetros son utilizadas por el planificador para asignar recursos a los usuarios y priorizar los paquetes de cada conexión. La planificación está centralizada en la estación base, ya que determina los recursos concedidos a cada estación móvil. Sin embargo, el planificador de las estaciones móviles sigue seleccionando qué conexiones se sirven en cada oportunidad de transmisión que les concede la estación base.

Los implementación realizada de las capas PHY y MAC de Mobile WiMAX soporta comunicaciones bidireccionales utilizando TDD. Las funcionalidades implementadas son las establecidas como obligatorias por el WiMAX Forum:

- Capa física:
  - Soporta los cinco perfiles definidos por el WiMAX Forum: 3.5 MHz, 5 MHz, 7.5 MHz, 8.75 MHz, or 10 MHz. Tamaño de FFT de 512 y 1024 subportadoras.
  - Los prefijos cíclicos se pueden configurar con una longitud de 1/4, 1/8, 1/16 y un 1/32. Es estándar sólo exige una longitud de 1/8.
  - Estructura de trama TDD con número fijo de símbolos OFDMA con una longitud total de 5 ms.
  - Estructura de símbolo PUSC. Este esquema distribuye los datos para cada usuario por todas las frecuencias.
  - Codificación de canal:
    - Modulaciones y tasa de códigos (convolucionales) soportados: QPSK 1/2, QPSK 3/4, 16-QAM 1/2, 16-QAM 3/4, 64-QAM 1/2, 64-QAM 2/3, and 64-QAM 3/4.
    - Decodificación *soft* (3 *soft-bits*) con algoritmo de Viterbi.
    - Soporte de códigos de repetición.
  - Sincronización en el DL basada en las propiedades del preámbulo y correlación cruzada.
  - Implementado el mecanismo de *ranging* en el enlace ascendente (UL) para sincronizar la transmisión del UL en tiempo y frecuencia. También se soporta el envío de códigos de *ranging* para hacer solicitudes de ancho de banda.
- Capa MAC:
  - Clasificación de paquetes y supresión de cabeceras en la subcapa de convergencia.
  - Conexiones de gestión y transporte.
  - Soporte para ARQ.
  - Planificador que respeta los requisitos de QoS.

La implementación se basa en una arquitectura hardware SDR de bajo coste formada por módulos FPGA y DSP que permite implementar todas las funcionalidades obligatorias del estándar WiMAX. Se siguió una metodología de desarrollo para la capa física pensada para la implementación de tareas de procesado de señal con una arquitectura heterogénea, que permite aprovechar la potencia de procesado de las FPGAs facilitando la flexibilidad de las

tareas implementadas. La implementación bidireccional final se realizó con éxito en el hardware seleccionado aprovechando al máximo los recursos y distribuyendo las tareas entre las FPGAs y los DSPs de forma equilibrada. Se muestra el uso de recursos de cada tarea implementada, incluyendo el uso de la FPGA y una estimación del tiempo de procesado de las tareas del DSP. Destacan los recursos de la FPGA requeridos por la tarea de sincronización en la estación móvil, y la carga de procesado en el DSP que implica la estimación e igualación de canal. También se proponen las modificaciones en la arquitectura hardware necesarias para implementar la versión evolucionada del estándar, conocida como Advanced Air Interface y definida en el estándar 802.16m.

La implementación ha sido validada de forma reproducible mediante diferentes mediciones de rendimiento realizadas y con la ayuda de un emulador de canal en tiempo real, implementado en una FPGA. Los resultados obtenidos muestran las distintas figuras de mérito considerando los escenarios de referencia recomendados por el WiMAX Forum: los canales ITU-R peatonales A y B, y vehicular A. Estos modelos de canal son soportados por el emulador de canal desarrollado. Los resultados obtenidos son los siguientes:

- Tasa de error de bit (BER) en canal AWGN para todas las modulaciones y códigos con respecto a la E_b/N_0. Sirve como validación de la correcta implementación de los algoritmos de codificación y decodificación de canal. El decodificador de Viterbi con 3 *soft-bits* consigue el rendimiento esperado alcanzando una BER de 10^{-6} con 5 y 15,5 dB de E_b/N_0 para las modulaciones QPSK 1/2 y 64-QAM 3/4, respectivamente.
- Error en la estimación del desfase en tiempo durante el proceso de *ranging*. El algoritmo implementado no se ve afectado en exceso por los efectos de los canales. Los peores resultados se obtienen para el canal peatonal A, con el que se observa una desviación típica del error de 6,4 muestras (1,6 µs) con 2 dB de SNR.
- BER y tasa de error de trama (FER) en los canales ITU-R con respecto a la SNR. Los resultados muestran como el canal peatonal A tiene las peores tasas de error de bit, pero mejora sus resultados al evaluar las tramas recibidas sin errores. Esto se debe a que este canal tiene muy poca selectividad en frecuencia y las tramas recibidas, o no contienen ningún error, o bien contienen muchos errores, lo cual empeora la BER pero no la FER. El resto de canales tienen mayor selectividad en frecuencia y se observa como los resultados en el UL son mejores que en el DL debido a la mayor densidad de pilotos y a que la estimación de canal en el UL se realiza en tiempo y frecuencia. Los resultados del canal vehicular A muestran claramente la influencia de las altas velocidades en los resultados, que empeoran cuanto mayor sea la velocidad.
- Tasas de datos alcanzadas utilizando ARQ en los canales ITU-R con QPSK 1/2 y QPSK 3/4. Para el canal peatonal A siempre es mejor utilizar la modulación QPSK 3/4. Para el canal peatonal B, se obtienen tasas de transferencia mayores utilizando QPSK 1/2, excepto a partir de los 29 dB de SNR en el UL. Para el canal vehicular A, siempre se obtienen mejores resultados con QPSK 1/2.

Las pruebas realizadas permiten evaluar el rendimiento real del sistema WiMAX completo en condiciones de propagación realistas. Los resultados de las mediciones confirman que la implementación propuesta es adecuada para los escenarios modelados con los modelos de canal mencionados.

A.2 Simulación de redes de comunicaciones en sistemas de transporte

En las últimas décadas la industria ferroviaria ha ido evolucionando sus sistemas de señalización convencionales hacia sistemas basados en comunicaciones que exigen infraestructuras fiables y tolerantes a fallos. En esta memoria nos centramos en los entornos de metro, en los que se suele utilizar el sistema CBTC para gestionar el tráfico de forma eficiente y segura.

Los sistemas CBTC pueden ser desplegados con cualquier tecnología de comunicaciones que cumpla sus requisitos de fiabilidad y baja latencia de paquetes. Habitualmente se utiliza infraestructura Wi-Fi por su bajo coste y por no necesitar el uso de bandas de transmisión licenciadas. Sin embargo, es necesario utilizar soluciones Wi-Fi con modificaciones propietarias para gestionar de forma correcta la transición entre los puntos de acceso desplegados a lo largo de la vía. Además, la tecnología Wi-Fi es susceptible de sufrir interferencias y no proporciona comunicaciones de largo alcance, obligando a la instalación de muchos puntos de acceso. Los estándares 4G y 5G son una buena alternativa que proporcionan mayor alcance y eficiencia espectral, soportan mejor la movilidad e incluyen mecanismos de QoS más robustos que Wi-Fi. Su mayor desventaja es la necesidad de utilizar bandas de frecuencia licenciadas y el mayor coste del equipamiento.

En entornos de metro hay otros servicios que requieren comunicaciones inalámbricas con el tren además de CBTC. Normalmente se utilizan tecnologías radio separadas para proporcionar estos servicios adicionales (por ejemplo, TETRA para la seguridad pública), lo que da lugar a un aumento en los costes de despliegue y mantenimiento de la infraestructura. En este trabajo se evalúa el uso de una sola tecnología inalámbrica para todas las aplicaciones, reduciendo los costes operacionales. Esta infraestructura debe soportar los diferentes requisitos de QoS de las aplicaciones, especialmente las de misión crítica. Los servicios y requisitos considerados son los siguientes:

- Servicios de misión crítica.
  - CBTC: Sistema de señalización y control. Requiere un retardo máximo de 100 ms y una pérdida de paquetes menor del 0.1%.
  - Voz: Servicio de seguridad pública permite comunicarse a los conductores con el centro de control. Al igual que CBTC, requiere comunicaciones con bajo retardo. Se recomienda que el retardo no sobrepase los 150 ms.

- Aplicaciones para el operador de metro.
  - Circuito Cerrado de Televisión (CCTV): Videovigilancia de los vagones del tren. La señal de vídeo se envía desde los trenes al centro de control o de seguridad. Este servicio necesita un gran ancho de banda pero tolera retardos de hasta 500 ms.
  - Videovigilancia de los andenes: Esta señal de vídeo se envía al tren para que el conductor pueda ver el estado del andén antes de que el tren llegue a la estación. Al igual que CCTV, requiere una tasa alta de datos pero permite retardos de medio segundo.
  - Mantenimiento: Telemetría para supervisar el estado de los sensores y equipos del tren. También se pueden incluir otras operaciones de mantenimiento, como la actualización de los sistemas del tren. En principio, este servicio no tiene requisitos de tiempo real y se puede proporcionar con transmisiones *best-effort*.
- Servicios para los pasajeros.
  - Información a los pasajeros: Consiste en los mensajes multimedia mostrados a los viajeros, como la próxima parada. Si no se muestra información de entretenimiento (noticias, publicidad), el servicio no requerirá grandes transmisiones de datos. Se toleran retardos largos que se pueden satisfacer con una prioridad *best-effort*.
  - Internet a bordo: Proporciona conectividad dentro de los trenes para dar acceso a Internet a los pasajeros. Este servicio no se considera en este trabajo.

Los despliegues de comunicaciones en los metros requieren un gran esfuerzo de planificación y la realización de campañas de medida para asegurar la cobertura a lo largo de toda la línea. Se pueden utilizar cables radiantes o antenas distribuidas dentro los túneles. Las soluciones de cable radiante proporcionan una cobertura más estable que el uso de antenas, pero tienen mayor coste. La planificación radio es más compleja con las antenas porque hay muchos factores que afectan a la propagación de las ondas electromagnéticas dentro de los túneles. Por este motivo se deben realizar mediciones de propagación dentro de los túneles para seleccionar y ajustar correctamente los modelos de canal radio utilizados para el cálculo de cobertura. También es importante realizar simulaciones de red para poder evaluar el cumplimiento de los requisitos ante distintas situaciones y prevenir posibles problemas.

Para la realización de estas simulaciones se ha seleccionado el simulador ns-3. Se trata de un simulador de redes de código abierto que se puede modificar totalmente para adaptarse a nuestras necesidades. A continuación se describen las funcionalidades destacadas del simulador y las mejoras que se realizaron para adaptarse a entornos ferroviarios:

- Proporciona librerías para facilitar el desarrollo de los modelos y la ejecución de las simulaciones: gestión de la configuración y parámetros de las simulaciones, generación de variables aleatorias, gestión de eventos temporales, generación de tráfico de red, etc.
- Implementa la pila de protocolos IP (IP, UDP, TCP, etc.).
- Incluye múltiples modelos de propagación. Permite implementar canales de propagación selectivos en frecuencia. También se tiene en cuenta el tipo de antenas utilizadas y su

orientación.

- Dispone de diversos modelos de movilidad y permite desarrollar modelos propios. Se ha desarrollado un modelo específico para trenes, que reproduce el recorrido de los trenes en la línea de metro estableciendo las velocidades máximas dentro y fuera de las estaciones, y la aceleración máxima cuando se acelera o frena el tren.
- Módulo LTE. Simula el funcionamiento de una red LTE en modo FDD. Implementa toda la pila de protocolos LTE y la red troncal (EPC). Ha sido necesario mejorar este módulo con las siguientes características:
  - Planificador con soporte de QoS de cada flujo. Los planificadores disponibles no son capaces de priorizar los distintos flujos de cada usuario, solo son capaces de asignar distintas prioridades entre usuarios. Se ha implementado la priorización de flujos descrita en el estándar para este fin, denominada *Logical Channel Prioritization* (LCP).
  - Planificador *proportional fair* (PF) para el UL. El simulador sólo dispone de un planificador *round robin* para el enlace ascendente. Se implementó el planificador PF para repartir los recursos de forma equitativa teniendo en cuenta el estado del canal de cada usuario. La implementación de este planificador tiene que respetar que las transmisiones de cada usuario deben ser contiguas en frecuencia, debido a la modulación SC-FDMA utilizada en el UL de LTE.
  - Se han adaptado los métodos de reúso de frecuencias para los despliegues en el túnel. Como los despliegues se realizan a lo largo de la vía y no en celdas hexagonales, se ha modificado el factor de reúso a 2. De esta forma se limitan las interferencias entre celdas aprovechando mejor el espectro utilizable.
- Módulo Wi-Fi. Es capaz de simular los estándares Wi-Fi hasta 802.11ac. Sin embargo, ha sido necesario utilizar el estándar 802.11a por errores en la implementación de la agregación de paquetes. También se han activado los mecanismos de QoS de 802.11e con colas separadas para cada categoría de acceso. Ha sido necesario añadir soporte para transiciones rápidas entre puntos de acceso con las siguientes características:
  - La implementación está bastante idealizada puesto que se asume que los clientes Wi-Fi de los trenes conocen su posición y los detalles del despliegue Wi-Fi (la posición de cada punto de acceso y el canal Wi-Fi en el que opera). De esta forma, los clientes saben cual es el punto de acceso más cercano y a qué canal Wi-Fi deben cambiar para conectarse a él.
  - Se desarrollaron tres métodos diferentes para conectarse a un punto de acceso una vez que ya se está operando en su canal Wi-Fi:
    - *PassiveBeaconWait*: El cliente recibe paquetes baliza (*beacons*) enviados por los puntos de acceso. Pasado un tiempo predeterminado, se conecta al punto de acceso del que se recibió el *beacon* con mejor SNR.
    - *ActiveProbing*: El cliente envía paquetes especiales (*probe requests*) que son

respondidos por los puntos de acceso que estén operando en ese canal. Pasado un tiempo (en nuestro caso 20 ms), se conecta al mejor punto de acceso.

* *FastHandover*: El cliente se conecta directamente puesto que ya conoce el punto de acceso más cercano. El proceso de conexión puede durar alrededor de 1 ms si no se pierden paquetes.

– Durante este proceso de *handover* los paquetes que se quieran enviar desde el cliente se perderán. También se pierden los paquetes que están en las colas del punto de acceso que se está dejando puesto que no se reenvían al siguiente punto de acceso.

Este simulador también permite caracterizar de forma precisa el comportamiento de las aplicaciones y servicios desplegados en el metro. Se han implementado generadores de tráfico adaptados a cada aplicación:

- Flujos con tamaño de paquete y tasa de transmisión fijos. Usado para las aplicaciones CBTC, mantenimiento, e información para los pasajeros.
- Simulación de tráfico de vídeo generado a partir de ficheros de vídeo reales. Se usa para las aplicaciones de videovigilancia.
- Flujo de voz IP, utilizando un tamaño de paquetes y tasa de datos fijas, pero con periodos de silencio cuya duración sigue una distribución estadística.

Los flujos de información de cada aplicación se mapean en las distintas clases de QoS (LTE) o categorías de acceso (Wi-Fi) en función de sus requisitos. Los servicios críticos tienen prioridad máxima y por tanto se les asignan las prioridades 1 y 2 en LTE y la categoría de voz (AC_VO) en Wi-Fi. El resto de aplicaciones se configura con prioridad *best-effort*.

También se han desarrollado modelos de propagación radio dentro de los túneles para realizar las simulaciones de la forma más realista posible. La propagación radio en túneles se suele caracterizar por el efecto de guía de ondas que tiende a aparecer a partir de determinadas distancias. Además, la propagación depende en gran medida de las características físicas del túnel, como sus dimensiones o el material y rugosidad de sus paredes. Además, la presencia de curvas y estaciones de metro, así como las dimensiones de los vagones de los trenes, modifican significativamente el canal radio.

En la bibliografía hay multitud de artículos centrados en el estudio del modelo de propagación del canal radio en túneles. Los modelos de canal se pueden clasificar en dos grupos: deterministas y empíricos. Los modelos de canal deterministas simulan el comportamiento de las ondas radio para predecir la potencia y el retardo en recepción. Estos modelos pueden estar basados en la resolución de las ecuaciones de Maxwell, en el análisis del efecto de guía de ondas, o en métodos de trazado de rayos. Por otra parte, los modelos empíricos se basan en el análisis de las medidas obtenidas en túneles. A partir de estas medidas, tratan de generalizar el comportamiento del canal con expresiones matemáticas cuyos parámetros dependen del escenario.

En este trabajo se han desarrollado dos modelos de canal:

- Modelo de canal determinista: Se basa en un modelo de canal determinista que utiliza

el análisis modal para aproximar el efecto de guía de ondas en túneles rectangulares. Además, puede utilizarse en las regiones de propagación cercana y lejana del túnel, proporcionando resultados realistas. Para poder utilizar este modelo en las simulaciones, se ha adaptado y mejorado de la siguiente forma:
  - Se ha descrito el método para poder utilizar el modelo con túneles con sección no rectangular. Este método permite obtener el ancho y alto del túnel rectangular equivalente de túneles arqueados o circulares.
  - Se ha añadido al modelo las pérdidas por la rugosidad e inclinación de las paredes del túnel.
  - Se tiene en cuenta la pérdida de acople o inserción de las antenas transmisoras y receptoras dentro del túnel, en función de la cercanía a las paredes. Cuanto más cerca de las paredes, mayor es la pérdida.
  - En los tramos curvos se produce una pérdida de propagación superior. Para modelar esta pérdida adicional, se utiliza un modelo empírico que solo depende del radio de curvatura, la frecuencia de la señal y la polarización de las antenas.
  - También se tiene en cuenta los cambios de pendiente del recorrido, que se modelan de la misma forma que las curvas.
- Modelo basado en medidas: Este modelo se basa en los resultados de una campaña de medida realizada en una estación del Metro de Madrid. Este modelo está dividido en dos componentes:
  - Pérdida de propagación de gran escala. Se dividen las mediciones en dos tramos (estación y túnel) para ajustar un modelo de propagación logarítmico en cada uno.
  - Pérdida a pequeña escala (desvanecimiento). Se procesan las medidas obtenidas para eliminar la pérdida de propagación a gran escala y se calcula la densidad espectral de potencia recibida para cada distancia y banda de frecuencia considerada.

Se han realizado simulaciones en dos escenarios. Por una parte, se ha estudiado un escenario con tres estaciones con un despliegue LTE similar al del modelo de propagación basado en medidas. Por otra parte, se han estudiado los posibles despliegues en una línea completa de metro, utilizando el modelo de canal teórico para LTE y Wi-Fi.

El despliegue LTE con tres estaciones se diseñó para ajustarse a las condiciones de la campaña de medida: un eNB en el centro de cada estación configurado para utilizar un sistema LTE en modo FDD de 10+10 MHz de ancho de banda. Se ajustaron diversos parámetros del despliegue LTE, incluyendo el reúso de frecuencias y el algoritmo de *handover*. De esta forma se minimizaron las interferencias y se evitaron los problemas típicos del *handover*, como el efecto ping-pong.

El escenario de la línea de metro completa se utilizó para probar el modelo de canal teórico y comparar las dos tecnologías más utilizadas en los sistemas reales: una red LTE basada en antenas distribuidas (DAS) y una solución Wi-Fi personalizada. La línea de metro

se basa en la línea 3 de Metro Bilbao y se usa su trazado y características para realizar los cálculos de propagación con el modelo teórico. Se plantea un despliegue inicial con antenas directivas situadas cerca de las salidas de emergencia y estaciones, facilitando su instalación y mantenimiento. Las distintas características de las tecnologías Wi-Fi y LTE conducen a despliegues muy diferentes. LTE utiliza el modo FDD con 20+20 MHz de ancho de banda, transmitiendo en las frecuencias de 1869.9 MHz y 1774.9 MHz, y con potencia máxima de 34 dBm y 23 dBm en DL y UL, respectivamente. El despliegue Wi-Fi, en cambio, utiliza 8 canales de 20 MHz en la banda de 5 GHz, y su potencia de transmisión está limitada a 20 dBm. Estas diferencias hacen que la red LTE pueda utilizar las posiciones iniciales de las antenas, pero para el despliegue Wi-Fi ha sido necesario usar un despliegue diferente con antenas cada 400 m.

El rendimiento de LTE y Wi-Fi se ha evaluado en términos de tasa de datos, pérdida de paquetes y latencia. En ambos casos se ha conseguido el cumplimiento de los requisitos definidos:

- Latencia: Tanto con LTE como con Wi-Fi se cumple la restricción de que el retardo sea siempre inferior a 100 ms para el tráfico CBTC. Los demás servicios cumplen sus requisitos de retardo de forma adecuada.
- PER: El límite del 0,1% establecido para CBTC se cumple con ambas tecnologías. Los despliegues LTE necesitan una configuración de reúso de frecuencias apropiada para evitar las interferencias y cumplir este requisito. En el caso de Wi-Fi, solo se respeta el límite de paquetes perdidos cuando se utiliza el método de transición entre puntos de acceso *FastHandover*.

Gracias a las adaptaciones realizadas al simulador, los resultados obtenidos predicen el comportamiento de las diferentes tecnologías de forma apropiada y muestran la versatilidad del simulador para evaluar diferentes despliegues.

Appendix II

List of Acronyms

3GPP 3rd Generation Partnership Project
4G fourth generation
5G fifth generation
AAI Advanced Air Interface
AAS adaptive antenna system
ABS advanced base station
ADC analog-to-digital converter
AES advanced encryption standard
AMC adaptive modulation and coding
AMS advanced mobile station
AP access point
ARP Address Resolution Protocol
ARQ automatic repeat request
ASIC application-specific integrated circuit
ATM asynchronous transfer mode
AWGN additive white Gaussian noise
BER bit error ratio
BE best effort
BR bandwidth request
BSN block sequence number
BS base station
BTC block turbo code
BWA broadband wireless access
CARA Collision-Aware Rate Adaptation
CBTC communications-based train control
CCDF complementary cumulative distribution function
CCTV closed-circuit television
CDMA code-division multiple access

CFO carrier frequency offset
CID connection identifier
CINR carrier-to-interference-and-noise ratio
CMAC cipher-based message authentication code
COTS commercial off-the-shelf
CPS common part sublayer
CP cyclic prefix
CRC cyclic redundancy check
CS convergence sublayer
CTC convolutional turbo code
DAC digital-to-analog converter
DAS distributed antenna system
DDC digital down-converter
DFS Dynamic Frequency Selection
DL-MAP downlink map
DL downlink
DRR deficit round robin
DSP digital signal processor
DUC digital up-converter
EAP Extensible Authentication Protocol
EARFCN E-UTRA Absolute Radio Frequency Channel Number
EIRP effective isotropic radiated power
EPC Evolved Packet Core
ePDCCH enhanced PDCCH
EPS Evolved Packet switched System
ERTMS European Rail Traffic Management System
ETCS European Train Control System
EVM error vector magnitude
FCH frame control header
FDD frequency-division duplexing
FEC forward error correction
FER frame error rate
FFR fractional frequency reuse
FFT fast Fourier transform
FIFO first-in-first-out
FPGA field programmable gate array
FRMCS Future Railway Mobile Communication System
FUSC full usage of subchannels
GBR guaranteed bit rate

GO geometric optics
GPP general purpose processor
GSM-R GSM for Railways
GSM Global System for Mobile Communications
HARQ hybrid automatic repeat request
HDL hardware description language
HCS header check sequence
HFR hard frequency reuse
HLS high-level synthesis
HMAC hash-based message authentication code
HST high-speed train
ICI inter-carrier interference
ICIC Inter-Cell Interference Coordination
IFFT inverse fast Fourier transform
IP Internet Protocol
ISM industrial, scientific and medical
ITU-R ITU Radiocommunication Sector
JML Joint Maximum Likelihood
LC logical channel
LCP logical channel prioritization
LDPC low-density parity check
LoS line-of-sight
LSB least significant bit
LTE-A LTE-Advanced
LTE Long Term Evolution
LTE-U LTE-Unlicensed
LTE-LAA LTE Licensed Assisted Access
LoS line-of-sight
M2M machine-to-machine
MAC medium access control layer
MIMO multiple-input-multiple-output
MPDU MAC protocol data unit
MRTR Minimum Reserved Traffic Rate
MSTR Maximum Sustained Traffic Rate
MSB most significant bit
MSDU MAC service data unit
MSE mean squared error
MS mobile station
MT maximum throughput

MTU maximum transmission unit
MU-MIMO Multiple User MIMO
NLoS non-line-of-sight
NR new radio
NR-U new radio unlicensed
OCC operational control center
OFDMA orthogonal frequency-division multiple access
OFDM orthogonal frequency-division multiplexing
PAPR peak-to-average power ratio
PCFICH Physical Control Format Indicator Channel
PCI Peripheral Component Interconnect
PC personal computer
PDCCH Physical Downlink Control Channel
PDU protocol data unit
PER packet error ratio
PF proportional fair
PGA programmable gain amplifier
PGW packet data network gateway
PHS payload header suppression
PHY physical layer
PIS Passenger Information System
PKM privacy key management
PMP point-to-multipoint
PN packet number
PRB physical resource block
PRBS pseudorandom binary sequence
PSD power spectral density
PUSC partial usage of subchannels
QoS quality of service
QCI QoS Class Identifier
RB resource block
RLC Radio Link Control
ROHC RObust Header Compression
RRC Radio Resource Control
RR round robin
RSSI received signal strength indication
RSRP Reference Signal Received Power
RSRQ Reference Signal Received Quality
RTG receive/transmit transition gap

RTP Real-time Transport Protocol
SAP service access point
SA security association
SC single-carrier
SC-FDMA single-carrier FDMA
SDR software-defined radio
SDU service data unit
SFR soft frequency reuse
SINR signal-to-interference-plus-noise ratio
SISO single-input and single-output
SNR signal-to-noise ratio
SOFDMA scalable OFDMA
SS subscriber station
STA station
SU-MIMO Single User MIMO
SoC System-on-Chip
TBCC tail-biting convolutional code
TCP Transmission Control Protocol
TDD time-division duplexing
TDMA time division multiple access
TETRA Terrestrial Trunked Radio
TPC Transmit Power Control
TTG transmit/receive transition gap
TUSC tile usage of subchannels
UDP User Datagram Protocol
UE user equipment
UGS unsolicited grant service
UIC International Union of Railways
UL-MAP uplink map
UL uplink
UM Unacknowledged Mode
UMTS Universal Mobile Telecommunications System
VoIP voice over Internet Protocol
WLAN wireless local area network
WiMAX Worldwide Interoperability for Microwave Access
eNodeB Evolved Node B
ertPS extended rtPS
nrtPS non-real-time polling service
rtPS real-time polling service

References

[3GP14] 3GPP. *Policy and charging control architecture*. TS 23.203, version 8.15.0. 3rd Generation Partnership Project (3GPP), 2014.

[3GP18] 3GPP. *Medium Access Control (MAC) protocol specification*. TS 36.321, version 15.2.0. 3rd Generation Partnership Project (3GPP), 2018.

[AHM10] Sassan Ahmadi. ***Mobile WiMAX: A systems approach to understanding IEEE 802.16 m radio access technology***. Academic Press, 2010. ISBN: 9780123749642.

[AI+16] B. Ai, K. Guan, Z. Zhong, C. F. López, L. Zhang, C. Briso-Rodríguez, and R. He. "**Measurement and analysis of extra propagation loss of tunnel curve**". *IEEE Transactions on Vehicular Technology*, vol. 65, no. 4, 2016, pp. 1847–1858. ISSN: 1939-9359.
DOI: 10.1109/TVT.2015.2425218.

[ALL18] Ben Allen. *User and System Requirements (Telecommunications)*. Deliverable 3.1. Version 1.1. X2Rail-1, 2018. Online access: https://projects.shift2rail.org/download.aspx?id=5a0c552b-eac6-46bf-9f9d-c33df0a980d9.

[ALT06] Altera Corporation. **WiMAX OFDMA Ranging**. Application Note 430. 2006. Online access: https://www.intel.com/content/dam/www/programmable/us/en/pdfs/literature/technology/dsp/dsp-literature_2.pdf.

[ARH09] A.Q. Ansari, A. Rajput, and M. Hashmani. "**WiMAX Network Optimization - Analyzing Effects of Adaptive Modulation and Coding Schemes Used in Conjunction with ARQ and HARQ**". *Proc. of Seventh Annual Communication Networks and Services Research Conference, 2009. CNSR '09.* 2009, pp. 6–13.
DOI: 10.1109/CNSR.2009.12.

[BCA07] C. Briso-Rodriguez, J. M. Cruz, and J. I. Alonso. "**Measurements and Modeling of Distributed Antenna Systems in Railway Tunnels**". *IEEE Transactions on Vehicular Technology*, vol. 56, no. 5, 2007, pp. 2870–2879. ISSN: 1939-9359.
DOI: 10.1109/TVT.2007.900500.

[BHA+09] G. Bhanage, R. Mahindra, I. Seskar, and D. Raychaudhuri. "**Implication of MAC frame aggregation on empirical wireless experimentation**". *Proc. of GLOBECOM 2009 - 2009 IEEE Global Telecommunications Conference*. 2009, pp. 1–7.
DOI: 10.1109/GLOCOM.2009.5426069.

[BIT14] Naila Bouchemal, Nora Izri, and Samir Tohmé. "**MAC-LTE scheduler modeling and performance evaluation in LTE network**". *Proc. of 2014 IEEE 25th Annual International Symposium on Personal, Indoor, and Mobile Radio Communication (PIMRC)*. 2014, pp. 1007–1012.
DOI: 10.1109/PIMRC.2014.7136314.

[BN09] Aymen Belghith and Loutfi Nuaymi. "Scheduling Techniques for WiMax". *Current Technology Developments of WiMax Systems*. Ed. by Maode Ma. Dordrecht, Springer Netherlands, 2009, pp. 61–84. ISBN: 978-1-4020-9300-5.
DOI: 10.1007/978-1-4020-9300-5_4.

[CAR+13a] Ángel Carro-Lagoa, Pedro Suárez-Casal, P. Fraga-Lamas, J. A. García-Naya, L. Castedo, and A. Morales-Méndez. "**Real-Time Validation of a SDR Implementation of TDD WiMAX Standard**". *Proc. of 2013 Wireless Innovation Forum European Conference on Communications Technologies and Software Defined Radio (SDR-WInnComm-Europe 2013)*. 2013.

[CAR+13b] Ángel Carro-Lagoa, Pedro Suárez-Casal, José A. García-Naya, Paula Fraga-Lamas, Luis Castedo, and Antonio Morales-Méndez. "**Design and implementation of an OFDMA-TDD physical layer for WiMAX applications**". *EURASIP Journal on Wireless Communications and Networking*, vol. 2013, no. 1, 2013, p. 243. ISSN: 1687-1499.
DOI: 10.1186/1687-1499-2013-243.

[CAR+19] Ángel Carro-Lagoa, Tomás Domínguez-Bolaño, José Rodríguez-Piñeiro, Miguel González-López, and José A. García-Naya. "**Feasibility of LTE for train control in subway environments based on experimental data**". *Proc. of 2019 27th European Signal Processing Conference (EUSIPCO)*. 2019, pp. 1–5.
DOI: 10.23919/EUSIPCO.2019.8903070.

[CHU+11] G.C.H. Chuang, Pang-An Ting, Jen-Yuan Hsu, Jiun-You Lai, Shun-Chang Lo, Ying-Chuan Hsiao, and Tzi-Dar Chiueh. "**A MIMO WiMAX SoC in 90nm CMOS for 300km/h mobility**". *Proc. of IEEE International Solid-State Circuits Conference Digest of Technical Papers (ISSCC), 2011*. 2011, pp. 134–136.
DOI: 10.1109/ISSCC.2011.5746252.

[CKH11] Bonato Both C., R. Kunst, and F. Henes. "**Channel Encoding Block for Mobile WiMAX Networks Using Reconfigurable Hardware**". *Journal of Applied Computing*

Research, vol. 1, no. 2, 2011, pp. 69–75.
DOI: 10.4013/jacr.2011.12.01.

[CLC07] Kang-Chuan Chang, Jun-Wei Lin, and Tzi-Dar Chiueh. "**Design of a downlink baseband receiver for IEEE 802.16E OFDMA mode in high mobility**". *Proc. of IEEE International SOC Conference, 2007*. 2007, pp. 301–304.
DOI: 10.1109/SOCC.2007.4545479.

[COL+10] Rebeca Colda, Tudor Palade, Emanuel Pucchita, Irina Vermecan, and Ancuta Moldovan. "**Mobile WiMAX: System performance on a vehicular multipath channel**". *Proc. of Fourth European Conference on Antennas and Propagation (EuCAP), 2010*. 2010, pp. 1–5.

[COR07] Intel Corporation. *OFDMA PHY SAP Interface Specification for 802.16 Broadband Wireless Access Base Stations*. Tech. rep. 2007.

[CS94] R.V. Cox and C.E.W. Sundberg. "**An efficient adaptive circular Viterbi algorithm for decoding generalized tailbiting convolutional codes**". *IEEE Transactions on Vehicular Technology*, vol. 43, no. 1, 1994, pp. 57–68. ISSN: 0018-9545.
DOI: 10.1109/25.282266.

[DIM+09] K. Dimou, M. Wang, Y. Yang, M. Kazmi, A. Larmo, J. Pettersson, W. Muller, and Y. Timner. "**Handover within 3gpp lte: design principles and performance**". *Proc. of 2009 IEEE 70th Vehicular Technology Conference Fall*. 2009, pp. 1–5.
DOI: 10.1109/VETECF.2009.5378909.

[DOM+16] T. Domínguez-Bolaño, J. Rodríguez-Piñeiro, José A. García-Naya, and L. Castedo. "**The GTEC 5G link-level simulator**". *Proc. of 1st International Workshop on Link- and System Level Simulations (IWSLS)*. 2016, pp. 1–6.
DOI: 10.1109/IWSLS.2016.7801585.

[DOM+18] T. Domínguez-Bolaño, J. Rodríguez-Piñeiro, J. A. García-Naya, X. Yin, and L. Castedo. "**Measurement-based characterization of train-to-infrastructure 2.6 GHz propagation channel in a modern subway station**". *IEEE Access*, vol. 6, 2018, pp. 52814–52830. ISSN: 2169-3536.
DOI: 10.1109/ACCESS.2018.2870564.

[DUD+07] D. G. Dudley, S. F. Mahmoud, M. Lienard, and P. Degauque. "**On wireless communication in tunnels**". *Proc. of 2007 IEEE Antennas and Propagation Society International Symposium*. 2007, pp. 3305–3308.
DOI: 10.1109/APS.2007.4396243.

[EH94] Bradley Efron and D. V. Hinkley. ***An Introduction to the Bootstrap (CRC Monographs on Statistics & Applied Probability)***. First. Chapman & Hall, 1994. ISBN: 0412042312.

[ELS75] A. Emslie, R. Lagace, and P. Strong. "**Theory of the propagation of uhf radio waves in coal mine tunnels**". *IEEE Transactions on Antennas and Propagation*, vol. 23, no. 2, 1975, pp. 192–205. ISSN: 1558-2221.
DOI: 10.1109/TAP.1975.1141041.

[EME17] Hany M. El-Maghrabi, Samir F. Mahmoud, and Mostafa El-Said. "**Modal analysis of wave propagation in straight and curved arched tunnel based on equivalent rectangular tunnel model**". *ACES JOURNAL*, vol. 32, no. 9, 2017. ISSN: 1054-4887. Online access: https://aces-society.org/includes/downloadpaper.php?of=ACES_Journal_September_2017_Paper_3&nf=17-9-3.

[FON+11] O. Font-Bach, N. Bartzoudis, A. Pascual-Iserte, and D. López Bueno. "**A real-time MIMO-OFDM mobile WiMAX receiver: Architecture, design and FPGA implementation**". *Computer Networks*, vol. 55, no. 16, 2011, pp. 3634–3647. ISSN: 1389-1286.
DOI: 10.1016/j.comnet.2011.02.018.

[FOR+13] A. E. Forooshani, S. Bashir, D. G. Michelson, and S. Noghanian. "**A survey of wireless communications and propagation modeling in underground mines**". *IEEE Communications Surveys Tutorials*, vol. 15, no. 4, 2013, pp. 1524–1545. ISSN: 1553-877X.
DOI: 10.1109/SURV.2013.031413.00130.

[FS17] J. Farooq and J. Soler. "**Radio communication for communications-based train control (CBTC): a tutorial and survey**". *IEEE Communications Surveys & Tutorials*, vol. 19, no. 3, 2017, pp. 1377–1402. ISSN: 1553-877X.
DOI: 10.1109/COMST.2017.2661384.

[GRR17] Juan Moreno García-Loygorri, José Manuel Riera, and Carlos Rodríguez. "Urban Transport Systems". Ed. by Hamid Yaghoubi. IntechOpen, 2017. Chap. Wireless Communication Systems for Urban Transport, pp. 39–60. ISBN: 978-953-51-2873-1.
DOI: 10.5772/65585.

[GUA+12] Ke Guan, Zhangdui Zhong, José I Alonso, and Cesar Briso-Rodríguez. "**Measurement of distributed antenna systems at 2.4 GHz in a realistic subway tunnel environment**". *IEEE Transactions on Vehicular Technology*, vol. 61, no. 2, 2012, pp. 834–837. ISSN: 0018-9545.
DOI: 10.1109/TVT.2011.2178623.

[GUA+13] K. Guan, Z. Zhong, B. Ai, R. He, B. Chen, Y. Li, and C. Briso-Rodríguez. "**Complete propagation model in tunnels**". *IEEE Antennas and Wireless Propagation Letters*, vol. 12, 2013, pp. 741–744. ISSN: 1548-5757.
DOI: 10.1109/LAWP.2013.2270937.

[HCC09] C. Hsiao, Chi-Yun Chen, and T.-D. Chiueh. "**Design of a dual-mode baseband receiver for 802.11n and 802.16e MIMO OFDM/OFDMA**". *Proc. of International Symposium on VLSI Design, Automation and Test, 2009. VLSI-DAT '09.* 2009, pp. 331–334.
DOI: 10.1109/VDAT.2009.5158162.

[HED09] M. Heddebaut. "**Leaky waveguide for train-to-wayside communication-based train control**". *IEEE Transactions on Vehicular Technology*, vol. 58, no. 3, 2009, pp. 1068–1076. ISSN: 1939-9359.
DOI: 10.1109/TVT.2008.928635.

[HEJ14] Seyed Amin Hejazi. "Self-Organized Intelligent Distributed Antenna System in LTE". PhD thesis. Simon Fraser University, 2014. Online access: http://summit.sfu.ca/item/14020.

[HEM+08] M. Hempel, Wei Wang, H. Sharif, Ting Zhou, and P. Mahasukhon. "**Implementation and performance evaluation of Selective Repeat ARQ for WiMAX NS-2 model**". *Proc. of IEEE Conference on Local Computer Networks, 2008. LCN 2008. 33rd*. 2008, pp. 230–235.
DOI: 10.1109/LCN.2008.4664174.

[HK09] K. Ho and A. Kwasinski. "**Uplink Channel Estimation in WiMAX**". *Proc. of 2009 IEEE Wireless Communications and Networking Conference*. 2009, pp. 1–6.
DOI: 10.1109/WCNC.2009.4918011.

[HKJ10] A. Hrovat, G. Kandus, and T. Javornik. "**Four-slope channel model for path loss prediction in tunnels at 400 mhz**". *IET Microwaves, Antennas Propagation*, vol. 4, no. 5, 2010, pp. 571–582. ISSN: 1751-8733.
DOI: 10.1049/iet-map.2009.0159.

[HKJ14] A. Hrovat, G. Kandus, and T. Javornik. "**A survey of radio propagation modeling for tunnels**". *IEEE Communications Surveys Tutorials*, vol. 16, no. 2, 2014, pp. 658–669. ISSN: 1553-877X.
DOI: 10.1109/SURV.2013.091213.00175.

[HLR08] Thomas R. Henderson, Mathieu Lacage, and George F. Riley. "**Network simulations with the ns-3 simulator**". *Proc. of In Sigcomm (Demo)*. 2008. Online access: http://conferences.sigcomm.org/sigcomm/2008/papers/p527-hendersonA.pdf.

[HSI+11] Hsien-Wen Chang, M. Tseng, S. Chen, Ming-Hung Cheng, and S. Wen. "**Field trial results for integrated WiMAX and radio-over-fiber systems on high speed rail**". *Proc. of 2011 IEEE 22nd International Symposium on Personal, Indoor and Mobile Radio Communications*. 2011, pp. 2111–2115.
DOI: 10.1109/PIMRC.2011.6139887.

[HSU+11] Jen-Yuan Hsu, Chien-Yu Kao, Ping-Heng Kuo, and Pangan Ting. "**Configurable baseband designs and implementations of WiMAX/LTE dual systems based on multi-core DSP**". *Proc. of IEEE International SOC Conference (SOCC), 2011*. 2011, pp. 265–271.
DOI: 10.1109/SOCC.2011.6085146.

[HU+07] Su Hu, Gang Wu, Yong Liang Guan, Choi Look Law, Yanxin Yan, and Shaoqian Li. "**Development and performance evaluation of mobile WiMAX testbed**". *Proc. of IEEE Mobile WiMAX Symposium, 2007*. 2007, pp. 104–107.
DOI: 10.1109/WIMAX.2007.348688.

[IEE04a] IEEE. "**IEEE Standard for Communications-Based Train Control (CBTC) Performance and Functional Requirements**". *IEEE Std 1474.1-2004 (Revision of IEEE Std 1474.1-1999)*, 2004, pp. 1–45.
DOI: 10.1109/IEEESTD.2004.95746.

[IEE04b] IEEE. "**Standard for Local and metropolitan area networks - Part 16: Air Interface for Fixed Broadband Wireless Access Systems**". *IEEE Std 802.16-2004 (Revision of IEEE Std 802.16-2001)*, 2004, pp. 1–915.
DOI: 10.1109/IEEESTD.2004.8684627.

[IEE06] IEEE. "**IEEE Standard for Local and Metropolitan Area Networks - Part 16: Air Interface for Fixed and Mobile Broadband Wireless Access Systems - Amendment for Physical and Medium Access Control Layers for Combined Fixed and Mobile Operation in Licensed Bands**". *IEEE Std 802.16e-2005 and IEEE Std 802.16-2004/Cor 1-2005 (Amendment and Corrigendum to IEEE Std 802.16-2004)*, 2006, pp. 1–822.
DOI: 10.1109/IEEESTD.2006.99107.

[IEE08] IEEE. "**IEEE Recommended Practice for Communications-Based Train Control (CBTC) System Design and Functional Allocations**". *IEEE Std 1474.3-2008*, 2008, pp. 1–117.
DOI: 10.1109/IEEESTD.2008.4618623.

[IEE09] IEEE. "**IEEE Standard for Local and metropolitan area networks Part 16: Air Interface for Broadband Wireless Access Systems**". *IEEE Std 802.16-2009 (Revision of IEEE Std 802.16-2004)*, 2009, pp. 1–2080.
DOI: 10.1109/IEEESTD.2009.5062485.

[IEE11] IEEE. "**IEEE Standard for Local and metropolitan area networks Part 16: Air Interface for Broadband Wireless Access Systems Amendment 3: Advanced Air Interface**". *IEEE Std 802.16m-2011(Amendment to IEEE Std 802.16-2009)*, 2011.
DOI: 10.1109/IEEESTD.2011.5765736.

[IEE12a] IEEE. "**IEEE Standard for Air Interface for Broadband Wireless Access Systems**". *IEEE Std 802.16-2012 (Revision of IEEE Std 802.16-2009)*, 2012, pp. 1–2542. DOI: 10.1109/IEEESTD.2012.6272299.

[IEE12b] IEEE. "**IEEE Standard for WirelessMAN-Advanced Air Interface for Broadband Wireless Access Systems**". *IEEE Std 802.16.1-2012*, 2012, pp. 1–1090. DOI: 10.1109/IEEESTD.2012.6297413.

[IEE12c] IEEE. "**IEEE Standard for WirelessMAN-Advanced Air Interface for Broadband Wireless Access Systems Amendment 1: Enhancements to Support Machine-to-Machine Applications**". *IEEE Std 802.16.1b-2012 (Amendment to IEEE Std 802.16.1-2012)*, 2012, pp. 1–126. DOI: 10.1109/IEEESTD.2012.6328224.

[IEE13] IEEE. "**IEEE Standard for WirelessMAN-Advanced Air Interface for Broadband Wireless Access Systems –Amendment 2: Higher Reliability Networks**". *IEEE Std 802.16.1a-2013 (Amendment to IEEE Std 802.16.1-2012)*, 2013, pp. 1–319. DOI: 10.1109/IEEESTD.2013.6547982.

[IEE16] IEEE. "**IEEE Standard for Information technology – Telecommunications and information exchange between systems Local and metropolitan area networks – Specific requirements - Part 11: Wireless LAN Medium Access Control (MAC) and Physical Layer (PHY) Specifications**". *IEEE Std 802.11-2016 (Revision of IEEE Std 802.11-2012)*, 2016, pp. 1–3534. DOI: 10.1109/IEEESTD.2016.7786995.

[IEE18] IEEE. "**IEEE Standard for Air Interface for Broadband Wireless Access Systems**". *IEEE Std 802.16-2017 (Revision of IEEE Std 802.16-2012)*, 2018, pp. 1–2726. DOI: 10.1109/IEEESTD.2018.8303870.

[IEE20] IEEE. "**IEEE Draft Standard for Information Technology – Telecommunications and Information Exchange Between Systems Local and Metropolitan Area Networks – Specific Requirements Part 11: Wireless LAN Medium Access Control (MAC) and Physical Layer (PHY) Specifications Amendment Enhancements for High Efficiency WLAN**". *IEEE P802.11ax/D7.0, September 2020*, 2020, pp. 1–822. Online access: https://ieeexplore.ieee.org/servlet/opac?punumber=9186914.

[ISC07] P. Imperatore, E. Salvadori, and I. Chlamtac. "**Path Loss Measurements at 3.5 GHz: A Trial Test WiMAX Based in Rural Environment**". *Proc. of 3rd International Conference on Testbeds and Research Infrastructure for the Development of Networks and Communities, 2007. TridentCom 2007*. 2007, pp. 1–8. DOI: 10.1109/TRIDENTCOM.2007.4444709.

[ITU03] ITU-T. *Recommendation G.114: One-way transmission time. Recommendations on the transmission quality for an entire international telephone connection*. 2003. Online access: https://www.itu.int/rec/T-REC-G.114.

[ITU97] ITU-R. *Recommendation ITU-R M.1225: Guidelines for Evaluation of Radio Transmission Technologies for IMT-2000*. Tech. rep. ITU-R, 1997.

[KAH09] M.S. Khairy, M.M. Abdallah, and S.E.-D. Habib. "**Efficient FPGA Implementation of MIMO Decoder for Mobile WiMAX System**". *Proc. of IEEE International Conference on Communications, 2009. ICC '09*. 2009, pp. 1–5. DOI: 10.1109/ICC.2009.5198971.

[KHA+13] Arwa Khayat, Mohamed Kassab, Marion Berbineau, Mohamed Amine Abid, and Abdelfettah Belghith. "**LTE based communication system for urban guided-transport: a QoS performance study**". *Proc. of Communication Technologies for Vehicles*. Berlin, Heidelberg, Springer Berlin Heidelberg, 2013, pp. 197–210. ISBN: 978-3-642-37974-1. DOI: 10.1007/978-3-642-37974-1_16.

[KIM+06] J. Kim, S. Kim, S. Choi, and D. Qiao. "**CARA: Collision-Aware Rate Adaptation for IEEE 802.11 WLANs**". *Proc. of 25TH IEEE International Conference on Computer Communications (IEEE INFOCOM 2006)*. 2006, pp. 1–11. DOI: 10.1109/INFOCOM.2006.316.

[LB08] H. Lai and S. Boumaiza. "**WiMAX baseband processor implementation and validation on a FPGA/DSP platform**". *Proc. of Canadian Conference on Electrical and Computer Engineering, 2008. CCECE 2008*. 2008, pp. 001449–001452. DOI: 10.1109/CCECE.2008.4564781.

[LEE+09] Suk-Bok Lee, Ioannis Pefkianakis, Adam Meyerson, Shugong Xu, and Songwu Lu. "**Proportional Fair Frequency-Domain Packet Scheduling for 3GPP LTE Uplink**". *Proc. of IEEE INFOCOM 2009*. 2009, pp. 2611–2615. DOI: 10.1109/INFCOM.2009.5062197.

[LIU+17] Yu Liu, Ammar Ghazal, Cheng-Xiang Wang, Xiaohu Ge, Yang Yang, and Yapei Zhang. "**Channel measurements and models for high-speed train wireless communication systems in tunnel scenarios: a survey**". *Science China Information Sciences*, vol. 60, no. 101301, 2017. DOI: 10.1007/s11432-016-9014-3. Online access: https://arxiv.org/abs/1612.09534.

[LP09] P. Latkoski and B. Popovski. "**Delay and throughput analysis of IEEE 802.16 ARQ mechanism**". *Proc. of International Conference on Wireless and Optical Communications Networks, 2009. WOCN '09. IFIP*. 2009, pp. 1–5. DOI: 10.1109/WOCN.2009.5010534.

[MAH10] Samir F. Mahmoud. “Wireless transmission in tunnels”. *Mobile and Wireless Communications*. Ed. by Salma Ait Fares and Fumiyuki Adachi. Rijeka, IntechOpen, 2010. Chap. 1.
DOI: 10.5772/7700.

[MAO06] H.A. Mahmoud, H. Arslan, and M.K. Ozdemir. “**Initial Ranging for WiMAX (802.16e) OFDMA**”. *Proc. of IEEE Military Communications Conference, 2006. MILCOM 2006.* 2006, pp. 1–7.
DOI: 10.1109/MILCOM.2006.302240.

[MAS+12] E. Masson, Y. Cocheril, M. Berbineau, J. Ghys, V. Hovinen, and A. Roivainen. “**MIMO channel characterization in subway tunnel for train-to-wayside applications**”. *Proc. of 2012 12th International Conference on ITS Telecommunications*. 2012, pp. 732–736.
DOI: 10.1109/ITST.2012.6425278.

[MAT] Mathworks. *Simulink – Simulation and Model-Based Design*. Online access: https://www.mathworks.com/products/simulink.html.

[MB17] Émilie Masson and Marion Berbineau. “Railway Operators Needs in Terms of Wireless Communications”. *Broadband Wireless Communications for Railway Applications: For Onboard Internet Access and Other Applications*. Cham, Springer International Publishing, 2017, pp. 1–33. ISBN: 978-3-319-47202-7.
DOI: 10.1007/978-3-319-47202-7_1.

[MCR08] Christian Mehlführer, Sebastian Caban, and Markus Rupp. “**Experimental Evaluation of Adaptive Modulation and Coding in MIMO WiMAX with Limited Feedback**”. *EURASIP Journal on Advances in Signal Processing*, vol. 2008, 2008.
DOI: 10.1155/2008/837102.

[MIT92] J. Mitola. “**Software radios-survey, critical evaluation and future directions**”. *Proc. of [Proceedings] NTC-92: National Telesystems Conference*. 1992, pp. 13/15–13/23.
DOI: 10.1109/NTC.1992.267870.

[MIT95] J. Mitola. “**The software radio architecture**”. *IEEE Communications Magazine*, vol. 33, no. 5, 1995, pp. 26–38. ISSN: 1558-1896.
DOI: 10.1109/35.393001.

[MIT99] J. Mitola. “**Software radio architecture: a mathematical perspective**”. *IEEE Journal on Selected Areas in Communications*, vol. 17, no. 4, 1999, pp. 514–538. ISSN: 1558-0008.
DOI: 10.1109/49.761033.

[MKP07] M. Morelli, C.-C.J. Kuo, and M.-O. Pun. "**Synchronization Techniques for Orthogonal Frequency Division Multiple Access (OFDMA): A Tutorial Review**". *Proceedings of the IEEE*, vol. 95, no. 7, 2007, pp. 1394–1427. ISSN: 0018-9219. DOI: 10.1109/JPROC.2007.897979.

[MR10] Zaki F.W. Mohamed M.A. and Mosbeh R.H. "**Simulation of WiMAX Physical Layer: IEEE 802.16e**". *IJCSNS International Journal of Computer Science and Network Security*, vol. 10, no. 11, 2010.

[NEG+16] Giovanni Neglia, Sara Alouf, Abdulhalim Dandoush, Sebastien Simoens, Pierre Dersin, Alina Tuholukova, Jérôme Billion, and Pascal Derouet. *Performance Evaluation of Train Moving-Block Control*. Research Report RR-8917. Inria Sophia Antipolis, 2016. Online access: https://hal.inria.fr/hal-01323589.

[NOK16] Nokia. *Paris metro LTE trial: the SYSTUF project and its results*. White Paper. 2016. Online access: https://www.nokia.com/blog/lte-underground-stellar-results-paris-metro-line-14-trial/.

[NUA07] Loutfi Nuaymi. ***WiMAX: Technology for Broadband Wireless Access***. John Wiley & Sons, Ltd, 2007, pp. 69–80. ISBN: 9780470319055. DOI: 10 . 1002 / 9780470319055. Online access: http : / / dx . doi . org / 10 . 1002 / 9780470319055.

[OMI07] T. Ohseki, M. Morita, and T. Inoue. "**Burst Construction and Packet Mapping Scheme for OFDMA Downlinks in IEEE 802.16 Systems**". *Proc. of IEEE Global Telecommunications Conference, 2007. GLOBECOM '07*. 2007, pp. 4307–4311. DOI: 10.1109/GLOCOM.2007.819.

[PAL+10] M. Palkovic, P. Raghavan, M. Li, A. Dejonghe, L. Van der Perre, and F. Catthoor. "**Future software-defined radio platforms and mapping flows**". *IEEE Signal Processing Magazine*, vol. 27, no. 2, 2010, pp. 22–33. ISSN: 1053-5888. DOI: 10.1109/MSP.2009.935386.

[PAR+10] D. Pareit, V. Petrov, B. Lannoo, E. Tanghe, W. Joseph, I. Moerman, P. Demeester, and L. Martens. "**A Throughput Analysis at the MAC Layer of Mobile WiMAX**". *Proc. of IEEE Wireless Communications and Networking Conference (WCNC), 2010*. 2010, pp. 1–6. DOI: 10.1109/WCNC.2010.5506379.

[PAR+12] Daan Pareit, Bart Lannoo, Ingrid Moerman, and Piet Demeester. "**The History of WiMAX: A Complete Survey of the Evolution in Certification and Standardization for IEEE 802.16 and WiMAX**". *IEEE Communications Surveys Tutorials*, vol. 14, no. 4, 2012, pp. 1183–1211. ISSN: 1553-877X. DOI: 10.1109/SURV.2011.091511.00129.

[PBM11] Giuseppe Piro, Nicola Baldo, and Marco Miozzo. "**An LTE module for the ns-3 network simulator**". *Proc. of 4th International ICST Conference on Simulation Tools and Techniques (SIMUTools)*. Barcelona, Spain, 2011, pp. 415–422. ISBN: 978-1-936968-00-8.
DOI: 10.4108/icst.simutools.2011.245571. Online access: http://dl.acm.org/citation.cfm?id=2151054.2151129.

[PRO21] ns-3 project. *Ns-3 model library*. 2021. Online access: https://www.nsnam.org/docs/models/html/index.html.

[PW10] Phuong Thi Thu Pham and Tomohisa Wada. "**Effective scheme of channel tracking and estimation for mobile WiMAX DL-PUSC system**". *J. Comp. Sys., Netw., and Comm.*, vol. 2010, 2010, 6:1–6:9. ISSN: 1687-7381.
DOI: 10.1155/2010/806279. Online access: http://dx.doi.org/10.1155/2010/806279.

[ROD+13] José Rodríguez-Piñeiro, José A. García-Naya, Ángel Carro-Lagoa, and Luis Castedo. "**A testbed for evaluating LTE in high-speed trains**". *Proc. of 16th Euromicro Conference on Digital System Design (DSD 2013)*. 2013, pp. 175–182.
DOI: 10.1109/DSD.2013.27.

[ROD+20] Antonio J. Rodríguez, Roland Pastorino, Ángel Carro-Lagoa, Karl Janssens, and Miguel Á. Naya. "**Hardware acceleration of multibody simulations for real-time embedded applications**". *Multibody System Dynamics*, 2020, pp. 1–19.
DOI: 10.1007/s11044-020-09738-w.

[SA10] Z. Sun and I. F. Akyildiz. "**Channel modeling and analysis for wireless networks in underground mines and road tunnels**". *IEEE Transactions on Communications*, vol. 58, no. 6, 2010, pp. 1758–1768. ISSN: 1558-0857.
DOI: 10.1109/TCOMM.2010.06.080353.

[SAY+06] Alexander Sayenko, Olli Alanen, Juha Karhula, and Timo Hämäläinen. "**Ensuring the QoS Requirements in 802.16 Scheduling**". *Proc. of 9th ACM International Symposium on Modeling Analysis and Simulation of Wireless and Mobile Systems*. MSWiM '06. Torremolinos, Spain, ACM, 2006, pp. 108–117. ISBN: 1-59593-477-4.
DOI: 10.1145/1164717.1164737.

[SAY+07] Alexander Sayenko, Vitaliy Tykhomyrov, Henrik Martikainen, and Olli Alanen. "**Performance Analysis of the IEEE 802.16 ARQ Mechanism**". *Proc. of 10th ACM Symposium on Modeling, analysis, and simulation of wireless and mobile systems*. MSWiM '07. Chania, Crete Island, Greece, ACM, 2007, pp. 314–322. ISBN: 978-1-59593-851-0.
DOI: 10.1145/1298126.1298180. Online access: http://doi.acm.org/10.1145/1298126.1298180.

[SHE+10] Yushi Shen, Pamela C. Cosman, Laurence B. Milstein, and Eduardo F. Martinez. "**On Uplink Channel Estimation in WiMAX Systems**". *Int. J. Mob. Comput. Multimed. Commun.*, vol. 2, no. 2, 2010, pp. 67–77. ISSN: 1937-9412.
DOI: 10.4018/jmcmc.2010040105. Online access: http://code.ucsd.edu/pcosman/jmcmc.pdf.

[SJT09] Chakchai So-In, R. Jain, and A.-K. Tamimi. "**Scheduling in IEEE 802.16e Mobile WiMAX Networks: Key Issues and a Survey**". *IEEE Journal on Selected Areas in Communications*, vol. 27, no. 2, 2009, pp. 156–171. ISSN: 0733-8716.
DOI: 10.1109/JSAC.2009.090207.

[SUÁ+10] Pedro Suárez-Casal, Ángel Carro-Lagoa, José A. García-Naya, and Luis Castedo. "**A Multicore SDR Architecture for Reconfigurable WiMAX Downlink**". *Proc. of 13th Euromicro Conference on Digital System Design: Architectures, Methods and Tools (DSD), 2010*. 2010, pp. 801–804.
DOI: 10.1109/DSD.2010.108.

[SUÁ+15a] Francisco J. Suárez, Pelayo Nuño, Juan C. Granda, and Daniel F. García. "Chapter 7 - computer networks performance modeling and simulation". *Modeling and Simulation of Computer Networks and Systems*. Ed. by Mohammad S. Obaidat, Petros Nicopolitidis, and Faouzi Zarai. Boston, Morgan Kaufmann, 2015, pp. 187–223. ISBN: 978-0-12-800887-4.
DOI: https://doi.org/10.1016/B978-0-12-800887-4.00007-9.

[SUÁ+15b] Pedro Suárez-Casal, Ángel Carro-Lagoa, José A. García-Naya, Paula Fraga-Lamas, Luis Castedo, and Antonio Morales-Méndez. "**A real-time implementation of the Mobile WiMAX ARQ and physical layer**". *Journal of Signal Processing Systems*, vol. 78, no. 3, 2015, pp. 283–297. ISSN: 1939-8115.
DOI: 10.1007/s11265-014-0890-3.

[SV96] M. Shreedhar and G. Varghese. "**Efficient fair queuing using deficit round-robin**". *IEEE/ACM Transactions on Networking*, vol. 4, no. 3, 1996, pp. 375–385. ISSN: 1558-2566.
DOI: 10.1109/90.502236.

[TB02] F. Tosato and P. Bisaglia. "**Simplified soft-output demapper for binary interleaved COFDM with application to HIPERLAN/2**". *Proc. of 2002 IEEE International Conference on Communications. Conference Proceedings. ICC 2002 (Cat. No.02CH37333)*. Vol. 2. 2002, 664–668 vol.2.
DOI: 10.1109/ICC.2002.996940.

[TEXa] Texas Instruments. **14 bit, 125 MSPS Analog-to-Digital Converter (ADS5500)**. Online access: http://www.ti.com/product/ads5500.

[TEXb] Texas Instruments. **16 bit, 500 MSPS, 2x-16x Interpolating Dual-Channel Digital-to-Analog Converter (DAC5686)**. Online access: http://www.ti.com/product/dac5686.

[TOL15] Morten Tolstrup. "Tunnel radio planning". *Indoor Radio Planning: A Practical Guide for GSM, DCS, UMTS, HSPA and LTE*. John Wiley & Sons, Ltd, 2015, pp. 423–470. ISBN: 9781118913611.
DOI: 10.1002/9781118913611.ch11.

[WAN+16] C. Wang, A. Ghazal, B. Ai, Y. Liu, and P. Fan. "**Channel Measurements and Models for High-Speed Train Communication Systems: A Survey**". *IEEE Communications Surveys Tutorials*, vol. 18, no. 2, 2016, pp. 974–987. ISSN: 1553-877X.
DOI: 10.1109/COMST.2015.2508442.

[WAN+19] Shuo Wang, Li Zhu, Kun Xu, Lin Zhang, and Xuan Wang. "**Reliability evaluation for LTE based CBTC train ground communication systems**". *Journal of Advanced Transportation*, 2019. ISSN: 0197-6729.
DOI: 10.1155/2019/2689648.

[WEN+15] T. Wen, X. Lyu, D. Kirkwood, L. Chen, C. Constantinou, and C. Roberts. "**Co-simulation Testing of Data Communication System Supporting CBTC**". *Proc. of 2015 IEEE 18th International Conference on Intelligent Transportation Systems*. 2015, pp. 2665–2670.
DOI: 10.1109/ITSC.2015.428.

[WIM05] WiMAX Forum™. *Requirements and Recommendations for WiMAX Forum™ Mobility Profiles*. Tech. rep. 2005.

[WU+09] Yu-Jen Wu, Jung-Mao Lin, Hsin-Yi Yu, and Hsi-Pin Ma. "**A baseband testbed for uplink mobile MIMO WiMAX communications**". *Proc. of IEEE International Symposium on Circuits and Systems, 2009. ISCAS 2009.* 2009, pp. 794–797.
DOI: 10.1109/ISCAS.2009.5117874.

[WU+10] Yu-Jen Wu, Jung-Mao Lin, Hsin-Yi Yu, Szu-Chi Liu, and Hsi-Pin Ma. "**An SoC evaluation platform for dual link MIMO-OFDMA communications**". *Proc. of 5th International ICST Conference on Communications and Networking in China (CHINACOM), 2010*. 2010, pp. 1–5.

[WWX08] Ming Wu, Fei Wu, and Changsheng Xie. "**The Design and Implementation of WiMAX Base Station MAC Based on Intel Network Processor**". *Proc. of International Conference on Embedded Software and Systems Symposia, 2008. ICESS Symposia '08.* 2008, pp. 350–354.
DOI: 10.1109/ICESS.Symposia.2008.46.

[XILa] Xilinx. **LogiCORE IP - Convolutional Encoder v7.0**. Online access: https://www.xilinx.com/support/documentation/ip_documentation/convolution_ds248.pdf.

[XILb] Xilinx. **LogiCORE IP - Viterbi Decoder v7.0**. Online access: https://www.xilinx.com/support/documentation/ip_documentation/viterbi_ds247.pdf.

[XILc] Xilinx. **LogiCORE IP Fast Fourier Transform v7.1**. Online access: http://www.xilinx.com/support/documentation/ip_documentation/xfft_ds260.pdf.

[XILd] Xilinx. *Xilinx System Generator for DSP*. Online access: https://www.xilinx.com/products/design-tools/vivado/integration/sysgen.html.

[YAN10] Samuel C. Yang. ***OFDMA System Analysis and Design***. 1st. Norwood, MA, USA, Artech House, Inc., 2010. ISBN: 160807076X, 9781608070763.

[YUC+07] T. Yucek, M.K. Ozdemir, H. Arslan, and F.E. Retnasothie. "**A comparative study of initial downlink channel estimation algorithms for mobile WiMAX**". *Proc. of Mobile WiMAX Symposium, 2007. IEEE*. 2007, pp. 32–37.
DOI: 10.1109/WIMAX.2007.348698.

[ZAI+16] A. A. Zaidi, R. Baldemair, H. Tullberg, H. Bjorkegren, L. Sundstrom, J. Medbo, C. Kilinc, and I. Da Silva. "**Waveform and Numerology to Support 5G Services and Requirements**". *IEEE Communications Magazine*, vol. 54, no. 11, 2016, pp. 90–98. ISSN: 1558-1896.
DOI: 10.1109/MCOM.2016.1600336CM.

[ZBM13] Dizhi Zhou, Nicola Baldo, and Marco Miozzo. "**Implementation and validation of LTE downlink schedulers for ns-3**". *Proc. of 6th International ICST Conference on Simulation Tools and Techniques (SIMUTools)*. Cannes, France, 2013, pp. 211–218. ISBN: 978-1-4503-2464-9.
DOI: 10.4108/icst.simutools.2013.251608. Online access: http://dl.acm.org/citation.cfm?id=2512734.2512763.

[ZH97] Y. P. Zhang and Y. Hwang. "**Enhancement of rectangular tunnel waveguide model**". *Proc. of Proceedings of 1997 Asia-Pacific Microwave Conference*. Vol. 1. 1997, 197–200 vol.1.
DOI: 10.1109/APMC.1997.659338.

[ZHA+12] Y. Zhang, M. Wu, S. Ge, L. Luan, and A. Zhang. "**Optimization of time-to-trigger parameter on handover performance in LTE high-speed railway networks**". *Proc. of The 15th International Symposium on Wireless Personal Multimedia Communications*. 2012, pp. 251–255. Online access: https://ieeexplore.ieee.org/document/6398770.

[ZHA+14] Hongli Zhao, Li Zhu, Hailin Jiang, and Tao Tang. "**Design and performance tests in an integrated TD-LTE based train ground communication system**". *Proc. of 17th International IEEE Conference on Intelligent Transportation Systems (ITSC)*. 2014, pp. 747–750.
DOI: 10.1109/ITSC.2014.6957778.

[ZHA+16] Hongli Zhao, Yuan Cao, Li Zhu, and Wei Xu. "**Integrated train ground radio communication system based TD-LTE**". *Chinese Journal of Electronics*, vol. 25, no. 4, 2016, pp. 740–745.
DOI: 10.1049/cje.2016.06.005.

[ZHA03] Y. P. Zhang. "**Novel model for propagation loss prediction in tunnels**". *IEEE Transactions on Vehicular Technology*, vol. 52, no. 5, 2003, pp. 1308–1314. ISSN: 1939-9359.
DOI: 10.1109/TVT.2003.816647.

[ZTN08] G. Zaggoulos, M. Tran, and A. Nix. "**Mobile WiMAX system performance - simulated versus experimental results**". *Proc. of IEEE 19th International Symposium on Personal, Indoor and Mobile Radio Communications, 2008. PIMRC 2008*. 2008, pp. 1–5.
DOI: 10.1109/PIMRC.2008.4699670.